Epigenetic Therapies to Augment Radiation Response in Glioblastoma

by

Nareg Değirmenci

A Dissertation Submitted to the
Graduate School of Health Sciences
in Partial Fulfillment of the Requirements for
the Degree of

Doctor of Philosophy

in

Cellular and Molecular Medicine

June, 2024

Epigenetic Therapies to Augment Radiation Response in Glioblastoma

Koç University

Graduate School of Health Sciences

This is to certify that I have examined this copy of a doctoral dissertation by

Nareg Değirmenci

and have found that it is complete and satisfactory in all respects,
and that any and all revisions required by the final
examining committee has been made.

Committee Members:

Prof. Tuğba Bağcı Önder (Advisor)

Prof. Tevfik Tamer Önder

Assoc. Prof. Umut Şahin

Prof. Uğur Selek

Assoc. Prof. Nihal Karakaş

Date: June 2024

To my family,

ABSTRACT

Epigenetic therapies to augment radiation response in glioblastoma

Nareg Değirmenci
Doctor of Philosophy in Cellular and Molecular Medicine
28 June 2024

Glioblastoma is the most prevalent and aggressive type of brain tumor, presenting limited treatment options that include surgery, chemotherapy, and radiotherapy. Radiotherapy aims to induce DNA damage in tumor cells to eradicate them. However, despite nearly all cancer patients receiving radiotherapy, recurrence occurs. Therefore, it is crucial to understand the molecular mechanisms underlying poor radiotherapy response and identify novel treatments. While genetic alterations have been extensively studied in glioblastoma, the role of epigenetic modifications in regulating radiotherapy response remains unresolved.

In this study, we investigated the potential of epigenetic inhibitors as radiosensitizers in glioblastoma. A chemical screen was performed using a library of 152 small-molecule inhibitors targeting over 12 classes of epigenetic modifiers. Among them, Bromodomain-containing protein 9 (BRD9) inhibitors were identified as potent radiosensitizers. Combination treatment with ionizing radiation (IR) and BRD9 inhibitor, I-BRD9, decreased cell viability and colony formation ability of various glioblastoma cell lines. The IR treatment alone led to induction of DNA double-strand breaks (DSBs), which were repaired over time, as gauged by gH2AX staining. On the contrary, combination treatment with I-BRD9 led to delay in the clearance of gH2AX, indicating an attenuation of DNA repair. In parallel, long-term IR-exposed cell populations, as a model of IR-resistance, exhibited increased expression of BRD9 and low response to combination treatment. Complementary to chemical inhibition, CRISPR/Cas9-based ablation of BRD9 also sensitized glioblastoma cells to ionizing radiation. I-BRD9 and ionizing radiation treatment led to alterations in pathways related to cell cycle, DNA damage repair, Myc-, and E2F -targets, suggesting a link between BRD9, radiation-induced DNA damage repair, and cell cycle progression. Furthermore, cell cycle arrest at the G2/M phase was observed upon combination treatment.

Taken together, our findings suggest a regulatory role for BRD9 in radiotherapy response, highlighting the potential of targeting BRD9 as a therapeutic approach for glioblastoma. This study provides new insights into the molecular mechanisms underlying the poor response to radiotherapy and identifies a potential avenue for improving treatment outcomes in glioblastoma patients.

ÖZETÇE

Glioblastomada radyasyon cevabını arttıracak epigenetik terapilerin geliştirilmesi

Nareg Değirmenci

Hücresel ve Moleküler Tıp, Doktora

28 Haziran 2024

Glioblastoma, sınırlı tedavi seçenekleri olan en yaygın ve agresif beyin tümörü türüdür ve bu tedavi seçenekleri cerrahi müdahale, kemoterapi ve radyoterapiyi içerir. Radyoterapinin amacı, tümör hücrelerinde DNA hasarına neden olarak onları yok etmektir. Ancak, neredeyse tüm kanser hastaları radyoterapi almasına rağmen, nüks kaçınılmazdır. Bu nedenle, radyoterapiye zayıf yanıtın altında yatan moleküler mekanizmaları anlamak ve yeni tedaviler belirlemek çok önemlidir. Glioblastomada genetik değişiklikler kapsamlı bir şekilde incelenmişken, epigenetik modifikasyonların radyoterapi yanıtını düzenlemedeki rolü henüz çözülmemiştir.

Bu çalışmada, glioblastoma hücrelerinin radyasyon cevabını etkileyen epigenetik inhibitörlerin potansiyelini araştırılmıştır. 12'den fazla epigenetik düzenleyici sınıfı hedefleyen 152 moleküllü inhibitörden oluşan bir kütüphane kullanılarak kimyasal bir tarama gerçekleştirilmiştir. Bu tarama, düşük doz radyasyonun, kütüphanedeki kimyasalların düşük dozlarda kullanılmasıyla gerçekleştirilmiştir. Bu inhibitörler arasında, Bromodomain containing protein 9 (BRD9) proteinini hedefleyen inhibitörlerin hücrelerin radyasyona olan cevabını etkilediği gözlemlenmiştir. İyonize radyasyon ve düşük doz BRD9 inhibitörü I-BRD9'un kombinasyon tedavisinin, çeşitli glioblastoma hücre hatlarının hücre canlılığını ve koloni oluşturma yeteneğini azalttığı gösterilmiştir. Ayrıca, iyonize radyasyon DNA çift sarmal kırıkları oluşturmuş ve bu gH2AX boyamasıyla belirlenen bu kırıklar zaman içinde azalmışken, kombinasyon tedavisinde DNA hasar onarımında gecikme olduğu gözlemlenmiştir. Ek olarak, uzun süreli radyasyona maruz kalmış hücre popülasyonlarında, BRD9'un artan ekspresyonu ve kombinasyon tedavisine düşük yanıt gözlenmiştir. Kimyasal inhibisyona ek olarak, CRISPR/Cas9 tabanlı BRD9 ablasyonu da glioblastoma hücrelerini iyonize radyasyona duyarlı hale getirdiği gözlemlenmiştir. I-BRD9 ve iyonize radyasyon tedavisinin, hücre döngüsü, DNA hasar onarımı, Myc- ve E2F-hedefleri ile ilgili yolaklarda bozulmalara yol açtığı gösterilmiştir. Bu sonuçlar ışığında BRD9, radyasyonla indüklenen DNA hasar onarımı ve hücre döngüsü ilerlemesi arasında olası bir bağlantıyı işaret etmektedir. Ayrıca, kombinasyon tedavisi ile G2/M fazında hücre döngüsü durması gözlenmiştir.

Sonuç olarak, bulgular BRD9'un radyoterapi yanıtında düzenleyici bir rol oynadığını ve BRD9'u hedeflemenin glioblastoma için terapötik bir yaklaşım olarak potansiyelini vurgulamaktadır. Bu çalışma, radyoterapiye zayıf yanıtın altında yatan moleküler mekanizmalara yeni bir bakış açısı sunmakta ve glioblastoma hastalarında tedavi sonuçlarını iyileştirmek için potansiyel bir yol belirlemektedir.

TABLE OF CONTENTS

LIST OF TABLES

LIST OF FIGURES

ABBREVIATIONS

Acute myeloid leukemia	AML
Apyrimidic	AP
Ataxia-telangiectasia mutated kinase	ATM
Ataxia-telangiectasia mutated and Rad3-related protein	ATR
BRG1/BRM-associated factor	BAF
Blood brain barrier	BBB
Base Excision Repair	BER
Bromodomaing containing protein 9	BRD9
canonical BAF	cBAF
DNA-dependent protein kinase	DNA-PK
DNA methyltransferase	DNMT
Double-strand break	DSB
Epidermal growth factor receptor	EGFR
Enhancer of zeste homolog 2	EZH2
Glioblastoma	GBM
Glioma stem cells	GSCs
Gray	Gy
Hypoxia activated prodrugs	HAPs
Histone acetyltransferase	HAT
Histone deacetylase	HDAC
Homologous recombination	HR
Immortalized normal human astrocytes	I-NHA
Inhibitory Concentration	IC
Isocitrate dehydrogenase	IDH
Ionizing radiation	IR
Lysine demethylase	KDM
Knockout	KO
O6-Methylguanine DNA methyltransferase	MGMT
Milimolar	mM

Mismatch Repair	MMR
MRE11-RAD50-NBS1	MRN
Nanomolar	nM
Non-canonical BAF	ncBAF
Non-homologous end joining	NHEJ
Open chromatin region	OCR
Poly (ADP-ribose) polymerase	PARP
Polybromo-associated BAF	pBAF
Population Doubling Level	PDL
Polycomb repressive complex	PRC2
Arginine methyltransferase	PRMT
Radiation-induced DNA damage response	RIDD
Reactive Oxygen Species	ROS
Radiotherapy	RT
Single-strand break	SSB
Single-strand DNA	ssDNA
Signal transducer and activator of transcription 5	STAT5
Switch/sucrose non-fermentable	SWI/SNF
Topologically associated domain	TAD
Telomerase reverse transcriptase	TERT
Tumor microenvironment	TME
Temozolomide	TMZ
Micromolar	µM
Micrometer	µm
Principal component analysis	PCA
Differentially expressed genes	DEG

INTRODUCTION

1.1 Glioblastoma

Glioblastoma (GBM) is one the most prevalent and aggressive forms of primary brain tumors (Brandes et al., 2008). Glioblastomas are classified as grade 4 IDH-wildtype by the 2021 WHO Classification of Central Nervous System Tumors (Louis et al., 2021). Tumors are classified as glioblastoma if they harbor 1 or more following characteristics; loss of chromosome 10 and gain of chromosome 7, Epidermal growth factor receptor (*EGFR)* amplification, and telomerase reverse transcriptase (*TERT)* promoter mutation (Tesileanu et al., 2020). After the recent classification, all glioblastomas are considered IDH-wild type; and IDH-mutant tumors are categorized as grade 2, 3 or 4 IDH-mutant astrocytomas (Karschnia et al., 2023).

The age-adjusted global incidence for glioblastoma is less than 10 in 100.000, although it has increased in the last decade. Glioblastoma patients have a poor prognosis with a median survival of 15 months (Brem & Abdullah, 2017; Wirsching et al., 2016). Overall, the 5-year survival rate is one the lowest among all cancer types. Despite the recent improvements in molecular characterization of glioblastoma, therapeutic translations have not been available due to high infiltrative capacity, high tumor heterogeneity, and aggressive clinical evolution (Nguyen et al., 2018)(**Figure 1.1**).

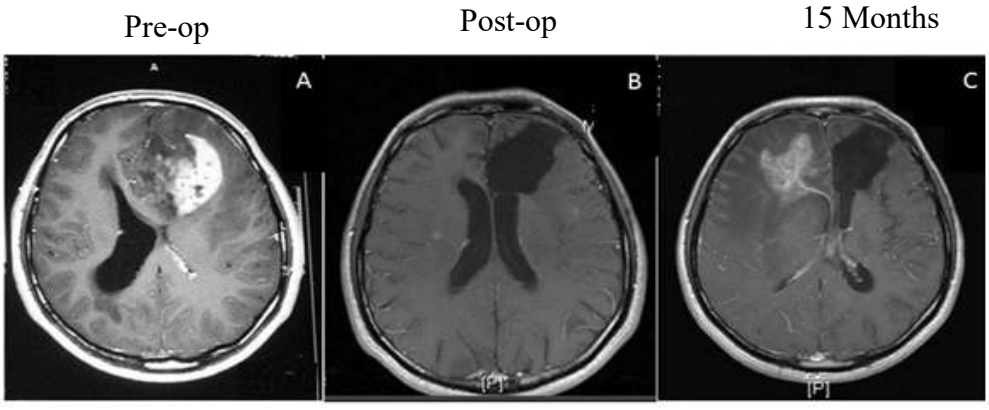

Figure 1.1 MRI image of a GBM patient with GBM tumor on right hemisphere, images taken pre-op, post-op and after 15 months (Seker-polat et al., 2022)

1.2 Therapy options for glioblastoma

Standardized GBM treatment involves surgical resection, followed by radiotherapy and chemotherapy, commonly with Temozolomide (TMZ) (Stupp et al., 2005). The primary objective of surgical resection is to remove the solid tumor without compromising the surrounding healthy tissue and to avoid damage to any neurological functions (Davis, 2016). Undefined tumor margins, high infiltrative capacity of the tumors, tumor location, and tumor pathophysiology are concepts that must be considered to ensure effective surgical resection (Grabowski et al., 2014).

To prevent recurrence and eliminate remaining tumor cells, surgical resection is followed by radiotherapy and chemotherapy.

The combined goal of radiotherapy and chemotherapy is to generate DNA damage, cause genomic instability, and ultimately eradicate tumor cells. As a chemotherapeutic agent for glioblastoma treatment, the golden standard is TMZ, a DNA alkylating agent (Friedman et al., 2000). TMZ administration is conducted with concomitant and adjuvant radiotherapy (Stupp et al., 2005). Even with current radiotherapy and TMZ treatments, recurrence occurs within a high percentage of glioblastoma patients (Ramirez et al., 2013).

1.2.1 Chemotherapy

1.2.1.1 Temozolomide (TMZ)

Temozolomide is a prodrug that is utilized as a benchmark chemotherapeutic agent in glioblastoma treatment (Sansom, 2009). Due to its physiochemical properties and small size, it confers the ability to penetrate the Blood-Brain Barrier (BBB) (Stupp et al., 2009). As a prodrug, it hydrolyzes to 5-(3- methyltriazen-1-yl) imidazole-4-carboxamide (MTIC) in a pH-dependent manner in the cell (Tong et al., 2021). After translocation of MTIC to the nucleus, it causes alkylation of DNA bases. As a result of the alkylation, a methyl group is added and N3-methyladenine (N3-MeA), N7-methylguanine (N7-MeG), and O6-methylguanine (O6-MeG) residues are formed (J. Zhang et al., 2011).

After the generation of DNA damage, cells activate DNA damage repair pathways such as Mismatch Repair (MMR), and Base Excision Repair (BER) (McFaline-Figueroa et al., 2015; Tomar et al., 2021; Yoshimoto et al., 2012). O6-methyl guanine is the most predominant residue generated by TMZ treatment, this damage is caused by a mismatch in DNA replication and activation of the MMR pathway resulting in the generation of DSBs and activation of a futile cycle of replication fork arrest, leading to apoptosis (Nakada et al., 2012; Shen et al., 2014). However, this generated damage, O6-methylguanine residue can be reversed by an enzyme, O6-methylguanine DNA methyl transferase (MGMT).

MGMT transfers the methyl group to itself from DNA bases, directly reversing the effect of TMZ (Stepanenko & Chekhonin, 2019) (**Figure 1.2**).

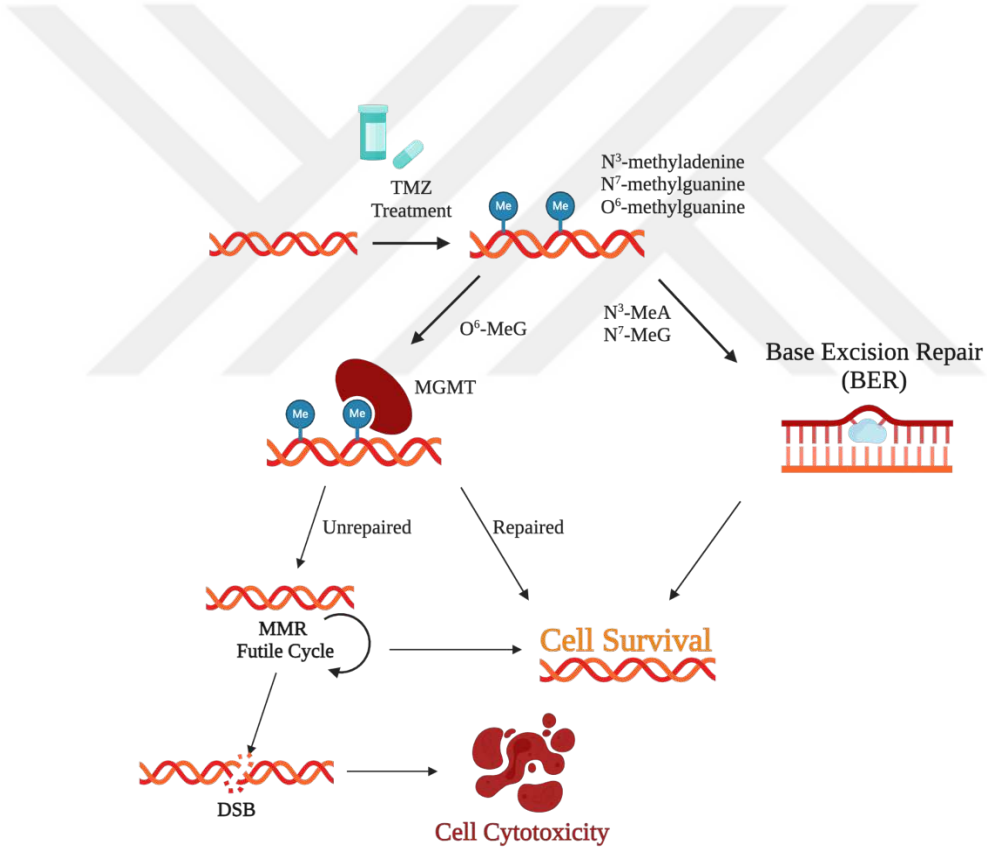

Figure 1.2 TMZ mechanism of action. Adapted from (Kohsaka & Tanak, 2013). Created in Biorender.

Therefore, MGMT expression level is highly correlated with TMZ response of glioblastoma tumors. MGMT's promoter methylation is considered a prognostic factor, as high TMZ response is observed in patients with high MGMT promoter methylation (Hegi et al., 2005; Perazzoli et al., 2015).

1.2.2 Radiotherapy

1.2.2.1 Mechanism of action of radiotherapy

Radiotherapy (RT) is one of the cornerstones in cancer treatment strategies. Since its discovery nearly a century ago, it remains as one of the most effective treatment options. Around 60% of all cancer patients receive RT during therapy, but in most cases, radiotherapy is combined with surgery, chemotherapy, immunotherapy, and stem cell transplantation (Baskar et al., 2012; Chapman et al., 2019) . Unfortunately, due to the location and nature of the tumor, RT is the only treatment for some cancer patients (Chaddad et al., 2019). Therefore, it is crucial to improve treatment strategies involving RT for effective treatment.

The effect of RT originates from high-frequency waves and particles targeting the tumor itself, causing minimal harm to surrounding healthy tissue (Baskar et al., 2014b). The effect of RT can be caused in two different ways, the direct and indirect effects. In the direct effect, ionizing radiation beams directly interact with DNA itself and generate various DNA damages resulting in high cytotoxicity. In the indirect effect, introduced ionizing radiation beams interact with various molecules in the cells, such as water molecules and proteins. Reactive oxygen species (ROS) are generated as radiation beams interact with water molecules (Desouky et al., 2015).

These radical groups cause either DNA damage itself or initiate radiation-induced stress response pathways, which ultimately lead to cell death (Hein et al., 2014) (**Figure 1.3**). Generation of radiation-induced oxidative stress causes disruption of the electron transport chain in mitochondria, lipid peroxidation, stimulation of inflammatory response, protein misfolding, and other various stress responses (Lomax et al., 2013; Reisz et al., 2014). The unit of radiation used in RT is defined as Gray (Gy), the absorption of one joule of radiation energy per kilogram of matter. For different cancer types, the total dose of ionizing radiation varies between 40 to 60 Gy overall, administered around 2 Gy per day (Matsui et al., 2022). The fractionation and dose calculations depend on the location and severity of the tumor and the quality of life of the patients.

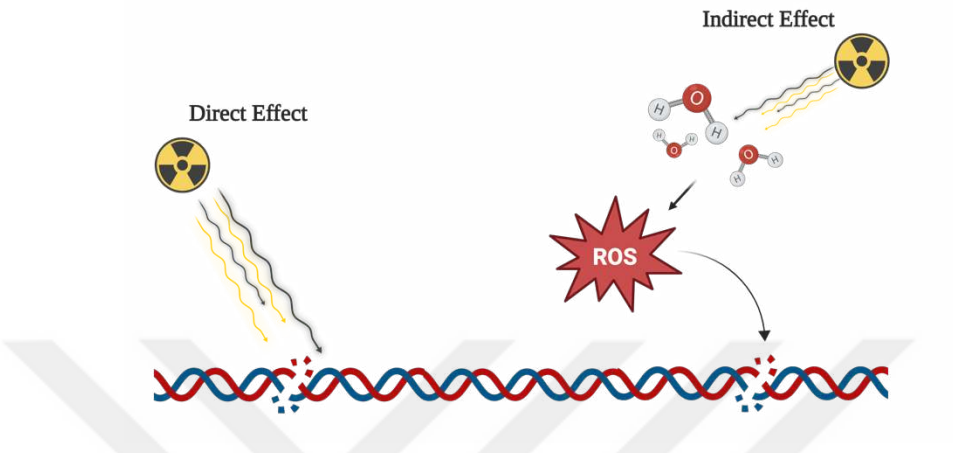

Figure 1.3 Radiotherapy mechanism of action. Adapted from (Desouky et al., 2015). Created in Biorender.

1.2.2.2 Radiation-induced DNA damage response (RIDD)

The beneficial outcomes of radiotherapy mainly come from the generation of various types of DNA damage. Radiation can induce various types of DNA damage; base mismatches, base oxidation, single-strand breaks (SSBs), apurinic or apyrimidic (AP) sites, and most importantly, double-stranded breaks (DSBs) (Goldstein & Kastan, 2015). The generation of DNA lesions initiates radiation-induced DNA damage response (RIDD), which comprises a set of signaling pathways for the recognition and repair of DNA damage (Lomax et al., 2013). Ring openings, abasic lesions, and SSBs are recognized and repaired by BER machinery, involving DNA glycosylases and apurinic endonucleases (APE1) (Wallace, 2014).

DSBs, which are the most cytotoxic lesions created by IR, are recognized by the MRE11-RAD50-NBS1 (MRN) complex (Goodarzi & Jeggo, 2013). After the recruitment of initiator kinases ataxia-telangiectasia mutated and Rad3-related protein (ATR), DNA-dependent protein kinase (DNA-PK), and ataxia-telangiectasia mutated kinase (ATM), phosphorylation of histone variant H2AX occur (Awasthi et al., 2016). The generated

γH2AX causes signal transduction and recruitment of other repair factors, triggering the activity of downstream effectors (Kinner et al., 2008).

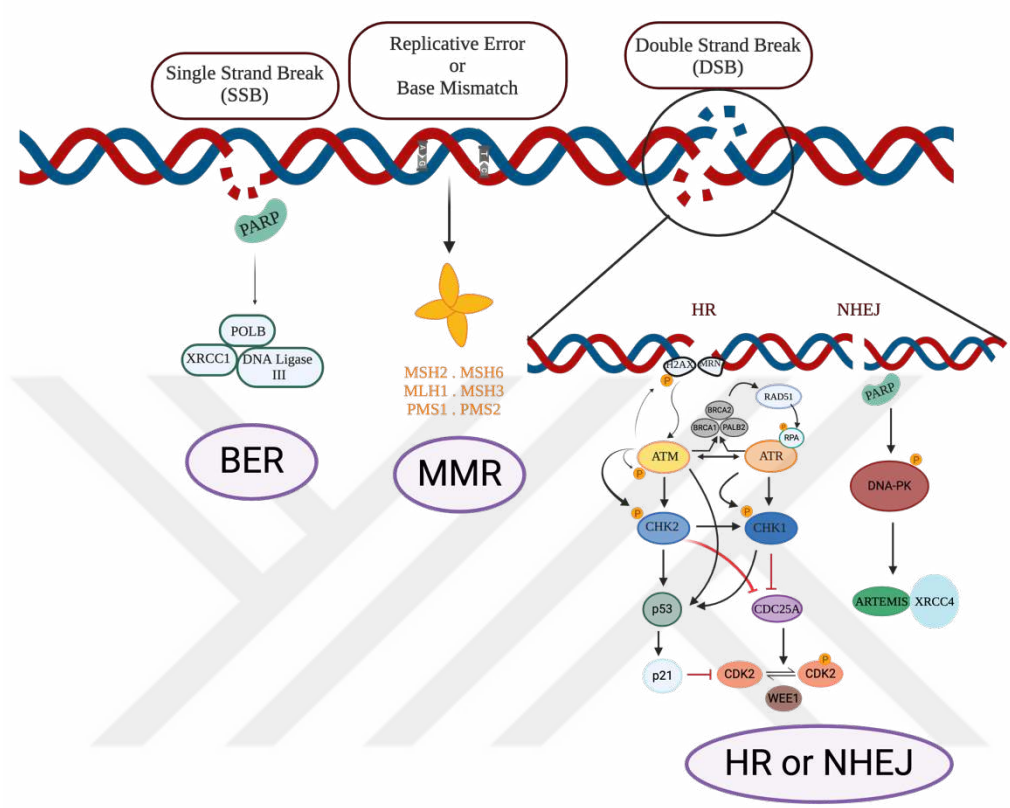

Figure 1.4 Commonly generated DNA damage types and pathways involved in radiation-induced DNA damage (RIDD). Adapted from (Pilié et al., 2019). Created in Biorender.

Depending on the current cell cycle stage and chromosomal conformations, there are three different primary pathways to repair DNA DSBs: homologous recombination (HR), non-homologous end-joining (NHEJ), and alternative end joining (Aparicio et al., 2014). HR pathways use homologous chromosomes as a template to repair DNA DSB. HR pathway initiates with the digestion of DNA to produce single-strand DNA (ssDNA) overhangs (**Figure 1.4**). This resection is tightly controlled during the cell cycle, such that it only occurs during S and G2 phases. On the other hand, NHEJ is a more error-prone alternative for DNA DSB repair, since it does not use a homologous template for repair (Lord & Ashworth, 2012). NHEJ is initiated by the Ku70/Ku80 heterodimer complex and recruitment of DNA-PKc which facilitates DNA ligation (Torgovnick & Schumacher, 2015). The dysfunction and/or deficiency of all repair pathways leads to

increased DNA instability and sensitization to IR (O'Connor, 2015). Increased damage burden ultimately leads to genomic instability, cell cycle arrest, and cell death (Erasimus et al., 2016).

1.2.2.3 Determination of time, dose and fractionation in radiotherapy

As RT generates DNA damage and cytotoxicity to tumor cells, surrounding healthy tissues and organs may also be affected. It is crucial to determine the dose, fractionation schedule, and targeted therapies to prevent local and systemic side effects caused by RT (Balentova & Adamkov, 2015). The considerations are dependent on tumor size, tumor location, vascularization and oxygenation status of the tumor. The total dose of radiation, dose per fraction, overall treatment time, time interval between fractions, and dose rates are also vital parameters to consider increasing the therapeutic effect of radiation therapy(H. H. W. Chen & Kuo, 2017; Mann et al., 2018). For this, the concept called "6Rs of Radiotherapy" is described to increase treatment efficacy.

The 6Rs of radiotherapy are as follows; repair of recovery of sublethal damage, redistribution, reoxygenation, repopulation, radiosensitivity, and remote bystander effect(Marcu et al., 2015). All these points emphasize providing enough time for healthy cells to recover, not allowing tumor cells to repair their damaged DNA, oxygenating tumors to increase the generation of ROS, minimizing the cytotoxic effect on high-proliferating healthy cells, implementing targeted therapies to make tumor cells more radiosensitive and minimize remote bystander effect (Boustani et al., 2019; Gérard et al., 2019; Mallick et al., 2020; Marín et al., 2015; Moeller et al., 2007; Pajonk et al., 2010) (**Figure 1.5**).

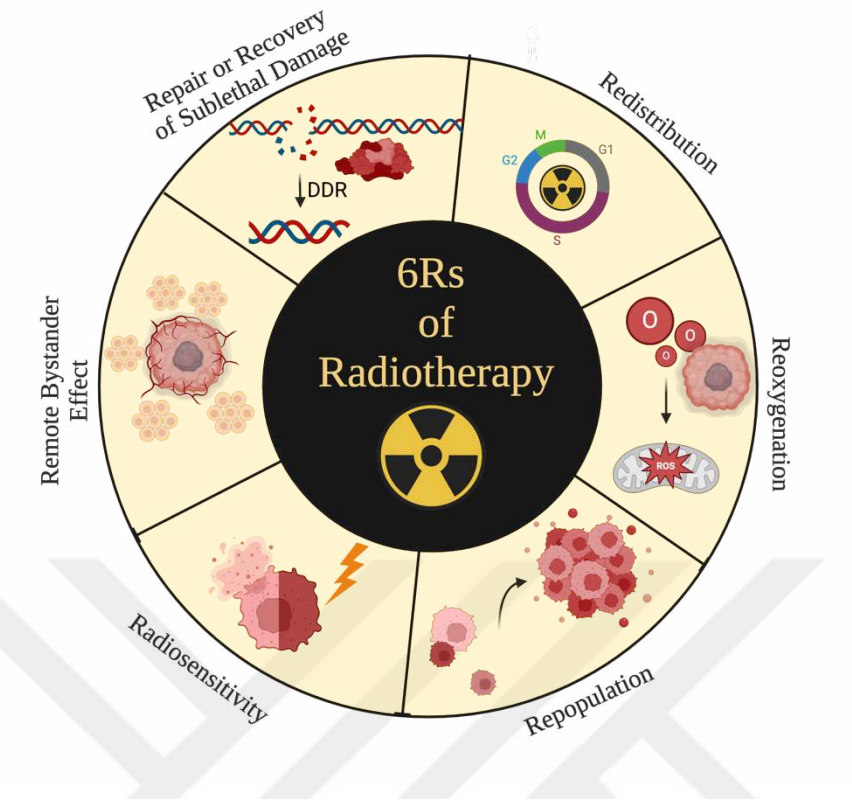

Figure 1.5 6R's of radiotherapy. Adapted from (Boustani et al., 2019). Created in Biorender.

1.2.3 Other treatment options

Various immunotherapy strategies are being investigated in clinical trials for glioblastoma, including immune checkpoint inhibitors like those targeting FASL, PD-1, EGFR vIII, and CTLA-4 (An et al., 2018; Huang et al., 2021). Poor immunogenicity of GBM and immunosuppressive conditions in the tumor microenvironment (TME) are considered as the main causes of resistance to immunotherapies (Di Nunno et al., 2023). Chimeric antigen receptor (CAR) T cell therapy (CAR-T), tailored to individual tumor antigen profiles, offers another avenue (Lin et al., 2022). CAR-T cell therapy provides selective elimination of tumor cells independent from major histocompatibility complex (MHC). With the success in *in* vitro and *in* vivo studies(Li et al., 2024; N. Zhu et al., 2024), CAR-T cell therapy targeting different tumor antigens are now investigated in clinical trials and few pre-clinical studies(Montoya et al., 2024). Dendritic cell therapy, a form of personalized medicine, aims to target multiple glioblastoma antigens using tumor lysates, RNA, peptides, and cancer stem cell products (Huang et al., 2021). One of the main obstacles in the development of effective GBM treatment is the BBB permeabilization of chemotherapeutic agents. For this, extensive research is conducted on targeted delivery systems such as BBB permeable agents, nanoparticles, and BBB manipulation. Another innovative form of therapy is tumor-treating fields (TTFields), which have an anti-proliferating effect on tumor cells by implementing low-intensity electrical fields (Ornelas et al., 2019; Stupp et al., 2017). This FDA-approved treatment causes inhibition of cell division, TTFields present promising results in clinical trials with minimum side effects and high tolerance by GBM patients (Michelhaugh et al., 2018).

1.3 Therapy resistance in GBM

Despite the advances in chemo-/radio-therapy and understanding the molecular landscape of the tumors, poor prognosis and tumor recurrence are highly common in GBM patients. Tumor recurrence is highly interconnected with therapy resistance, which may occur stochastically or may have been acquired during treatment, called intrinsic or acquired resistance. Cellular heterogeneity, TME, the effect of hypoxia, cancer-associated fibroblasts, glioma stem cells (GSCs) and chromatin dynamics are pivotal

factors in therapy resistance in glioblastoma (Auffinger et al., 2015; Bakir et al., 2020; Virga et al., 2019; Wu et al., 2023).

1.3.1 Resistance to chemotherapy

As TMZ is the golden standard option chemotherapeutic agent for GBM treatment, TMZ resistance is one of the earliest-characterized mechanisms in tumor recurrence and therapy resistance (Lu & Shervington, 2008). Cytotoxicity of TMZ arises from the generation of O6-MeG, which causes replication-associated DNA DSB (J. Zhang et al., 2011). This lesion is reversed by MGMT, where therapy response is highly associated with MGMT expression levels in GBM patients (Wickström et al., 2015). TMZ resistance is associated with high expression of MGMT. Promoter methylation status is a predictive biomarker for TMZ response and resistance (Andreoli et al., 2008) . Although MGMT is the most predictive biomarker, there are MGMT-independent mechanisms that cause chemoresistance. As TMZ does not cause DNA DSB directly, unrepaired damaged bases and futile DNA repair cycle cause collapse of replication fork. (Yi et al., 2019) Aberrations in various DNA damage response pathways such as BER and MMR also cause chemoresistance (Lu & Shervington, 2008). Increased expression levels of MMR proteins such as MSH6, MLH1, and PMS2 also confer chemoresistance (Perazzoli et al., 2015).

Poly (ADP-ribose) polymerase (PARP) is an important effector of apoptosis which is involved in the BER system. After recognition of SSB by PARP, PARP-SSB complexes may ultimately lead to genomic instability. PARP inhibition is also studied for TMZ resistance in GBM. Olaparib and rucaparib, well-studied PARP inhibitors, show chemosensitization when combined with TMZ in MGMT-deficient GBM populations, causing synthetic lethality (Annovazzi et al., 2017). It is also reported that important cellular pathways such as Notch, NFκB, Hedgehog, and Wnt/β-catenin pathways have various roles in chemoresistance (Wickström et al., 2015).

1.3.2 Resistance to radiotherapy

Around 60% percent of cancer patients receive RT in their treatment regimen. In some cases, where the tumor is inoperable and/or chemotherapy is not an option, RT remains the only treatment option. One of the main objectives of effective RT is to cause maximum cytotoxicity to tumor cells while limiting the bystander effect on healthy tissues and organs.

Despite the current advances in radiation oncology, RT resistance, or radioresistance remains a challenge (H. H. W. Chen & Kuo, 2017). Radioresistance can either be acquired or innate. DNA damage repair, cell cycle alterations, tumor microenvironment, GSCs, hypoxia, and oxidative stress are various factors that cumulatively cause radioresistance in GBM (Chaddad et al., 2019).

1.3.2.1 Repairing of DNA damage

As effect of RT to control cancer predominantly depends on how cells respond to the resulting DNA damage, the ability of the cells to repair the generated damage is an essential determinant of RT response. As RT causes DNA damage to create genomic instability, these generated lesions may lead the cells to cell death if not repaired. However, these lesions may also cause radioresistance by different adaptive mechanisms (Jeggo et al., 2016). Cells become adapted to survive with an increased burden of DNA damage by adopting various compensatory cellular processes. The inherent DNA damage response and repair efficiency of cancer cells differ even within a tumor, leading to cellular resistance and weakened therapeutic outcome (Han et al., 2017). The expression of genes and proteins involved in DNA DSB repair have an influence on the resulting repair process, hence the regulation of these elements can make cancer cells more resistant or more sensitive to RT (Yard et al., 2016).

Starting from the recognition of DNA damage by various proteins and activation of downstream effectors, targeting DDR proteins are commonly employed to enhance therapy response. DSB repair and recognition is one of the most extensively studied DDR events in the context of radiation response. Although the majority of the cytotoxicity originates from DSB, deficiencies in other DNA repair pathways can alter RT response (Goldstein & Kastan, 2015; Hakem, 2008). In addition, cancer cells exhibiting therapy

resistance usually compensate the deficient repair pathways with complementary pathways to preserve genomic integrity (Burgess & Misteli, 2015). Despite the fact that cancer cells usually upregulate the DNA damage repair pathways or prefer compensatory pathways, one of the survival mechanisms is to adapt and survive in spite of futile cycle of unrepaired DNA damages.

The earliest event in DSB generation is phosphorylation of H2AX, which could serve as an indicator for DNA DSB generation and repair efficiency of the cells. Prolonged clearance of γH2AX could serve as an indicator for deficiency in DDR machinery, or vice versa. Indeed, our previous work has shown in clinically relevant radioresistant models that, after exposure to 60 Gy of radiation *in vitro*, pathways related to DNA damage response and repair were upregulated in GBM cells (Pinarbasi-Degirmenci et al., 2022).

Targeting upstream of DDR or downstream pathway of choice, NHEJ or HR, are possible options for radiosensitization. For this, effector DDR kinases such as CHK1, CHK2, ATM, and ATR are potential targets for radiosensitization (Pilié et al., 2019; Squatrito et al., 2010). Currently, various inhibitors targeting not only these effector kinases, but also other DNA damage repair pathways elements such as DNA-PKc, Wee1, DNA LIG4 are potential targets for radiosensitization (Cheng et al., 2022). In addition, it is shown that a combination of Topoisomerase and PARP inhibition causes sensitization of cells to IR (Nickoloff et al., 2017).

1.3.2.2 Role of cell cycle

Cell cycle is a complex and intricate process, which ensures successful cell division with protecting genome integrity. This process involves a large number of regulatory proteins, such as cyclins, cyclin dependent kinases (CDKs), CDK inhibitors (CKIs) and also proteins involved in cell cycle checkpoints (Jamasbi et al., 2022a). Cell cycle checkpoints ensure succession of cell cycle events, and deficiencies in those pathways result in cell cycle arrest. Cell cycle arrest provides protection to cells before progression to the next phase of the cell cycle. Cell cycle arrest provides time and resource to solve the problem before progression. IR causes various damages which result in cell cycle arrest (Jamasbi et al., 2022b). In addition, sensitivity to IR differs for each phase of the cell cycle.

This is caused by the availability and activation of DNA damage repair pathways and vulnerability of the genome, since there is an ongoing cell division (J. Chen, 2016).

Radioresistant GBM cells have also altered cell cycle progression. Normally, IR-induced DNA damages cause cell cycle arrest allowing cells to repair the DNA damage before cell cycle progression and cell division (Shaltiel et al., 2015). Tumor cells and especially therapy-resistant cell populations usually have defective cell cycle checkpoints. For this reason, targeting proteins involved in cell cycle progression, cell cycle checkpoints, and cell cycle arrest may cause radiosensitization (Hauge et al., 2023). G1 checkpoint defect is commonly observed in most cancer cells because of the mutations in the key regulators of G1 checkpoints, such as p53. Therefore, G2/M checkpoint is crucial for cancer cell survival (Barnaba & LaRocque, 2021). Targeting G2/M modulators is one of the options to cause mitotic catastrophe and ultimately cell death. In the context of RT, G2/M arrest usually occurs after IR, and resolution is observed around 4h post-IR. The duration of G2/M arrest increases with increasing dose of IR(Dillon et al., 2014). After some point where cell cycle recovery becomes impossible, cell death occurs as a result of mitotic catastrophe. The expression levels and deficiency of some G2/M checkpoint regulators such as PLK1, ATM and CHK1 alter cell cycle progression after IR-induced DNA damage (Vlatkovic et al., 2022).

1.3.2.3 Role of oxidative stress

The indirect effect of IR is to cause radiolysis of water molecules in the cell and generate ROS. Generated ROS may alter mitochondrial permeability, which further stimulates ROS production (Baskar et al., 2014). Dysfunctions in the mitochondria may lead to adaptive responses of metabolic pathways involved in radioresistance development (R. Liu et al., 2022). Beside mitochondria, cell membrane is another cellular compartment affected from increased ROS levels in the cells. ROS accumulation causes high levels of lipid peroxidation, which triggers ferroptosis, ultimately triggering structural and functional damage to the cell (W. Kim et al., 2019). One of the adaptive mechanisms of tumor cells to escape from radiation-induced ferroptosis is rewiring glutathione metabolism by an upregulation of proteins such as GPX4 and Nrf2 and its

downstream protein, SLC7A11 (Lei et al., 2021a). Upregulation of these proteins lowers peroxidation levels in the cells, therefore preventing cells to enter ferroptosis.

For both apoptosis and ferroptosis, p53 status of the tumor cells are crucial. p53 is involved in both redox pathways and apoptotic pathways, which eventually regulates radiotherapy efficacy (B. Liu et al., 2014).

1.3.2.4 Role of hypoxia

Hypoxia is the state of low oxygen levels, which is an important driver for molecular adaptations of solid tumors, affecting therapy response, tumor recurrence, and patient survival (Horsman et al., 2012). GBM tumors generally have hypoxic tumor cores, where oxygen levels drop to nearly 0.7% in tumor core, as opposed to the normal oxygen levels of around 5% in the brain (Rakotomalala et al., 2021).

With low oxygen, the effect of radiotherapy gradually decreases, as direct and indirect effect of IR is gradually decreases in the absence of oxygen. Oxygen plays an essential role in the stabilization of radiation-induced DNA damage by providing unpaired electrons that generate covalent bonds with DNA (Dewhirst et al., 2008). In addition, oxygen availability alters immune cell infiltration and pH of microenvironment of tumor, which affects therapy response. Activation of DDR kinases ATM and ATR also occurs due to hypoxia-induced replication stress (Begg & Tavassoli, 2020). Low oxygen levels cause modifications on proteome and transcriptome, which leads to alterations in radiotherapy response. Therefore, increasing intratumoral oxygen levels is an alternative approach to increasing radiosensitivity in hypoxic tumors. Recently developed hypoxia-activated prodrugs (HAPs) could be effective alternatives for radiosensitization. In addition, combining radiotherapy with DNA damaging agents or DDR inhibitors are potential avenues in treatment of hypoxic tumors (Bouleftour et al., 2021).

1.3.2.5 Role of chromatin architecture

With the recent advances in sequencing and microscopy-based technologies, the 3D structure of the genome is being discovered. The 3D organization of the chromatin influences gene expression, gene regulation, cell differentiation, and cell proliferation (Canela et al., 2017). The 3D structure of spatial and genomic distribution of IR-induced

DNA damage caused by radiation helps better understand DNA repair processes.

It is recently shown that different hierarchical chromatin structures respond differently to IR, genes in open chromatin regions (OCRs) are more susceptible to IR-induced DNA damage. On the contrary, genes in tightly packed heterochromatin regions are more protected from IR-induced damage by nucleosomes (Sanders et al., 2020) . In addition, loop anchors and topologically associated domains (TADs) are more vulnerable to IR (Zheng et al., 2023). All these chromosomal organizations lead to transcriptional regulation and therefore affect the radiation response of tumor cells. Recently it is shown that upon UV-exposure, cells favor to increase accessibility of repair elements and alterations in the boundaries around TADs (Kaya & Adebali, 2024).

1.4 Epigenetics

The chromatin organization is crucial for nucleosome positioning, chromatin accessibility, and transcriptional regulation (Kouzarides, 2007). Changes in the chromatin structure are regulated by epigenetic processes. Epigenetics was first described by Conrad Waddington, where gene regulation and expression occur without altering the DNA sequence itself (Inbar-Feigenberg et al., 2013). Epigenetic modifications are reversible. Tightly packed nucleosome regions are called heterochromatin regions, associated with repressed gene expression. Whereas nucleosomes found in more relaxed conformation are called euchromatin regions and are associated with active transcription (Crusio et al., 2021). Different types of epigenetic marks orchestrate the regulation of gene expression such as DNA methylation at CpG dinucleotides, covalent modifications of histone proteins, ncRNAs, and other complementary mechanisms, facilitating transcriptional activation or repression (Etcheverry et al., 2010; Kouzarides, 2007) .

Histones are regulated with modifications on DNA or lysine, serine, or arginine amino acids on histone tails. These modifications are described as "histone code" and dictate transcriptional regulation (Bannister & Kouzarides, 2011). Acetylation, methylation, butyrylation, and ubiquitinylation are modifications that occur on histone tails (Millán-Zambrano et al., 2022) .

The proteins that carry out post-translational modification on histone tails can be classified into three categories: writers, readers, and erasers. "Writers" are the group of enzymes that facilitate the addition of histone marks. DNA methyltransferases (DNMTs), histone methyltransferases, kinases, SUMO ligases, ubiquitin ligases, and histone acetyltransferases (HATs) are writer enzymes (Nicholson et al., 2015). "Reader" proteins are involved in the recognition of histone marks and provide interaction with transcriptional machinery. Bromodomains, chromodomains, and Tudor domains are proteins that are classified as writer proteins (Yun et al., 2011). Lastly, the removal of histone marks is facilitated by the group of enzymes called "erasers", such as histone demethylases, histone deacetylases (HDACs), lysine demethylases (KDMs), phosphatases, SUMO proteases, and deubiquitinases (**Figure 1.6**).

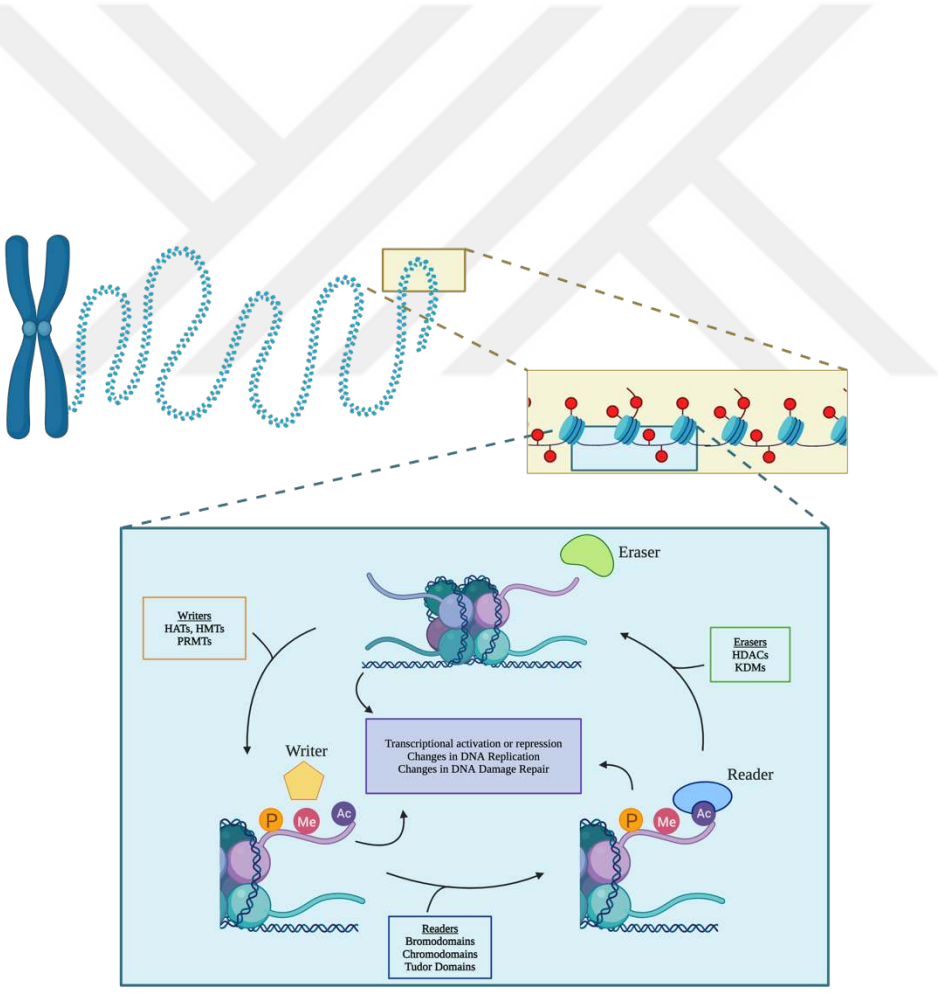

Figure 1.6 Epigenetic modifications. Adapted from (Feinberg et al., 2016). Created in Biorender.

1.4.1 Role of epigenetic modifications in GBM progression and therapy response

Cancer progression is not only driven by genomic alterations, but also by epigenetic modifications, transcriptional activation of oncogenes, and transcriptional repression of tumor suppressor genes. One of the most influential factors in tumor progression and therapy response is the "epigenetic landscape" of cancers (Jones et al., 2016). Among other cancer types, GBMs also have altered epigenome that affects therapy response. There are different subgroups defining the genomic and epigenomic characteristics of GBMs (Gusyatiner & Hegi, 2018). One of the well-studied predictive biomarkers that is implemented into clinical applications is MGMT promoter methylation. Hypermethylation of MGMT promoter leads to TMZ sensitization (Hegi et al., 2005).

There are various epigenetic alterations and therapeutic targets defined in GBM. It is shown that Enhancer of zest homolog 2 (EZH2), an enzymatic component of Polycomb Repressive Complex (PRC2) and a lysine demethylase, is upregulated in some GBM patients. (Sak et al., 2017). Furthermore, for a subgroup of pediatric gliomas, the H3K27M mutation is identified (Uddin et al., 2022). This mutation causes a decrease in methylation of histone H3 and leads to transcriptional activation, also inhibition of PRC2 complex generation of CpG hypomethylated phenotype, and aberrant activation of gene expression. PRC2 complex is regulated by KDM6A and KDM6B lysine demethylases. Lysine demethylases are commonly targeted chromatin modifying enzymes, which are extensively studied in therapy response both in preclinical and clinical trials (Kayabolen et al., 2020; Kurt et al., 2017; Saraç et al., 2020). Recently, members of arginine methyltransferase (PRMT) family members, PRMT1, PRMT5, and PRMT2 are shown to be overexpressed in glioblastoma cells and they could be potential predictive biomarkers for GBM prognosis (Jarrold & Davies, 2019; Sachamitr et al., 2021).

Isocitrate dehydrogenase 1/2 (IDH) mutations are found in newly classified IDH-mutant astrocytomas. This mutation causes the generation of an oncometabolite, D-2-hydroxyglutarate (D2HG), which disrupts cellular metabolism and epigenetic regulation by inhibition of TET methylcytosine dioxygenase 2 (TET2), KDM4 and JHDM1 (Kayabolen et al., 2021).

HDACs also have high expression status which changes the transcriptomic profile of cancer cells resulting in the evasion of cell death. For this reason, HDAC inhibitors are potential targets for sensitization of cells to therapies. Vorinostat, Belinostat, Romidepsin, and Panobinostat are FDA-approved HDAC inhibitors, for which clinical trials as monotherapies and combination treatments are still ongoing (McClure et al., 2018; Ramaiah et al., 2021).

1.5 Radiation-induced epigenetic alterations

Even though more than half of cancer patients receive RT, the relation of RT and epigenetic elements is currently not well defined or utilized for improvement of therapy response. Currently, there are no epigenetic biomarkers identified for IR response for GBM (Merrifield & Kovalchuk, 2013). After exposure to IR, epigenetic alterations take place, and certain chromatin modifications lead to cancer progression and poor therapy response. The IR-induced changes in chromatin accessibility influence radiotherapy response, as it affects the access of DNA repair machinery to DNA lesions. Therefore, histone modifications have an important effect on IR-induced DNA damage response (Smits et al., 2014). Epigenetic events that modify DDR and repair machinery are likely targets for the radiosensitization of cells (Peng et al., 2021).

The most known radiation-induced histone modification is the phosphorylation of H2AX by ATM. γH2AX is crucial for the initiation of DDR and repair of DNA DSB, which also is an indicator of the DNA repair capacity of the cells (Christmann & Kaina, 2017; Karakaidos et al., 2020). The trimethylation of histone H3 on lysine 27 (H3K27me3) is associated with chromosome condensation, and the inhibitor of H3K27me3 GSKJ4 is studied for radiosensitization (Katagi et al., 2019). HDACs, which serve as transcriptional repressors, are also important in radiation response. HDAC inhibitors cause a delay in the recondensation of chromatins after repair, therefore cells become more susceptible to IR-induced DNA damage. There are various trials to combine Epi-drugs and radiotherapy as an effective treatment strategy (J. G. Kim et al., 2014). HDAC inhibitors Panobinostat, Vorinostat, and Belinostat have been combined with radiotherapy in clinical trials, but this caused high cytotoxicity (Ling et al., 2023) .

1.6 Bromodomain containing protein 9 (BRD9)

The switch/sucrose non-fermentable (SWI/SNF) complex, which is an ATP-dependent chromatin remodeling complex, remodels nucleosomes and is involved in various biological processes, such as proliferation, splicing, gene regulation, and cellular differentiation (Hohmann & Vakoc, 2014). These complexes, also known as BRG1/BRM-associated factor (BAF) complexes, are key regulators of nucleosome positioning. Mammalian SWI/SNF complexes can be classified into three subfamilies: canonical BAF (cBAF), polybromo-associated BAF (PBAF), and non-canonical BAF (ncBAF) complexes (Hodges et al., 2016; Inoue et al., 2019).

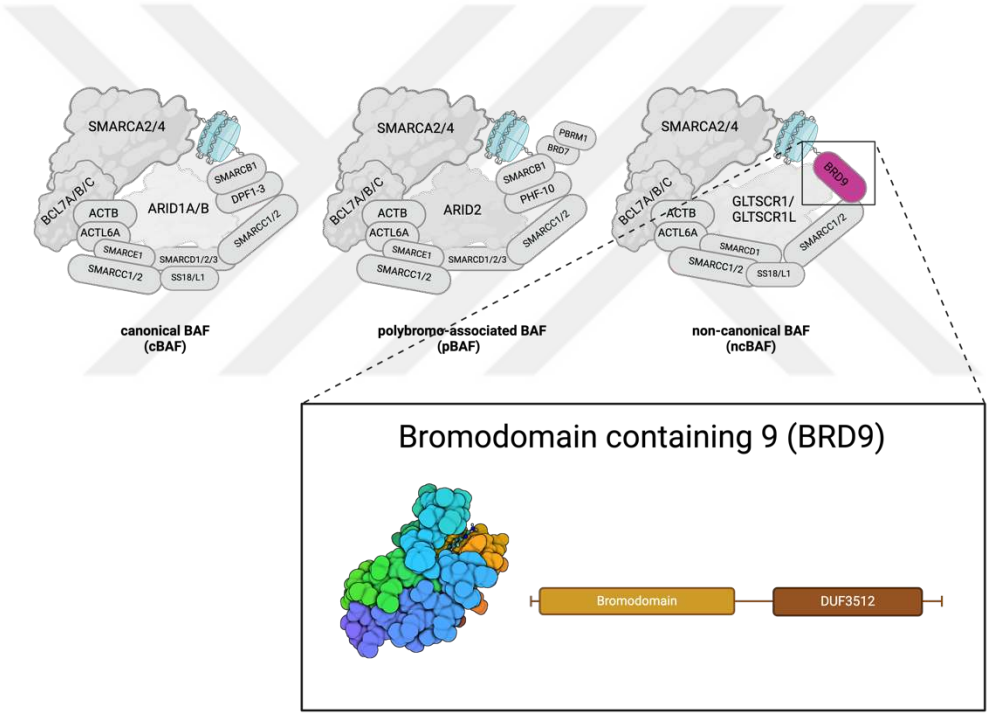

Figure 1.7 SWI/SNF complexes and structure of BRD9. Adapted from (Hohmann & Vakoc, 2014; X. Zhu et al., 2020). Created in Biorender.

SWI/SNF complexes usually consist of 12–15 subunits and are the most frequently mutated chromatin regulators in cancer, with at least nine subunits recurrently mutated and in 20% or more of all cancers collectively (Kadoch et al., 2013).

Bromodomain containing 9 (BRD9) is an exclusive subunit of the ncBAF complex. BRD9 harbors a single bromodomain, that recognizes acetylated lysine on histones and non-histone proteins, and a DUF3512 domain, which facilitates the interaction with SWI/SNF complex. BRD9 binds to acetylated and butyrylated histones, mainly H3K27ac, H4K5ac, and H4K8ac (Karim & Schönbrunn, 2016; X. Zhu et al., 2020) (**Figure 1.7**).

Recently, it has been shown that BRD9 is involved in human somatic cell reprogramming, inhibiting epigenetic barriers in cell reprogramming (Gatchalian et al., 2018; Sevinç et al., 2022). In addition, BRD9 has been shown to regulate DNA repair by orchestrating the complex formation of Rad51 and Rad54, two major proteins involved in double-strand break repair, suggesting non-epigenetic mechanisms regulated by BRD9 as well (Zhou et al., 2020).

1.6.1 Implications of BRD9 in cancer and treatment options

The tumor biological functions of BRD9 are mainly due to epigenetic modification mediated by its bromodomain. BRD9 protein is found to be differentially expressed among different cancer types. Indeed, BRD9 is overexpressed in cervical cancer and BRD9 is a specific vulnerability to rhabdoid tumors through SMARCB1 (Krämer et al., 2017). It is shown that BRD9 is enriched downstream of the *MYC* promoter, which drives its transcription (Bell et al., 2019). Studies have confirmed that BRD9 plays an oncogenic role in multiple cancer types, by regulating tumor cell growth (Hohmann et al., 2016; Weisberg et al., 2022). BRD9 overexpression induces the activation of signal transducer and activator of transcription 5 (STAT5) in Acute myeloid leukemia (AML) cells, promoting cell proliferation and tumorigenesis (Del Gaudio et al., 2019). Whole exome sequencing revealed that BRD9 is one of the susceptibility genes for melanoma, involved in pathways such as cell proliferation, DNA replication, and DNA repair (Hipólito et al., 2024) . In addition, studies have demonstrated that BRD9 acts as a co-factor to stabilize

the structure of the SS18-SSX fusion and to maintain its oncogenic transcription in synovial sarcoma (SS) (Brien et al., 2018).

Accumulating knowledge suggests that rewiring the epigenome of tumor cells through bromodomain targeting might serve as a promising anticancer approach (Du et al., 2023; Wang et al., 2019) . Compared to other bromodomain proteins, BRD9's role in cancer is less well-defined (Cochran et al., 2019). Besides small molecule inhibitors, proteolysis-based degrader systems for BRD9 have revealed efficacy on cancer cells (Clark et al., 2015; Martin et al., 2016; Remillard et al., 2017; Theodoulou et al., 2016). Indeed, the BRD9 degrader compound is being tested in Phase 1 clinical trials for Synovial Sarcoma (NCT04965753). Despite all the current knowledge, the mechanism of action of BRD9 and its role in cancer progression and therapy response is yet to be elucidated.

1.7 Aim of the thesis

The overarching goal of this thesis is to elucidate epigenetic mechanisms regulating radiotherapy response and the role of BRD9 in radiation response to establish new radiosensitization therapies for glioblastoma.

MATERIALS AND METHODS

2.1 Cell culture

Human Glioblastoma cell lines U373, U87-MG, Human Embryonic Kidney cells (HEK293T), and Prostatic adenocarcinoma cell lines (PC-3) were received from the American Tissue Type Culture Collection (USA). Human breast cancer cell line MDA-MB-231 cells were a kind gift from Robert Weinberg (MIT, Boston, USA). Immortal normal human astrocytes (I-NHA) was a kind gift from Tim Chan from Memorial Sloan Kettering Cancer Center (MSKCC). U373$^{60\ Gy}$ irradiation survivor cell population was generated in our laboratory (Pinarbasi-Degirmenci et al., 2022). All parental and irradiated cell populations cells were cultured in DMEM (Gibco, Gaithersburg, MD, USA) supplemented with 10% FBS (Gibco, Gaithersburg, MD, USA) and 1% Penicillin-Streptomycin (Gibco, Gaithersburg, MD, USA). All cells were maintained at 37 °C in a humidified incubator with 5% CO_2. GBM4 and MGG119 cell lines were established by Dr. Hiroaki Wakimoto from patient-derived models, at Massachusetts General Hospital (MGH) (Wakimoto et al., 2014). GBM4 and MGG119 were cultured as neurospheres in GBM/EF medium consisting of Neurobasal medium (Gibco, USA) with 7.5 ml L-Glutamine, 1X B-27 supplement (Gibco, USA), 0.5X N-2 supplement (Gibco, USA), 0.5 ml heparin solution (0.2%, Stemcell Technologies, Canada), 0.5% Pen/Strep, FGF (20 ng/ml) and EGF (20 ng/ml).

2.2 Chemicals and reagents

The drug libraries consisting of 125 compounds were provided by Dr. Udo Oppermann (University of Oxford, UK), the composition of the library is listed in **Table 2.1**. I-BRD9 is purchased from Selleckchem (Catalog #S7835). BRD7/BRD9 PROTAC degrader (VX185), BRD7/BRD9 inhibitor (BI-7273) and BRD9 inhibitor (BI-9654) were from the opnMe platform (https://opnme.com/), granted by Boehringer Ingelheim.

MSCV-Cterm_3xFL_BRD9-PGK-Puro-IRES-GFP was a gift from Christopher Vakoc (Addgene plasmid # 75122; http://n2t.net/addgene:75122; RRID:Addgene_75122).

2.3 Irradiation experiments *in vitro* and *in vivo*

All irradiation experiments were performed in XStrahl CIX2 Cabinet X-Ray Irradiator located at KUTTAM Animal Research Facility (KUARF). For *in vitro* experiments, cell-seeded plates were placed in the irradiator cabin and exposed to radiation at 195 kV - 10 mA according to the desired exposure. For *in vivo* whole-body irradiation optimization experiments, 4-6 weeks old C56BL/6 mice were either exposed to 1 Gy or 2 Gy daily dose of radiation for 10 days (in total 10 Gy or 20 Gy). On days 5,10 and 15, mice were weighed, and blood samples were collected and analyzed. After completing 10 Gy, for metabolic activity measurement, mice were placed into metabolic cages for 5 days and metabolic activity was analyzed. All experiments were performed in KUARF with appropriate conditions and all protocols were approved by the Koç University Ethics Committee.

2.4 Epigenetic drug screen

The epigenetic chemical probe library was constructed by the Structural Genomics Consortium (SGC) by Dr. Udo Oppermann (Oxford University) and kindly provided for epigenetic drug screening. Accordingly, U373 and U87 cells were seeded as 1000 cells/well into round bottom 96-well plates. The next day, cells were treated with a drug library with 1/10th of the working concentration (0.1X). On day 3, cells were exposed to a single dose of IR (4 Gy). After 24 hours, cells were trypsinized and 90% of collected cells were seeded into 6 well-plates for further clonogenic assays and remaining 10% of collected cells were seeded into a new black 96-well plate for Cell-Titer Glo (CTG) assay to assess cell viability. On day 7, CTG assay and on day 10 crystal violet staining for clonogenic assay was performed. The list and targets of drugs are shown in **Table 2.1.**

Table 2.1. Composition of epigenetic drug library

Compounds	**Class/Target**	**Working Con. (1X) (µM)**
AMI-1	Arginine methyltransferase - PRMT	50
SGC707	Arginine methyltransferase - PRMT3	1
TP-064	Arginine methyltransferase - PRMT4	1
TP-064N	Arginine methyltransferase - PRMT4	1
MS049	Arginine methyltransferase - PRMT4, PRMT6	1
MS409N	Arginine methyltransferase - PRMT4, PRMT6	1
GSK591	Arginine methyltransferase - PRMT5	1
LLY-283	Arginine methyltransferase - PRMT5	1
MS023	Arginine methyltransferase - Type I PRMTs	1
GSK8814	Bromodomains - ATAD2	10
GSK8815	Bromodomains - ATAD2	10
GSK2801	Bromodomains - BAZ2A, BAZ2B	1
BAZ2-ICR	Bromodomains - BAZ2A, BAZ2B	1
BAY-299	Bromodomains - BRD1, TAF1	1
RVX-208	Bromodomains - BRD2, BRD3, BRD4, BRDT (BET, BD2)	5
(+)-JQ1	Bromodomains - BRD2, BRD3, BRD4, BRDT (BET)	1
PFI-1	Bromodomains - BRD2, BRD3, BRD4, BRDT (BET)	5
I-BET	Bromodomains - BRD2/3/4	1
I-BRD9	Bromodomains - BRD9	10
TP-472	Bromodomains - BRD9	1
TP-472N	Bromodomains - BRD9	1
LP99	Bromodomains - BRD9, BRD7	1
BI-9564	Bromodomains - BRD9, BRD7	1
GSK6853	Bromodomains - BRPF1/2/3	1
GSK9311	Bromodomains - BRPF1/2/3	1
PFI-4	Bromodomains - BRPF1B	1
CBP/BRD4 (0383)	Bromodomains - CBP, BRD4(1)	5
NVS-CECR2-1	Bromodomains - CECR2	1

NVS-CECR2-C	Bromodomains - CECR2	1
I-CBP112	Bromodomains - CREBBP, EP300	1
SGC-CBP30	Bromodomains - CREBBP, EP300	1
(-)-JQ1 (inactive)	Bromodomains - Negative control	1
Bromosporine	Bromodomains - pan-Bromodomain	1
OF-1	Bromodomains - pan-BRPF	5
NI-57	Bromodomains - pan-BRPF	1
GSK4027	Bromodomains - PCAF, GCN5	1
GSK4028	Bromodomains - PCAF, GCN5	1
L-Moses	Bromodomains - PCAF, GCN5	1
D-Moses	Bromodomains - PCAF, GCN5	1
SMARCA	Bromodomains - SMARCA, PB1	2,5
PB1/SMARCA	Bromodomains - SMARCA, PB1	1
PFI-3	Bromodomains - SMARCA2/4, PB1(5)	1
TRIM24/BRPF	Bromodomains - TRIM24/BRPF	10
GSK864	Dehydrogenase	5
5-Azacitidine	DNA methyltransferase (DNMT) -	10
5-Azadeoxycitidine	DNA methyltransferase (DNMT) - DNMT1/3	5
CXD101	HDAC -	1
PCI-24781	HDAC -	10
Romidepsin	HDAC -	1
Mocetinostat	HDAC -	10
CI-994	HDAC - 1,2,3,(8)	1
Valproic acid	HDAC - aliphatic acid compounds	1000
RGFP966	HDAC - HDAC3	10
Rocilinostat	HDAC - HDAC6	10
Tubastatin A HCl	HDAC - HDAC6	10
PCI-34051	HDAC - HDAC8	5
Belinostat	HDAC - hydroxamic acids	5
SAHA	HDAC - hydroxamic acids	2,5
Trichostatin A	HDAC - hydroxamic acids - Class I & II	0,5
Entinostat	HDAC - ortho-amino anilides	0,5
EX 527	HDAC - SIRT1	1
SRT1720	HDAC - SIRT1 (indirect?) activator	1

AGK2	HDAC - SIRT2	10
TMP269	HDAC -4, 5, 7 &9	10
TMP195	HDAC -4,5,7,9	1
Santacruzamate	HDAC 2	50
C646	Histone acetyltransferase (HAT) p300/CBP	1
A-485	Histone acetyltransferase (HAT) p300/CBP	1
A-486	Histone acetyltransferase (HAT) p300/CBP	1
Methylstat (Ester)	Histone demethylase	2,5
KDOBA67	Histone demethylase	10
KDM5-C70	Histone demethylase - JARID1	10
ML324	Histone demethylase - JMJD2E	5
(E)-JIB-04	Histone demethylase - Pan JmjC	0,05
SGC0946	Histone methyltransferase - DOT1L	7,5
GSK343	Histone methyltransferase - EZH2	3
UNC1999	Histone methyltransferase - EZH2	1
UNC2400	Histone methyltransferase - EZH2	1
CPI-360	Histone methyltransferase - EZH2 and EZH1	10
CPI-169	Histone methyltransferase - EZH2, EZH1	10
UNC0642	Histone methyltransferase - G9a, GLP	1
UNC0638	Histone methyltransferase - G9a, GLP	1
A-366	Histone methyltransferase - G9a, GLP	2
PFI-2	Histone methyltransferase - SETD7	2
LLY-507	Histone methyltransferase - SMYD2	1
BAY-598	Histone methyltransferase - SMYD2	1
PFI-5	Histone methyltransferase - SMYD2	1
Chaetocin	Histone methyltransferase - SUV39H1	0,05
A-196	Histone methyltransferase - SUV420H1/H2	1
K00135	Kinase inhibitor - ATP competitive - PIM	1
5-Iodotubercidin	Kinase inhibitor - ATP mimetic - Haspin	1
SGI-1776	Kinase inhibitor - Haspin	10
CHR-6494	Kinase inhibitor - Haspin	1
KDOAM-25a	Lysine demethylases - JARID	1
KDOAM32	Lysine demethylases - JARID	1
GSK J4	Lysine demethylases - JMJD3, UTX, JARID1B	10
KDOPZ-32a	Lysine demethylases - KDM5	1

Tranylcypromine	Lysine demethylases - LSD1	20
GSK-LSD1 (irreversible)	Lysine demethylases - LSD1	0,5
GSK2879552	Lysine demethylases - LSD1	10
GSK J5 (inactive)	Lysine demethylases - Negative control	10
IOX1 (5-carboxy-8HQ)	Lysine demethylases - pan-2-OG	40
KDOOA012000	Lysine demethylases KDM2	1
A-395	Methyl Lysine Binder - EED	1
A-395N	Methyl Lysine Binder - EED	1
UNC1215	Methyl Lysine Binder - L3MBTL3	5
OICR-9429	Methyl Lysine Binder? - WDR5	1
TDO20824a	Methyl Lysine Binder/tudor domain -Spin1	1
TDO20826a	Methyl Lysine Binder/tudor domain -Spin1	1
GSK484	Peptidyl arginine deiminase (PAD4)	1
GSK106	Peptidyl arginine deiminase (PAD4)	1
Olaparib	Poly ADP ribose polymerase (PARP)	1
Rucaparib	Poly ADP ribose polymerase (PARP)	10
IOX2	Prolyl-Hydroxylases - PHD2 (EGLN1)	10
MAZ1805	tRNA Synthetase	1
MAZ1392	tRNA Synthetase	1
Bortezomib	Proteasome	0,1
Carfilzomib	Proteasome	0,1
Temozolomide		
Doxorubicin	Topoisomerase 2	1
Taxol	Tubulin	0,01
Vincristine	Tubulin	0,01
Staurosporine	Protein Kinases	0,01
Cyclophosphamide	DNA Crosslinks	10
MS-275	HDAC	2,5

2.5 Clonogenic assay

All cells were seeded as 200-250 cells/well to 12-well plates as triplicates and treated with corresponding inhibitors for 3 days. After treatment, cells were exposed to single doses of ionizing radiation of 2-4-6-8 Gy for each plate and incubated for 10-14 days. For Cas9-expressing gRNA-transduced cells, cells were seeded at day 6 post-transduction. These cells were irradiated the next day and incubated for 10-14 days. For the staining of the clonogenic assay, first, the culture media was aspirated, and wells were gently washed with 1x PBS twice, and colonies were fixed with ice-cold methanol for 5 minutes. After fixation, wells were washed with 1x PBS twice and stained with crystal violet for 15 minutes. Following the staining, crystal violet was removed from the wells, and plates were washed. After the plates were dried, colonies were scanned and colony densities for each well were quantified with Adobe Photoshop CC 2019 (USA).

2.6 Cell viability assays

2.6.1 MTT assay

For adherent cells, an MTT assay was used to assess cell viability. Cells were seeded as 750 cells/well, treated with the corresponding drug on day 1, and/or exposed to IR treatment on day 3. On day 5, MTT solution dissolved in sterile PBS (3 mg/ml) was added as 1:4 of the initial medium per well and incubated for 4 hours at 37°C. After incubation, the culture medium was aspirated, and 100 µl DMSO was added. Plate shaker was used to dissolve the crystals and absorbance reading was performed in Synergy H1 Reader (Biotek, USA) at 570 nm wavelength.

2.6.2 Cell-Titer Glo (CTG) assay

For suspension cells, cell viability was assessed with Cell Titer-Glo® (CTG) Luminescent Cell Viability Assay. Firstly, cells were seeded as 500 cells/ well to 96-well black culture plated and next day treated with the selected inhibitor. After 3 days, all plates were irradiated. On day 7, CTG reagent was directly added to cells at 1:10 of the culture medium. After 2 minutes of shaking and 8 minutes of incubation, luminescence levels of each well were measured using a plate reader (BioTek's Synergy H1, Winooski, VT, USA).

For each method, survival was described as a percentage of viable cells in each sample compared with DMSO control groups.

2.7 Immunofluorescent staining

Cells were seeded on 24-well plates on coverslips as 10.000 cells/well. After the BRD9 inhibitor and irradiation treatment, the media was removed, and cells were gently washed with PBS twice. Cells were fixed with ice-cold 4% PFA for 5 minutes at room temperature. After PBS wash, fixed cells were treated with 0.1% Triton X-100 for 5 minutes for permeabilization and washed with PBS. The blocking step was performed with 250 µL SuperBlock IHC Blocking Solution (ScyTek Laboratories, Logan, UT, USA) at room temperature for 15 minutes. After washing wells with PBS, coverslips were incubated with primary antibodies diluted in a blocking solution overnight at 4 °C. Coverslips were washed with PBS and incubated with respective secondary antibodies diluted in a blocking solution at room temperature for 1 hour in the dark. Finally, coverslips were mounted with Mounting Medium with DAPI (Abcam, USA). Images are taken at Zeiss Axio Imager M1 at 40x magnification. Foci numbers were counted for each condition and normalized to untreated control groups. All primary and secondary antibodies used in immunofluorescence staining are listed in **Table 2.2**.

Table 2.2. List of primary and secondary antibodies used in immunofluorescence staining

Antibody Target	Brand/Catalog Number	Dilution
Phospho-Histone H2A.X (Ser139)	Millipore/05-636	1:1000
53BP1	Novus/NB100-304	1:1000
BRD9	Invitrogen/PA5-110872	1:1000
Alexa Fluor® 488 Anti-IgG Secondary Antibody	Invitrogen	1:1000
Alexa Fluor® 594 Anti-IgG Secondary Antibody	Invitrogen	1:1000

2.8 Western blotting

Cell pellets were lysed in an appropriate volume of lysis buffer (1% NP40, 150 mM NaCl, 1 mM EDTA, 50 mM Tris-HCl (pH 7.8), 1 mM NaF) containing 0.1 mM PMSF, and 1X protease inhibitor cocktail (complete Protease Inhibitor Cocktail Tablets, Roche). Following 30 minutes of incubation in the lysis buffer, the lysates were sonicated and centrifuged (12,000 rpm, 4 ◦C, 15 min). Samples were denatured in 4 × SDS Laemmli sample buffer at 95 °C for 5 minutes. To ensure equal protein loading, Pierce™ BCA (Bicinchoninic Acid) Protein Assay (Thermo Fisher, Waltham, MA, USA) was used, and calculations of protein concentration were performed accordingly. For immunoblotting, equal amounts of protein were loaded and separated by SDS-polyacrylamide gel electrophoresis and transferred onto a PVDF membrane by Trans-Blot® TurboTM RTA Mini PVDF Transfer Kit (Biorad, Philadelphia, PA, USA). Next, the membranes were blocked with 5% non-fat dry milk in TBS-T (20 mM Tris-HCl, pH 7.8, 150 mM NaCl, 0.1%, v/v Tween-20) at room temperature for 1 hour. After blocking, the membrane was incubated with primary antibodies diluted in corresponding diluent overnight at 4 °C. Next day, the membranes were washed three times with 1x TBS-T for 15 minutes. Membranes were incubated with appropriate horseradish peroxidase coupled secondary antibodies (Cell Signaling, 1:10,000) for 1 hour, and the membrane was washed three times with 1x TBS-T. Blots were incubated with ClarityTM Western ECL Substrate (Biorad, Philadelphia, PA, USA) and visualized using an Odyssey Scanner (LiCor Biosciences, Lincoln, NE, USA). Used antibodies are listed in **Table 2.3.**

Table 2.3 Primary antibodies used in Western Blot

Antibody	Brand/Catalog Number	Dilution
BRD9	Invitrogen/PA5-110872	1:1000
GAPDH	Cell Signaling/97166S	1:2000

2.9 Quantitative Real-Time PCR (qRT-PCR)

To determine mRNA expressions for respective genes, corresponding cell pellets were collected, and RNA isolation was performed with NucleoSpin® RNA Isolation Kit according to the manufacturer's protocols (Macherey-Nagel). RNA concentrations were measured with Nanodrop. 900 ng of each cDNA was obtained by using M-MLV Reverse Transcriptase (Invitrogen) with reverse transcriptase reaction. mRNA expression levels of desired genes were detected by LightCycler® 480 SYBR Green I Master (Roche). Used primer sequences are listed in **Table 2.4**.

Table 2.4 qRT-PCR Primer Sequences

Gene	Sequence of Forward Primer (5'-3')	Sequence of Reverse Primer (5'-3')
BRD9	ATGTTCCATGAAGCCTCCAG	AGCTCCTTCTTCACCTTCCC
p53	GGTGACACGCTTCCCTGGATT	AGGGGGACAGAACGTTGTTTTCAG
p21	GGCAGACCAGCATGACAGATTT	AAGATGTAGAGCGGGCCTTTGA
MYC	TACAACACCCGAGCAAGGAC	GAGGCTGCTGGTTTTCCACT
PLK1	GCCGTACTTGTCCGAATAGTCC	GCCGTACTTGTCCGAATAGTCC
AURKA	GCAACCAGTGTACCTCATCCTG	AAGTCTTCCAAAGCCACTGCC
TOP2A	GTGGCAAGGATTCTGCTAGTCC	ACCATTCAGGCTCAACACGCTG
CDKN2A	AGTCTGCAGTTAAGGGGGCA	ATCATCATGACCTGGTCTTCTAGG
CDK1	GGAAACCAGGAAGCCTAGCATC	GGATGATTCAGTGCCATTTTGCC
H2AX	ACTCAACTCGGCAATCCAAG	GGGTT AGCTGCAGAATTCCA
CCNB1	ATGACATGGTGCACTTTCCTCC	GCCAGGTGCTGCATAACTGG
CCNB2	AGAGCAAGGCATCAGAAA	CAACCCACCAAAACAACA
RAD51	CTTTGGCCCACAACCCATTTC	ATGGCCTTTCCTTCACCTCCAC
GAPDH	AGCCACATCGCTCAGACAC	GCCCAATACGACCAAATC

2.10 RNA-sequencing and analysis

Total RNAs of cells were isolated using the Macherey-Nagel NucleoSpin® RNA Isolation Kit. After ensuring the isolation of high-quality RNA, samples were shipped for sequencing. For U373 BRD9 NT1-KO and U87 BRD9 NT1- KO samples, libraries were prepared and sequenced using 24 million single-end reads per sample at Oxford University NDORMS by Adam Cribbs. For U373 I-BRD9 and ionizing radiation-treated samples, libraries were prepared and sequenced based on protocols of the BGISEQ-500 platform. FASTQ files were uploaded into Genialis Expressions Platform (Texas, USA) and analyzed with RNA-seq SALMON pipeline. According to differential expression data, volcano plots were generated, with log2(FC)=1 and 0.05% FDR cut-offs.

Also, heat map representations were used for selected gene sets to visualize differential expressions. Pathway analysis was performed with the Enrichr gene list enrichment analysis tool directly linked to the Genialis website and with Gene Set Enrichment Analysis (GSEA) by MSigDB.

2.12 Guide RNA (gRNA) cloning

Guide RNAs were designed to target the BRD9 gene by using designed using Chopchop gRNA design tool (Labun et al., 2019). All oligonucleotides corresponding to gRNAs were synthesized at Macrogen Europe Laboratories as top and bottom strands. Oligonucleotides were annealed using T4 Polynucleotide Kinase (NEB). The backbone plentiGuide-Puro (Addgene) vector was digested using BsmI (NEB) followed by agarose gel electrophoresis and digested plasmid was isolated from the gel using Gel and PCR clean-up kit (MN). Annealed insert and digested backbone were ligated using T4 DNA Ligase (NEB). Next, the ligated product was transformed into chemically competent bacteria for plasmid amplification. Following plasmid isolation, samples were sequenced. gRNA sequences were listed in **Table 2.5.**

Table 2.5 Used gRNA Sequences

Name	Sequence
BRD9-g1-F	CACCGCTTGACGGACAGTACCGCAG
BRD9-g1-R	AAACCTGCGGTACTGTCCGTCAAGC
BRD9-g2-F	CACCGCTTCGCCAACTTGTAGTACA
BRD9-g2-R	AAACTGTACTACAAGTTGGCGAAGC
BRD9-g3-F	CACCGAGGATCAACCGGTTCCTCCC
BRD9-g3-R	AAACGGGAGGAACCGGTTGATCCTC
BRD9-g4-F	CACCGACTCCAGTTACTATGATGAC
BRD9-g4-R	AAACGTCATCATAGTAACTGGAGTC
BRD9-g5-F	CACCGCTTCGCCAACTTGTAGTACA
BRD9-g5-R	AAACTGTACTACAAGTTGGCGAAGC
BRD9-g6-F	CACCGCTTGACGGACAGTACCGCAG
BRD9-g6-R	AAACCTGCGGTACTGTCCGTCAAGC

2.13 Lentiviral packaging

Lentiviral packaging was used for Cas9, GFP, and gRNAs. $2.5x10^6$ 293T cells were seeded per 10cm petri dish. The next day, a 2500 ng vector was mixed with 2250 ng of pxPAX2 and 255 ng of VSVG-plasmids in 200 µL serum-free DMEM. Then this solution was added to 15 µL Fugene 6 (Roche, USA) containing 200 µL serum free DMEM. The mixture was then added to each 10 cm petri dish drop by drop.

Following transfection, the medium was collected on 48^{th} and 72^{nd} hour and stored at +4 °C. Then, to concentrate infectious particles, the collected medium was filtered through 45 µm filters and aliquoted in small amounts for further experiments.

2.14 Cas9 activity assay

To estimate the time required for the completion of Cas9 activity in more than 80% of the cells, cells were transduced with Cas9-expressing lentiviral vectors with Blasticidin selection (Addgene # 52962) with MOI:1.0. After the selection was completed, cells were post-transduced with GFP-expressing lentiviral vectors with Hygromycin selection with MOI:0.4. Then, stably Cas9 and GFP expressing cells were

transduced with either plentiGuide_T1 (GFP targeting gRNA) or plentiGuide_NT1 (non-targeting control gRNA) with Puromycin selection. From the selection day on, every 3 days, cells were trypsinized, and $1/10^{th}$ of cell suspension was analyzed on flow cytometry for GFP positive cells percentage in the population.

After the GFP-positive cell percentage in the population fell under 20% and stabilized on the next measurements, the optimum day count was chosen accordingly.

2.15 Determination of doubling time

The doubling time was calculated using the equation below, where the logarithm of the number of cells collected was divided by the logarithm of the number of cells initially seeded and then normalized by 3.32 (log2). The cumulative doubling time was obtained by summing all the previously calculated doubling times.

$$PD = 3.32 (\log2 (\text{Collected Cell Count}) - \log2 (\text{Seeded Cell count}))$$

2.16 Primary GBM sphere quantification

After I-BRD9 and IR treatment of GBM4 and MGG119 cells, images for each condition are captured. The diameter of each sphere is measured with ImageJ.

2.17 Cell cycle assay

For the assessment of the cell cycle, the Muse Cell Cycle Assay kit was used (Luminex) according to the instructions. Briefly, cells were collected with trypsin and washed 2x with sterile PBS. 70% ethanol was used as a fixative as $1x10^6$ cells per 1 ml of ethanol for a minimum of 3 hours at -20 °C. Following fixation, cells were centrifuged at 300xg for 5 minutes and washed once with PBS to discard ethanol. 150 µL of Cell Cycle reagent was added to the fixed cells and incubated for 30 minutes at room temperature in the dark. Reads were taken with a Muse Cell Analyzer.

2.18 Dual H2AX activation assay

Cells were harvested from 6-well plates following the corresponding treatment, and H2AX activation was quantified with The Muse® H2AX Activation Dual Detection Kit (MCH200101) according to the manufacturer's protocol. After collecting the cells after treatment of irradiation and/or BRD9 inhibitor, cells were fixed, permeabilized and stained with both total and phosphorylated H2AX antibodies. After incubation with antibodies for 30 minutes at room temperature, samples were run immediately to obtain optimum results.

2.19 Annexin/PI staining

Annexin/PI staining was performed with BD Pharmingen™ FITC Annexin V Apoptosis Detection Kit I according to the manufacturer's protocol. Cells were detached with Trypsin and collected with condition media. Cells washed with 1x PBS containing 1% FBS. 100 µl of cell suspension containing ~$1x10^5$ cells stained with 5 µl FITC and 2 µl PI and incubated at dark around 15 at RT. Cells were analyzed with CytoFlex Flow Cytometer, obtaining 10.000 events per sample.

2.20 Statistical analysis

All normalizations were performed on non-radiated or untreated samples, denoted as 100% using GraphPad Prism version 9.0 (USA) and Microsoft Excel 2018. Significance analysis was performed with student's t-test and two-way ANOVA (n.s denote not significant, for p-values, *, ** and *** denote $p < 0.05$, $p < 0.01$ and $p < 0.001$ respectively, two-tailed Student's t-test).

RESULTS

3.1 Epigenetic library screen on U373 glioblastoma cells

To identify novel epigenetic modifiers that alter radiotherapy response in GBM, a library screen was conducted using a chemical probe library. This library consists of around 125 chemicals, targeting nearly 25 classes of epigenetic modifiers. In this screen setup, the chemical library was combined with a single-pulse 4 Gy IR treatment. As a screen strategy, U373 glioblastoma cells were seeded to 96-well plates as 1000 cells/well, cells were treated with a low working dose (0.1X) of the chemical library. On day 3, cells were exposed to 4 Gy IR. On day 4, cells were trypsinized and 10% of cells were seeded to a new 96-well plate, a CTG assay was then performed to quantify cell viability (**Figure 3.1**).

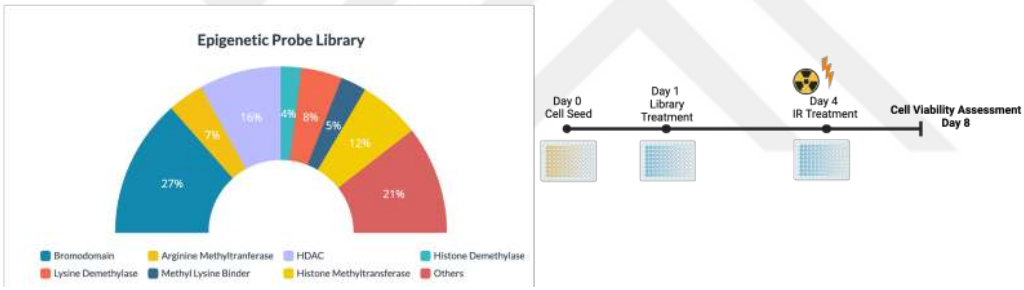

Figure 3.1 Epigenetic chemical library. Composition of epigenetic chemical library and implemented experimental setup for U373 cells

The radiosensitization effect of chemical inhibitor is calculated as "%Drug Only"-"% Drug+IR (4Gy)". IR exposure itself decreased the cell viability to 68%, potential radiosensitizer candidates were identified by taking this result as a reference. In addition, this library screen was also conducted on U87 cells, the results are presented in **Appendix B.**

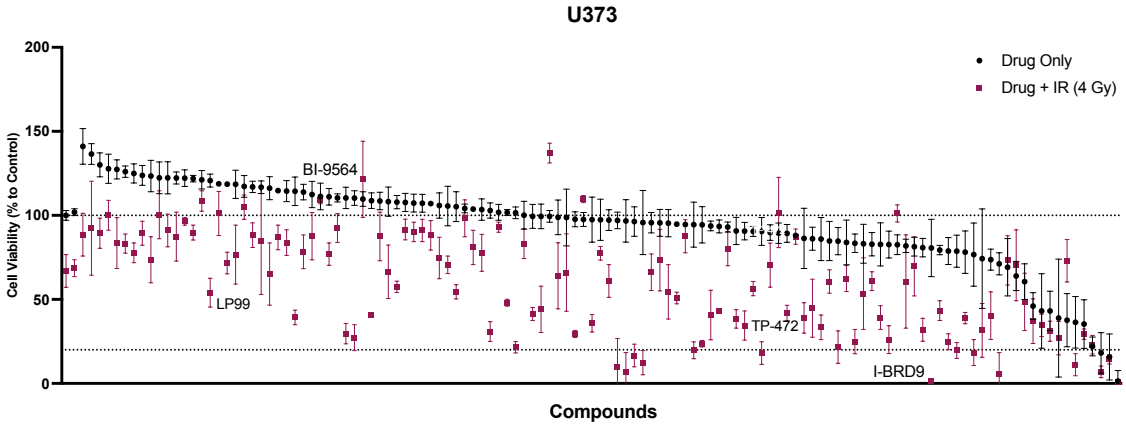

Figure 3.2 Epigenetic library screen. Scatter plot representation of epigenetic drug screen on U373 cells. Colored dots show the changes in cell viability when Taxol given epigenetic chemical is combined with IR.

Some of the compounds did not have a combinatorial effect on cell viability with IR treatment. Also, few of the compounds have high cytotoxicity when applied as monotherapy. These were not selected a for further experiments due to high cytotoxicity. To identify potential radiosensitizers, top hits were selected from chemicals that represent high cytotoxicity only when combined with IR.

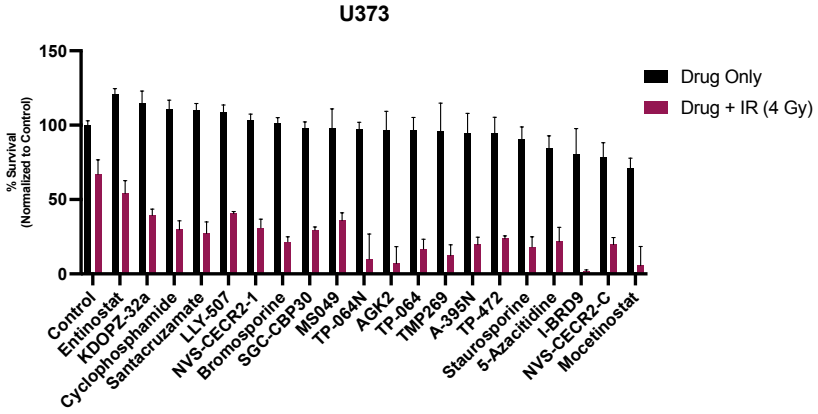

Figure 3.3 Top 20 selected hit chemicals as potential radiosensitizer for U373 cells

In this selected hit list, there were a few HDAC inhibitors such as Mocetinostat and Entinostat, and three chemotherapeutic agents; Cyclophosphamide, Staurosporine, and 5-azacitidine. Chemical inhibitors targeting different Bromodomains were candidates for novel radiosensitizers. From those, inhibitors targeting Bromodomain containing 9 protein were selected for this study, as I-BRD9 and TP-472, two BRD9 inhibitors were listed in the top 20 lists for radiosensitizers shown in **Figure 3.3**.

3.2 Establishment of the treatment regimen of BRD9 inhibitors with IR

To identify the most effective treatment regimen and whether the timing of BRD9 inhibitor treatment alters radiation response in GBM cells, three different experimental setups were prepared. This optimization experiment was only conducted with I-BRD9, a selective BRD9 inhibitor which was identified as a hit in the chemical library screen. As schematically represented in **Figure 3.4A,** in **pre-treatment**, cells were treated with I-BRD9 on day 1 after cell seeding. These cells were treated with I-BRD9 (2 µM) for 3 days, and at day 4 cells were exposed to IR (4 Gy). In **co-treatment**, both I-BRD9 (2 µM) and IR (4 Gy) treatment were performed on day 4 simultaneously.

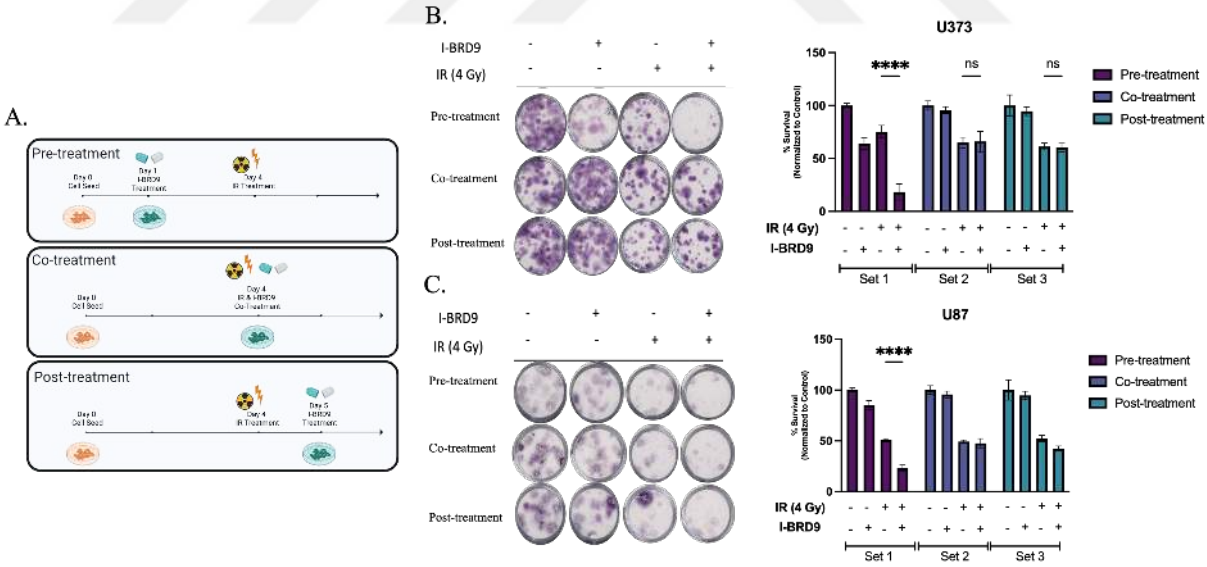

Figure 3.4 Establishment of treatment regimen for BRD9 inhibitors A. Schematic representation of experimental flow. B. Representative images of U373 colonies and quantification of colonies after treatment with I-BRD9 (2 µM) and IR (4 Gy) in different orders. C. Representative images of U87 colonies and quantification of colonies after treatment with I-BRD9 (2µM) and IR (4 Gy) in different orders.

Lastly, for **post-treatment**, I-BRD9 (2 μM) treatment was performed 24 hours after IR (4 Gy) treatment. Colony formation assays performed on U373 and U87 cells show that I-BRD9 treatment before IR treatment causes sensitization, especially more prominent cytotoxicity was observed on U373 cells, whereas no significant change was observed in colony numbers in co-treatment and post-treatment. In addition, for both cell lines, combination treatment did not exhibit an additive effect when compared with IR only conditions in **Figure 3.4B, C.**

These results suggest that early treatment of I-BRD9 may prime the cells to irradiation and make them more radiosensitive. This priming may have potentially originated from not short-term cytotoxicity of BRD9i, but a long-term alteration in chromatin architecture and transcription landscape of the cells.

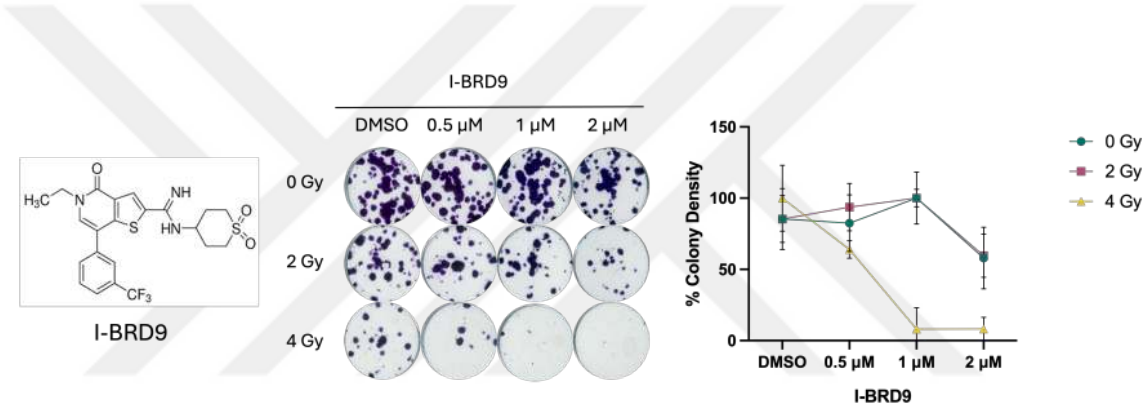

Figure 3.5 I-BRD9 radiosensitization on U373. Chemical structure of I-BRD9. Representative images of colonies and Quantification of colony densities after treated with various doses of I-BRD9 and IR.

After the establishment of this treatment regimen, different BRD9 inhibitors were combined with IR to observe the radiosensitization. Firstly, I-BRD9, a BRD9-specific inhibitor with high efficacy, is combined with different doses of IR.

Long-term clonogenic assay results show that in combination with different doses of I-BRD9 and IR; 4 Gy IR combined with 1 μM of I-BRD9 markedly affected the colony formation ability of U373 cells (**Figure 3.5**).

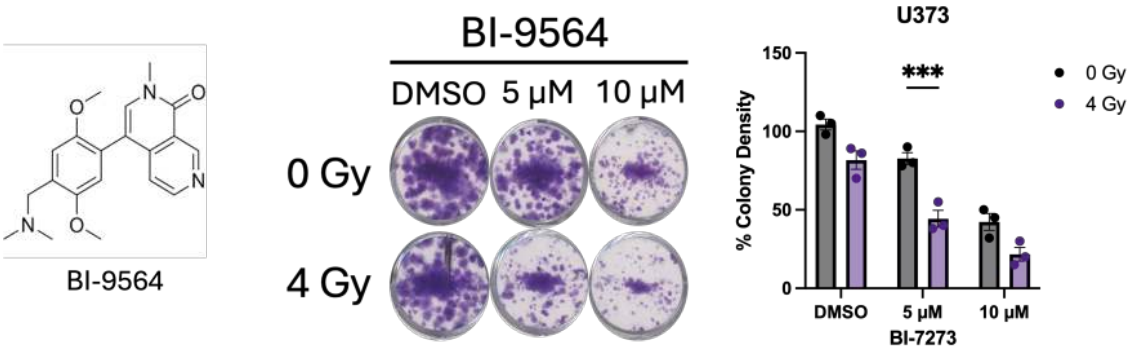

Figure 3.6 BI-9564 treatment in combination with IR on U373 cells Chemical structure of BI-7273. Representative images of colonies and quantification of colony densities after treated with various doses of BI-7273 and IR.

A BRD9/BRD7 inhibitor BI-9564 was also combined with IR on U373 cells. Where the radiosensitization effect was observed in much higher doses (5 μM) when compared with I-BRD9, this inhibitor also showed a radiosensitization effect on U373 cells (**Figure 3.6**). A slight radiosensitization was also observed in the treatment of BI-7273, a BRD9/BRD7 inhibitor, when combined with IR.

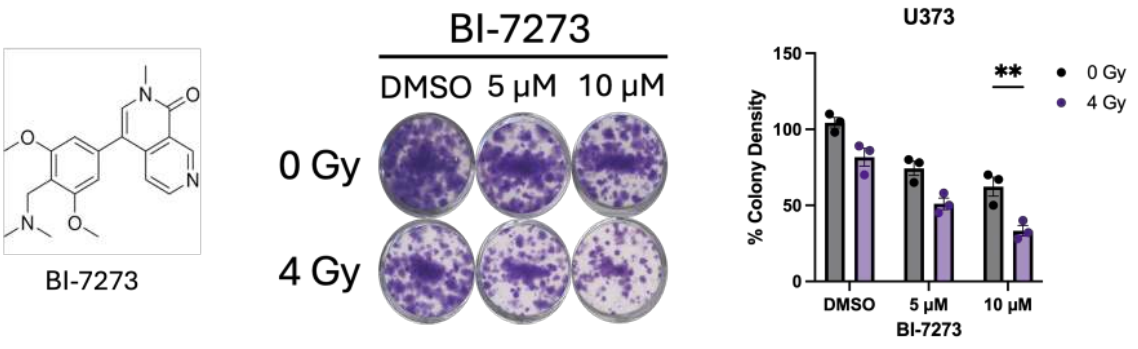

Figure 3.7 BI-7273 treatment in combination with IR on U373 cells. Chemical structure of BI-7273. Representative images of colonies and quantification of colony densities after treated with various doses of BI-7273 and IR.

10 µM BI-7273 treatment in combination treatment with 4 Gy IR significantly decreased the number of colonies as shown in **Figure 3.7**.

To support the role of BRD9 in radiation response, a PROTAC-based BRD9 degrader called VZ185 (Zoppi et al., 2019) was used to observe the radiosensitization effect. Proteolysis targeting chimeras (PROTAC) are useful tool to selectively degrade specific proteins in the cell (Békés et al., 2022). As shown in **Figure 3.8**, VZ185 has successfully degraded BRD9, and protein levels of BRD9 were decreased after 24 hours.

To sustain low BRD9 levels in the cell through protein degradation, treatment was repeated in cell culture media containing 500 nM or 1µM of VZ185 every day for three days until cells were exposed to IR (**Figure 3.9A**). The combination of 1 µM of VZ185 and 6 Gy or IR significantly decreased colony forming ability of U373 cells, as shown in **Figure 3.9B, C.** Again, this treatment required higher doses of IR compared with selective BRD9 inhibitors.

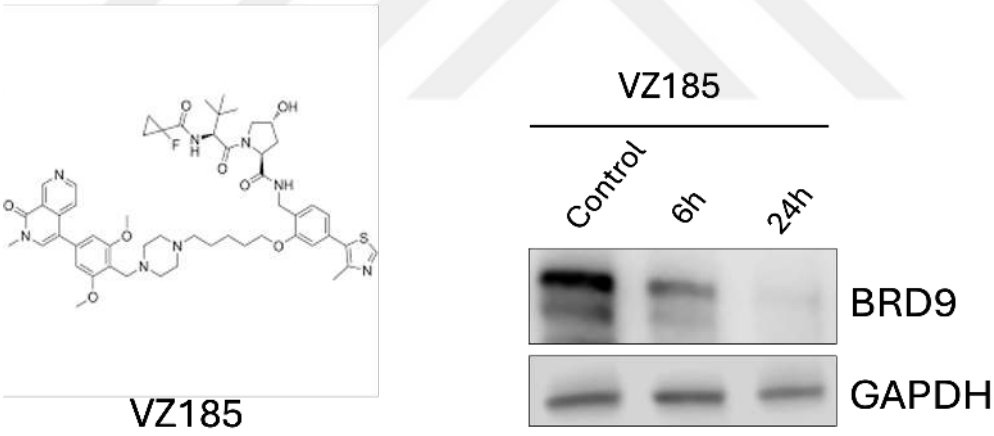

Figure 3.8 PROTAC-based BRD9 degrader. Chemical structure of VZ185 and BRD9 protein levels of U373 cells after treatment with VZ185 (1 µM).

Among all those three inhibitors, I-BRD9 has shown the most potent radiosensitization effect on U373 cells. Further on, the role of BRD9 in radiation response was investigated by mainly using I-BRD9.

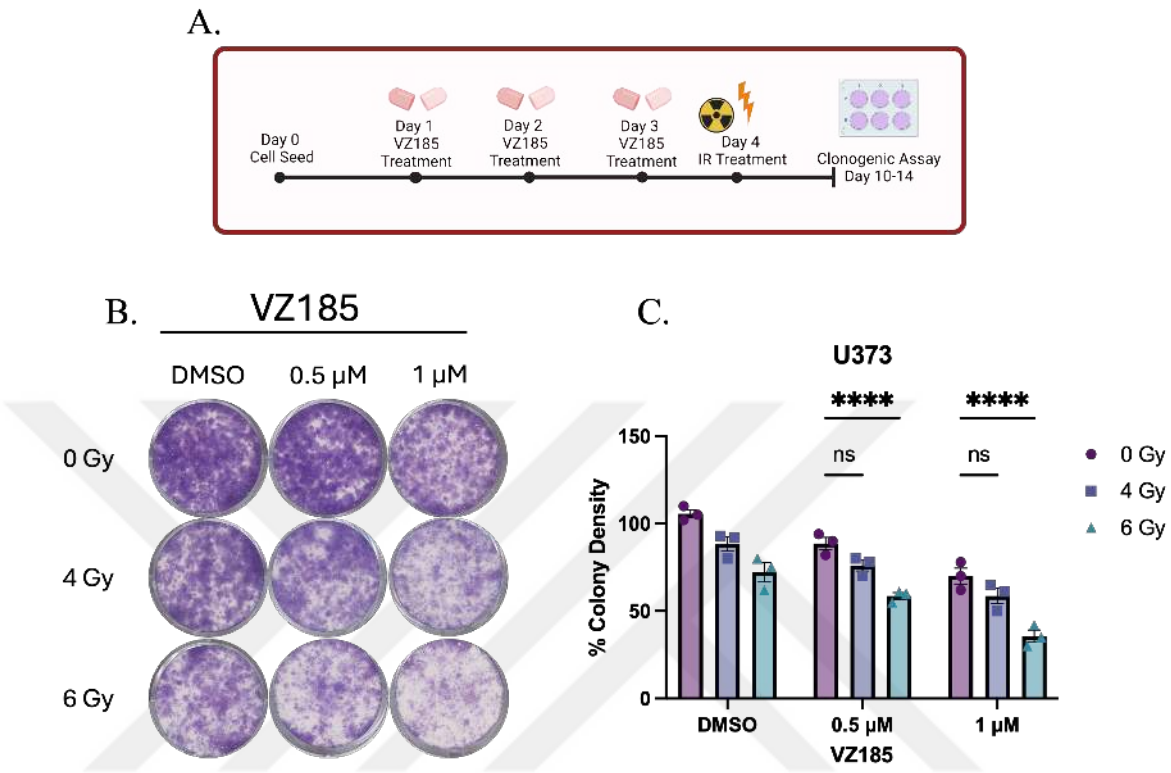

Figure 3.9 Effect of VZ185 on U373 cells. A. Schematic representation of VZ185 treatment strategy B. Representative images of U373 colonies after treatment with VZ185 and IR. C. Quantification of colony densities

3.3 Effect of I-BRD9 on non-malignant cell lines

To elucidate whether the radiosensitization effect of I-BRD9 is cancer-specific; the established treatment regimen was utilized on immortalized normal human astrocytes (I-NHA) as a non-malignant control group. Firstly, relative protein and gene expression levels of BRD9 were investigated in I-NHA, U373 and U87 cells. U373 was the cell line that has the highest protein levels of BRD9 (**Figure 3.10A**) also, the gene expression level of BRD9 was higher in U373 compared to both I-NHA and U87 (**Figure 3.10B)**.

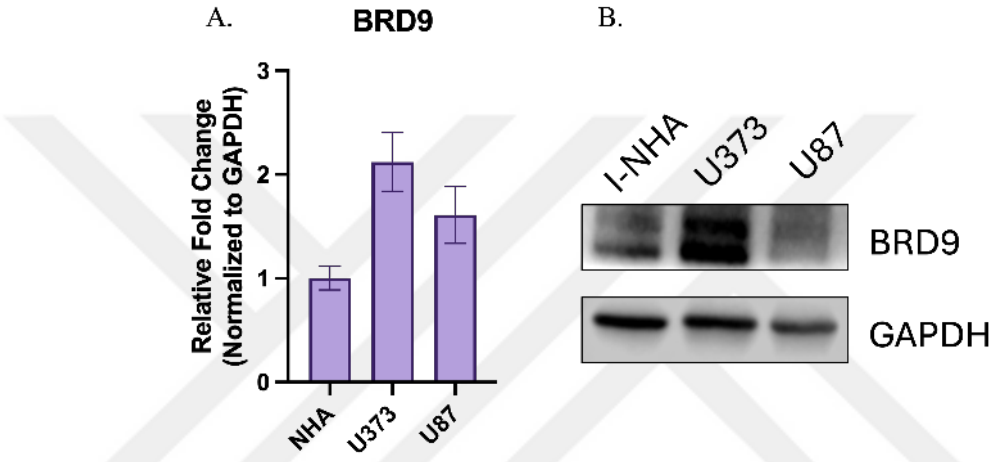

Figure 3.10 BRD9 levels in different cell lines. A. BRD9 gene expression levels I-NHA, U373 and U87 cell lines B. BRD9 protein levels in I-NHA, U373 and U87 cell lines

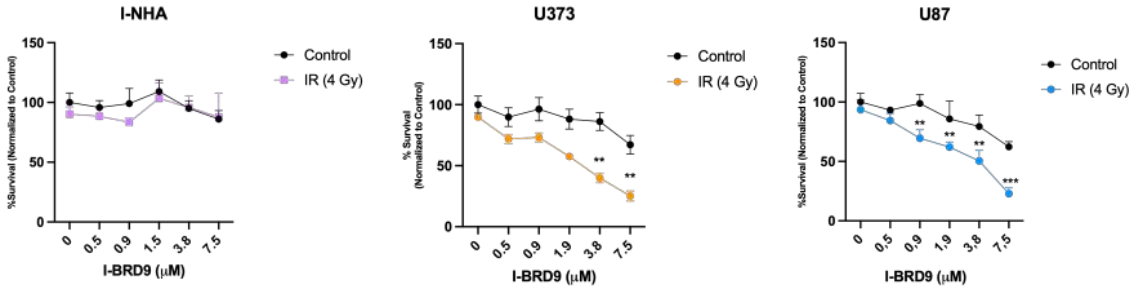

Figure 3.11 I-BRD9 dose response curves of different cell lines. Short-term cell viability results for I-NHA, U373 and U87 cells when treated with I-BRD9

The radiosensitization effect of I-BRD9 was not observed in I-NHA cells, IR treatment also did not affect the cell viability. The most effective response observed in short-term cell viability assay was in U373 cells. U87 cells were also affected slightly, on the other hand, combination treatment did not have a cytotoxic effect on I-NHA cell viability, as shown in (**Figure 3.11**).

In addition to short-term cell viability assays, the same radiosensitization was also observed in U373 in long-term clonogenic assays. Supporting previous results, cell viability and colony formation abilities of I-NHA cells were not affected by combination treatment (**Figure 3.12**). These results showed that radiosensitization through BRD9 inhibition occurs in malignant cell lines, not having any cytotoxic effect on I-NHA. In addition, these results suggest that endogenous BRD9 levels may be critical for the effective inhibition of I-BRD9.

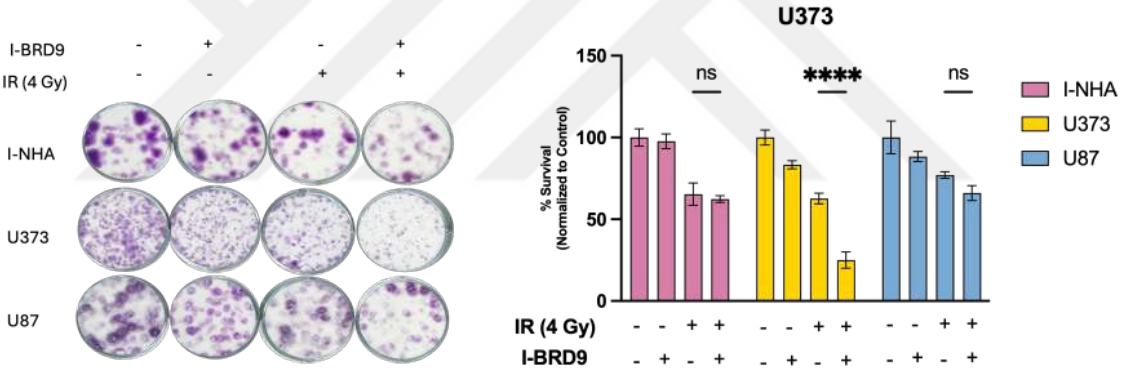

Figure 3.12 Representative images and quantification of clonogenic assay for I-NHA, U373 and U87 cell lines

3.4 Effect of I-BRD9 on different cell lines

To further investigate the role of BRD9 inhibition in radiation response, different cell lines were tested.

3.4.1 Effect of I-BRD9 on patient-derived primary GBM cells

To further investigate the effect of BRD9 in radiosensitization in glioblastoma, the established strategy was implemented on patient-derived primary GBM cell cultures. Unlike U373 and U87 cell lines, which adhere to a culture plate, these cells grow in suspension, supplemented with EF medium. For this purpose, GBM4 and MGG119 cell lines were used. To understand their response, different doses of I-BRD9 and ranged doses of ionizing radiation were implemented. As they grow in spheroids, the radiation response of primary cells might have differed from the U373 and U87 cell lines. Parallel with the established strategy, cells were treated with I-BRD9 on day 1. On day 4, GBM spheres were exposed to different doses of IR. The short-term cell viability was assessed with (CTG). In addition to cell viability, the number and diameter sizes of spheres for each condition were analyzed.

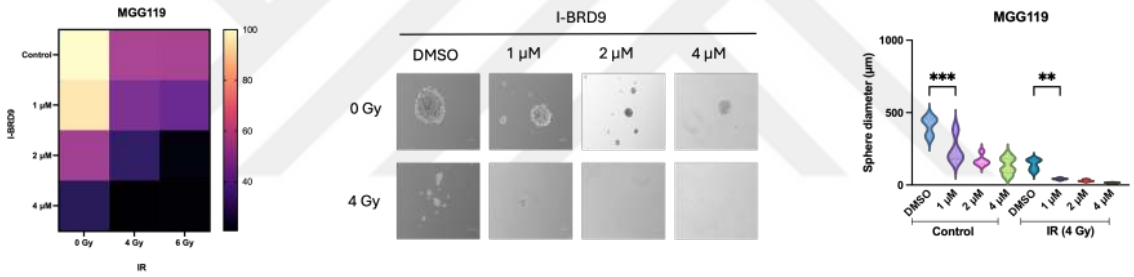

Figure 3.13 Radiation response of MGG119 cells after BRD9 inhibition Heatmap representation of short-term viability assay of MGG119 cells. Representative images of MGG119 spheres after treatment with I-BRD9 and IR and sphere diameter quantification. (Magnification:10X)

MGG119 cells were more sensitive to IR treatment, I-BRD9 treatment, and the combination treatment. Similar cytotoxicity was observed at 4 µM I-BRD9 and combination treatment of 2 µM I-BRD9 and 4 Gy IR. In addition, with an increased dose of I-BRD9, cell numbers were not affected significantly, but the sizes of spheres were significantly decreased (**Figure 3.13**).

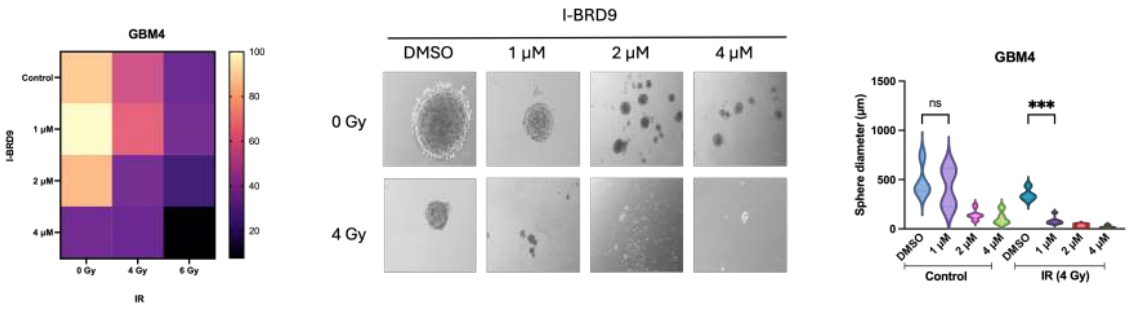

Figure 3.14 Radiation response of GBM4 cells after BRD9 inhibition. Heatmap representation of short-term viability assay GBM4 cells. Representative images of GBM4 spheres after treatment with I-BRD9 and IR and sphere diameter quantification. (Magnification:10X)

GBM4 cells were more resistant to both I-BRD9 and IR. But combination treatment again caused mild sensitization of the cells. Although initial cell numbers were the same in both GBM4 and MGG119 experiments, the GBM4 cell population doubled faster than the MGG119 cells. This might be the cause of larger spheres with a large number of cells. Again, I-BRD9 treatment alone did not affect significantly cell viability but caused the formation of smaller spheres. 4 Gy IR treatment also caused a small decrease in cell viability as expected (**Figure 3.14**). Strikingly, even in low doses, combination treatment caused the dissipation of cells and no viable spheres. These results show that BRD9 inhibition also radiosensitized primary GBM cells in suspension.

3.4.2 Effect of I-BRD9 on different cancer types

The effect of I-BRD9 was also investigated in different cancer types. Prostatic adenocarcinoma cell line (PC-3) and Breast cancer cell line (MDA-MB-231). PC3 has the highest BRD9 expression among three different cancer types. In contrast with BRD9 expression levels, MDA-MB-231 cells have higher radiosensitivity with I-BRD9 treatment. Although PC3 colony numbers were significantly decreased when I-BRD9 was combined with IR, the radiosensitization was more prominent in MDA-MB-231 cells, as shown in **Figure 3.15**.

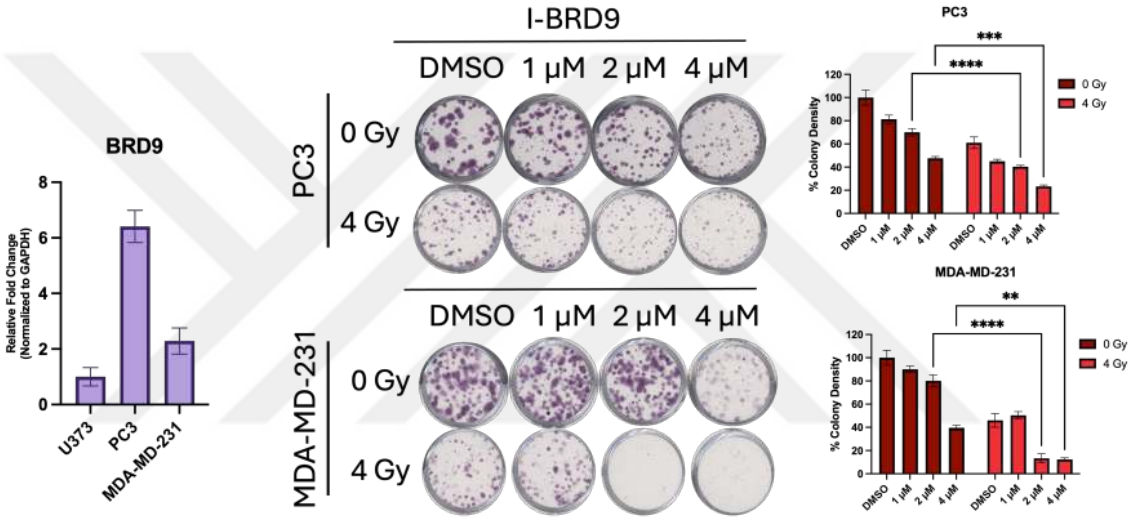

Figure 3.15 Effect of I-BRD9 and IR combination on prostate and breast cancer BRD9 expression levels on U373, PC3 and MDA-MD-231 cells. Representative images of clonogenic assay results and colony density quantifications of PC3 and MDA-MB-231 cells after different doses of I-BRD9 and IR treatment.

These results suggest that the radiosensitization effect of BRD9 inhibition is valid in malignant cell lines, and it is independent of BRD9 protein or gene expression levels.

3.5 Effect of I-BRD9 radiosensitization on apoptosis and DNA damage response

Since cell viability and colony formation abilities of U373 and U87 cells have decreased when treated with I-BRD9 and IR, Annexin/PI staining was performed for U373 and U87 cells to determine the level of apoptotic cells in the population. Both U373 and U87 cells were again treated with I-BRD9 for 3 days, and on day 4, cells were exposed to IR. Annexin/PI staining was performed 48 hours after IR treatment.

For U373 cells, I-BRD9 and IR single treatment did not increase the apoptotic cell population significantly. After 48 hours of combination treatment, the total apoptotic cell population increased by up to 40%, suggesting that combination treatment leads to apoptosis (**Figure 3.16**).

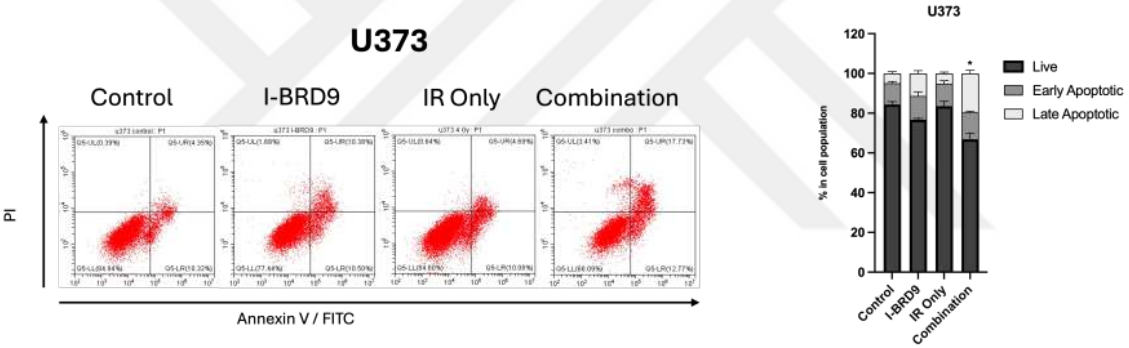

Figure 3.16 Annexin/PI Staining for U373 cells Representative images from Annexin/PI staining flow cytometry analysis and quantification of apoptotic cells for each condition. I-BRD9 (2 μM) and IR (4 Gy) treatments was performed following the established strategy.

The same pattern, but a stronger phenotype has been observed in U87 cells. Combination treatment caused higher percentages of both early apoptotic and late apoptotic cells in U87 cells. The total apoptotic cell percentage in the population has increased up to 60% (**Figure 3.17**).

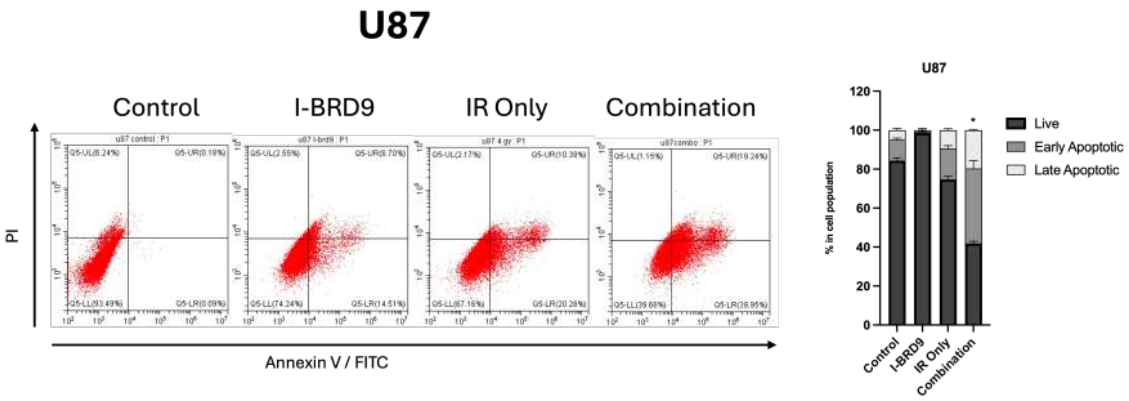

Figure 3.17 Annexin/PI Staining for U87 cells Representative images from Annexin/PI staining flow cytometry analysis and quantification of apoptotic cells for each condition. I-BRD9 (2 μM) and IR (4 Gy) treatments was performed following the established strategy.

These results suggest that I-BRD9 and IR combination treatment initiates apoptosis in both U373 and U87 cells 48 hours after IR treatment.

To support H2AX activation assay results, immunofluorescence staining was performed for the most two prominent markers for DNA damage response: phosphorylated H2AX and 53BP1 (**Figure 3.18A).** Immunofluorescent staining for γH2AX staining at four different time points again showed that I-BRD9-only treatment did not cause the formation of γH2AX foci. DSB formation by ionizing radiation was highest after 2 hours from IR treatment, foci clearance was gradually observed after 24 hours. On the contrary, combination treatment generated DSB nearly as IR-only treatment, but gH2AX foci clearance was slower (**Figure 3.18B**).

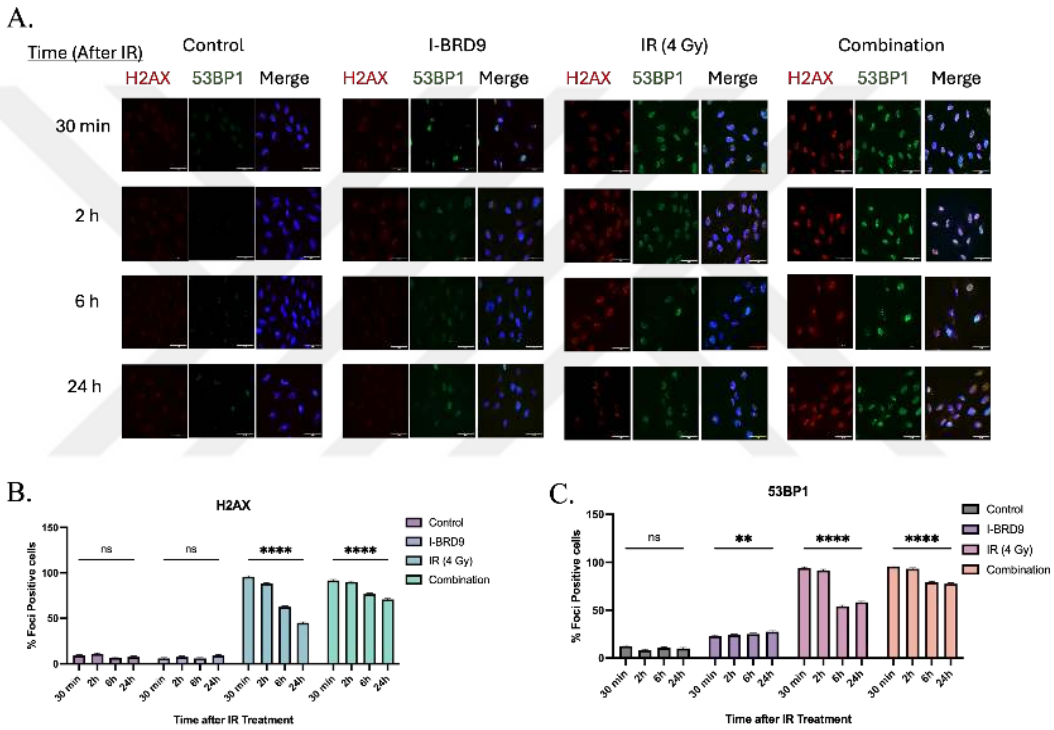

Figure 3.18 Immunofluorescent staining for U373 cells. A. Immunofluorescence staining of gH2AX and 53BP1 after different time points of IR treatment. (Scale bar: 50 μm, Red: γH2AX, Green: 53BP1, Blue: DAPI, n=120 for each condition). A. Representative images taken from different time points. B. Quantification of γH2AX foci positive cells C. Quantification of 53BP1 foci positive cells at different time points.

In addition to γH2AX staining, 53BP1 staining showed that prior I-BRD9 treatment increased the levels of 53BP1 compared to control cells. Again, IR treatment caused the generation of 53BP1 foci, and approximately 50% of foci were cleared 24 hours after IR treatment. Combination treatment also increased 53BP1 foci as much as IR-only

treatment, but similar to γH2AX, effective clearance of foci did not occur (**Figure 3.18C**). These results suggest that IR treatment itself generated DNA damage and induced DNA damage response, but when combined with prior I-BRD9 treatment, it caused impairment in DNA repair machinery and cells were unable to mitigate DNA damage burden.

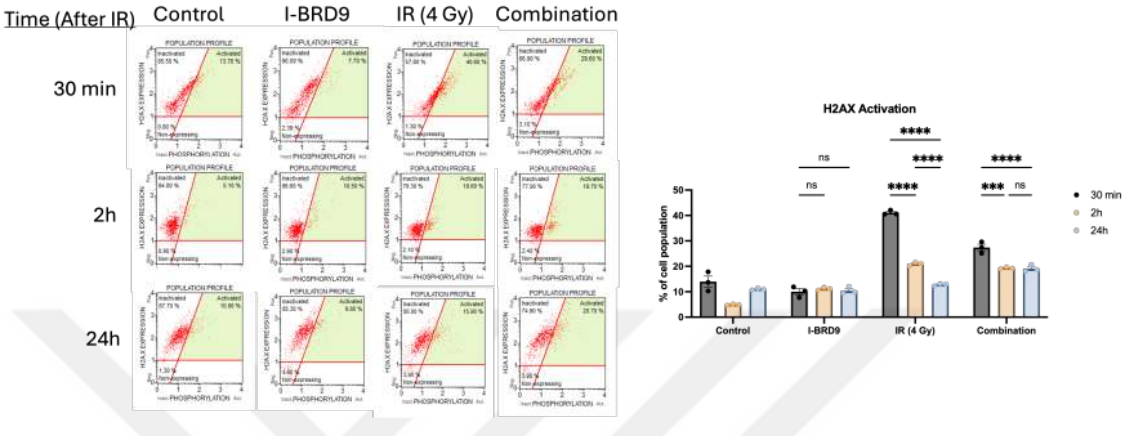

Figure 3.19 H2AX Activation assay for U373 cells. H2AX activation assay plots for different time points after IR treatment to U373 cells. And quantification of activated H2AX ratios after combination treatment. I-BRD9 (2 μM) and IR (4 Gy) treatments was performed following the established strategy.

To further investigate alteration in DSB formation and repair, flow cytometry-based H2AX activation assay was utilized to capture initial DSB formation via H2AX activation after different time points, 30 minutes, 2 hours, 24 hours. I-BRD9 treatment itself did not affect H2AX activation, the basal level of activated H2AX was preserved. As expected, the H2AX activation level was increased up to 40% at 30 minutes after IR treatment.

Activated H2AX levels gradually decreased in IR-only treated samples, showing functional repair machinery upon DNA damage generation. Combination treatment itself did not generate higher activated H2AX levels than IR-only treated samples. On the other hand, activated H2AX levels did not decrease in I-BRD9 and IR treatment samples, suggesting impaired DNA damage response and DNA repair machinery. In addition to activated H2AX and its clearance upon DNA repair, an increased percentage of inactive H2AX in I- BRD9 treated samples was observed. This could suggest that I-BRD9 itself did not cause phosphorylation of H2AX, but it might alter transcription and expression levels of H2AX (**Figure 3.19**).

3.6 Genetic ablation of BRD9 using CRISPR/Cas9 and its effect on radiosensitization

To complement the chemical approach, a CRISPR/Cas9-based genetic approach was employed to address the role of BRD9 in regulating radiotherapy response. For this, to determine the Cas9 efficiency in U373 and U87 cells, a Cas9 activity assay was performed. Cells were transduced with GFP-Hygro and selection was performed using Hygromycin. Next, these cells were transduced with Cas9 lentivirus and selected with Blasticidin. After selection, GFP targeting (T1) and non-targeting (NT1) lentiviruses were transduced to the cells. By using a flow cytometer, the GFP signal was measured every 3 days.

Results show that, for U373 cells, after day 13, around 70% Cas9 activity was observed (**Figure 3.20A**). For U87 cells, Cas9 efficiency has reached its peak around day 21, which was around 50% (**Figure 3.20B**). From these results, for completion of Cas9 activity, 13 days for U373 and 21 days for U87 cells were chosen as optimal.

After Cas9 activity, pLentiGuide constructs containing BRD9 guides targeting different sequences were transduced to U373 and U87 cells. To check whether BRD9 ablation causes a decrease in population doubling (PDL) time, PDL was calculated (**Figure 3.21**).

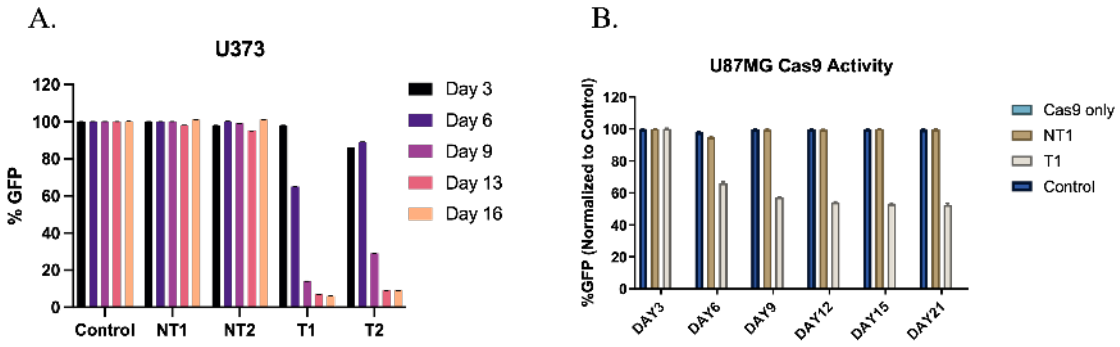

Figure 3.20 Cas9 Activity Assay A. %GFP levels for U373 cells. B. %GFP levels for U87 cells. Performed by Dr. Ezgi Yağmur Kala Kalkan

When compared with NT1-transduced cells, both BRD9 gRNAs decreased the growth rate of U373 cells (**Figure 3.21A**). U87 cells were affected more than U373 cells, and BRD9 knockout (KO) caused a significant decrease in growth rate, as shown in **Figure 3.21B**. These results suggest that, although genetic ablation of BRD9 does not have a cytotoxic effect as an essential gene, it decreases the growth rate.

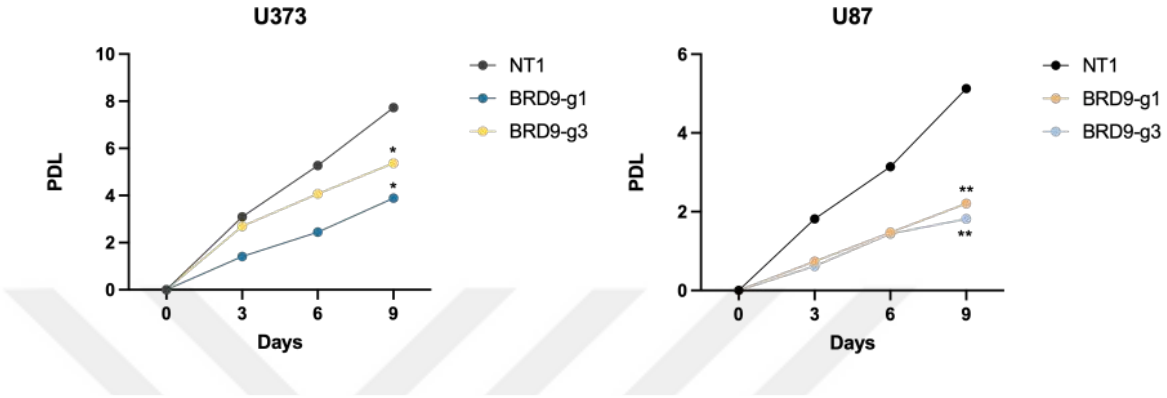

Figure 3.21 Growth curves of BRD9 guide transduced cells. A. B. Growth curves of U373-NT1, U373-BRD9-g1 and U373-BRD9-g3 cells. C. Growth curves of U87-NT1, U87-BRD9-g1 and U87-BRD9-g3 cells.

In addition to U373 and U87 cells, BRD9 KO was performed also on I-NHA cells. On day 6 after guide transduction to Cas9 expressing cells, colony formation assay was set for U373, U87, and I-NHA cells to observe the cell viability and radiosensitization effect of BRD9 loss.

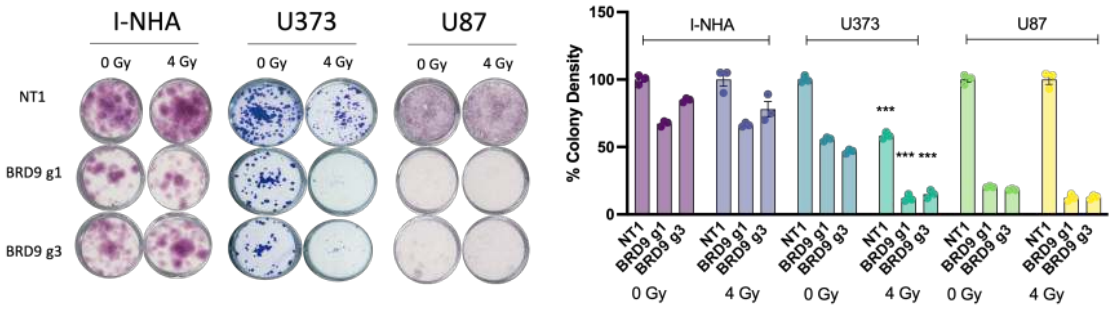

Figure 3.23 Clonogenic assay results upon BRD9 KO of U373, U87 and I-NHA cells. Representative images and quantification of colony formation assay of I-NHA, U373 and U87 NT1 and BRD9-KO cells after IR treatment.

As shown in **Figure 3.23**, I-NHA colony formation was slightly affected by BRD9 loss, but this effect was not strong; and no radiosensitization was observed in cells with BRD9 gRNAs. The most prominent radiosensitization effect was observed in U373 cells, where the BRD9 loss itself did not cause a marked reduction in cell viability; but dramatically radiosensitized cells as there were almost no quantifiable colonies after IR treatment. On the other hand, U87 cells were affected by BRD9 KO, where the colony formation dropped significantly with BRD9 loss. No further effect could be detected in IR treated conditions, as the BRD9 loss itself was already detrimental to cell growth.

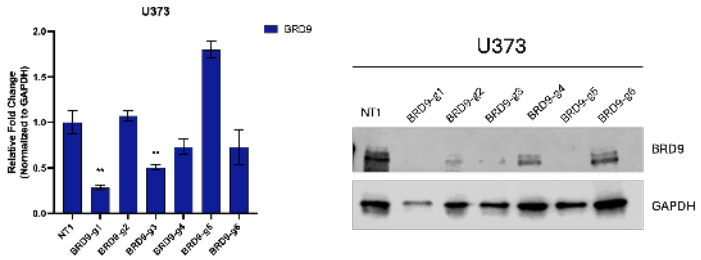

Figure 3.22 Changes in BRD9 expression levels and BRD9 protein levels upon BRD9 loss

For U373 cells, the BRD9 gene expression level and protein levels were also significantly decreased upon BRD9 KO (**Figure 3.22**). Few of the gRNAs did not efficiently cause a decrease in both protein level and gene expression levels.

3.6.1 Effect of BRD9 loss on IR-surv glioblastoma cells

As this study is focused on the role of BRD9 in the radiosensitization of glioblastoma cells, we also investigated BRD9's effects on long-term IR-exposed persistent cells. In our previous study, clinically relevant radiation survivor (IR-surv or U373$^{60\ Gy}$) cell populations were generated (Pinarbasi-Degirmenci et al., 2022). Accordingly, to implement a standardized radiotherapy regimen used in the clinic, U373 cells were exposed to IR for 2 Gy every day for 6 weeks, until the total dose reached to 40-60 Gy (**Figure 3.24A).**

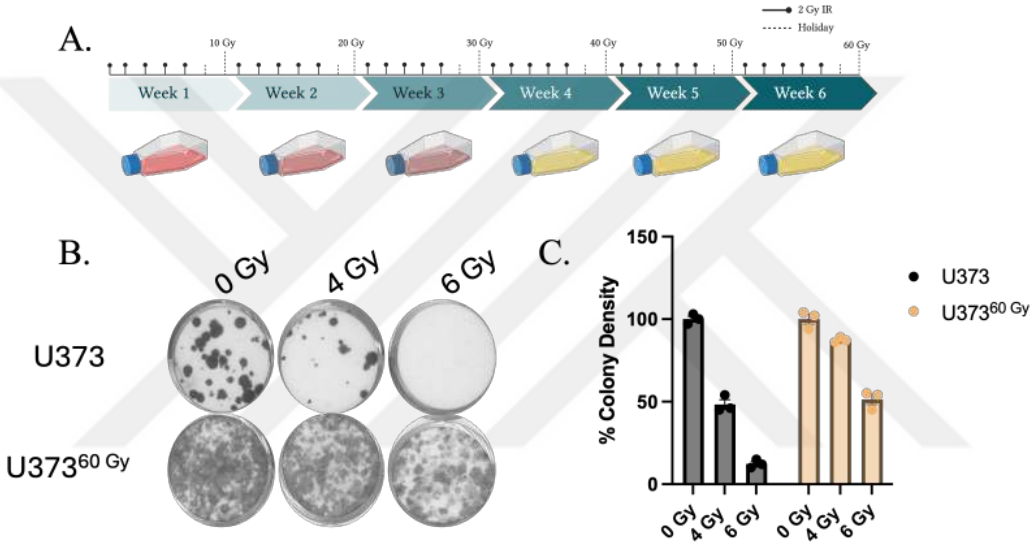

Figure 3.24 Generation of IR-surv cells and their response to IR. A. Schematic representation of generation of IR-surv cells. B. Representative colony images of parental and IR-surv U373 and U373$^{60\ Gy}$ cells. C. Quantification of colony numbers of U373 and U373$^{60\ Gy}$ cells.

When IR-surv and their matched parental cells were exposed to different doses of IR, as shown in figure **Figure 3.24B** and **Figure 3.24C,** parental U373 cells failed to form colonies after 6 Gy single-pulse IR and their colony numbers were significantly decreased, U373$^{60\ Gy}$ cells were not affected from IR as their parental match. This shows that IR-surv cells have a persistent phenotype in exposure to IR.

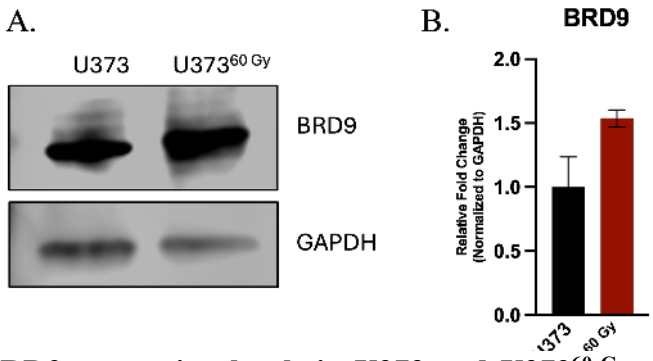

Figure 3.25 BRD9 expression levels in U373 and U373$^{60\ Gy}$ cells A. BRD9 protein levels of U373 and U373$^{60\ Gy}$ cells. B. BRD9 gene expression levels of U373 and U373$^{60\ Gy}$.

Since it was shown that BRD9 affects radiosensitization, we first compared the basal BRD9 expression levels in paired U373 and U373$^{60\ Gy}$ cells. As shown in **Figure 3.25A,** protein levels of BRD9 were slightly increased in U373$^{60\ Gy}$ compared to the parental cells. In addition, transcriptomic analysis was performed for U373 and U373$^{60\ Gy}$ cells (GEO Accession number GSE199862), and *BRD9* gene expression was upregulated upon long-term IR exposure. Indeed, *BRD9* was significantly upregulated in U373$^{60\ Gy}$ cell when compared with parental cells (**Figure 3.25B).**

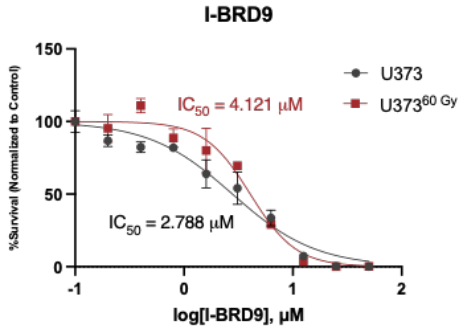

Figure 3.26 Dose response curve to I-BRD9

To investigate to response of IR-surv cells to BRD9 inhibition, a short-term cell viability assay was performed by treating these cells with I-BRD9. As shown in **Figure 3.26**, the IC_{50} value of U373 cells to I-BRD9 was 2.78 µM, whereas the IC_{50} value for $U373^{60\ Gy}$ cell was 4.121 µM. These results show that $U373^{60\ Gy}$ cells have a higher tolerance to I-BRD9, as the IC_{50} value is doubled after long-term IR exposure compared with its parental match. As a complementary approach, the radiation response of $U373^{60\ Gy}$ was investigated upon genetic loss of BRD9. Cas9 activity completion takes around 13 days for $U373^{60\ Gy}$, which is quite similar to parental U373 cells (**Figure 3.27**). No difference in Cas9 activity of parental and IR-surv cells provides better understanding of the effect of gene loss, since long-term clonogenic assays were conducted in parallel.

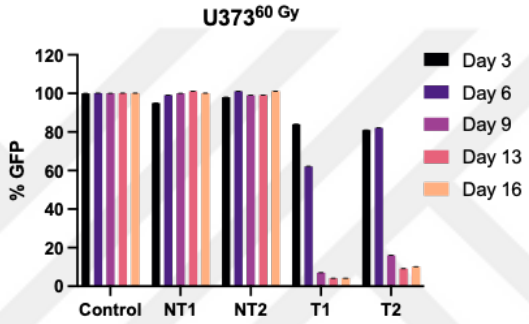

Figure 3.27 Cas9 Activity assay for $U373^{60\ Gy}$ cells

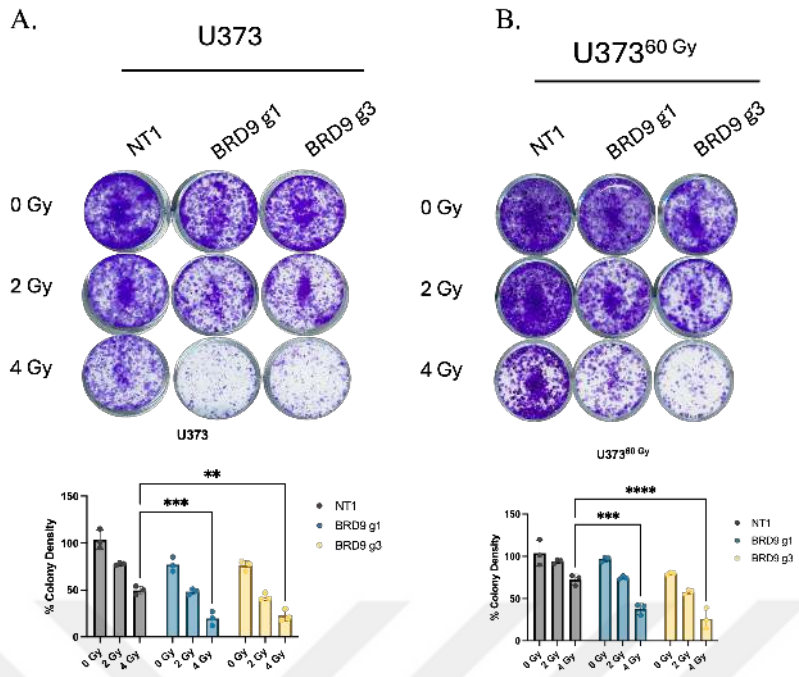

Figure 3.28 Clonogenic Assay results for U373 and U373^{60Gy} upon BRD9 KO

A. Representative images of colonies and quantification of colonies U373 cells upon IR exposure after BRD9 KO. B. Representative images of colonies and quantification of colonies U373$^{60\ Gy}$ cells upon IR exposure after BRD9 KO.

As shown in **Figure 3.28A**, BRD9-g1 and BRD9-g3 did not affect cell viability significantly. However, when these KO cells were exposed to IR, a slight decrease in colony numbers were observed when exposed to 2 Gy. In addition, in especially 4 Gy, colony numbers were significantly decreased. As for U373$^{60\ Gy}$ cells, again, IR treatment did not affect colony formation when compared with its parental pair. For BRD9-g1, a slight decrease in colony number was observed when compared with parental U373 cells. BRD9-g3 effectively sensitized U373$^{60\ Gy}$ cells as shown in **Figure 3.28B.**

These results suggest that long-term IR exposure causes upregulation of BRD9, and this causes higher tolerance to BRD9 inhibition. This alteration in radiation response can be partly reverted by BRD9 loss.

3.7 Effect of BRD9 overexpression on radiation response

To further investigate the effect of BRD9 expression in radiation response, BRD9 overexpression was performed on U373 and U87 cells. For this, retroviral expression vector MSCV-Cterm_3xFL_BRD9-PGK-Puro-IRES-GFP was transduced to U373 and U87 cells. As shown in **Figure 3.29**, BRD9 overexpression was successful after the transduction of the expression plasmid.

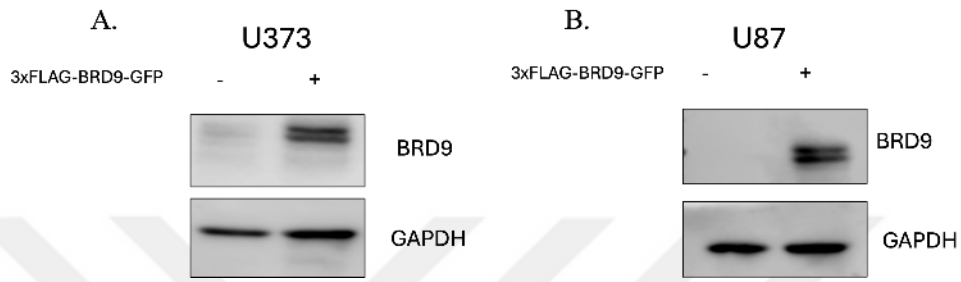

Figure 3.29 BRD9 overexpression on U373 and U87 cells A. BRD9 protein levels after transduction of expression plasmid to U373 cells B. BRD9 protein levels after transduction of expression plasmid to U87 cells

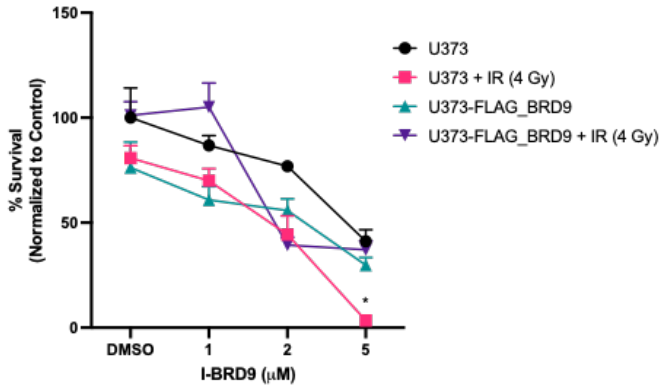

Figure 3.30 Cell viability results for BRD9 overexpressed cells. Cell viability assay of U373 parental and FLAG-BRD9 transduced cells treated with increasing dose of I-BRD9 and IR (4Gy)

To see the effect of overexpression in radiosensitization, a colony formation assay, and short-term cell viability assay were performed. From the short-term cell viability assay shown in **Figure 3.30**, BRD9 overexpressing cells were affected by increased doses of I-BRD9 and IR independently, but the radiosensitization effect was not observed.

We observed sensitization similar to previous experiments in U373 cells. On the other hand BRD9 overexpressing U373 cells did not respond to combination treatment. U373-FLAG_BRD9 cells were slightly affected by I-BRD9 treatment and IR treatment, as observed in colony number quantification, not combination effect was not observed when compared with their parental pairs, as shown in **Figure 3.31**.

These results suggest that the radiosensitization effect of BRD9 depends on the expression level of BRD9. Increased levels of BRD9 alter the efficacy of BRD9

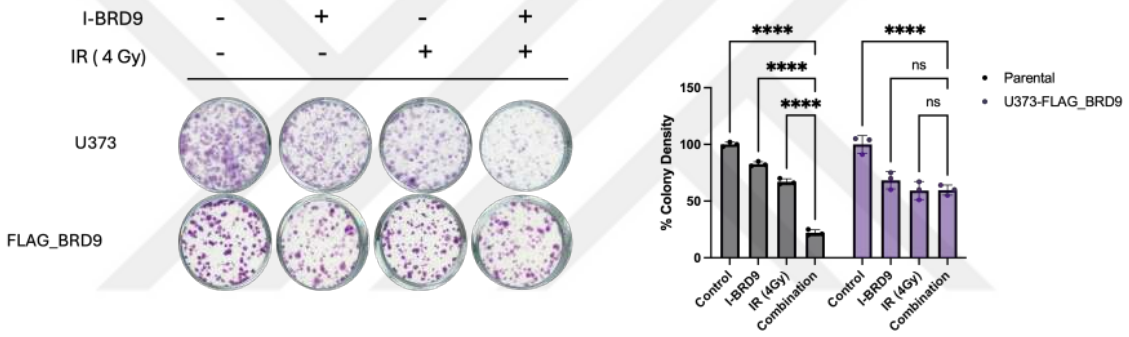

Figure 3.31 Colony formation assay after BRD9 overexpression Representative images and quantification of colony formation assays of U373 parental and FLAG-BRD9 transduced cells.

inhibition. To understand effect of BRD9 level comprehensively, future work is needed.

3.8 Transcriptomic alterations upon BRD9 perturbation

3.8.1 Transcriptomic analysis of U373 cells upon I-BRD9 and/or IR treatment

To understand the transcriptomic alterations upon BRD9 inhibition and its effect on radiation response, RNA sequencing was performed for U373 cells. As per previously established protocol, U373 cells were treated with I-BRD9 for 3 days, and on day 4, IR treatment was performed. RNA samples were collected 24 hours after IR treatment. After validating the RNA quality of the triplicate samples for each condition, samples were sent for RNA sequencing.

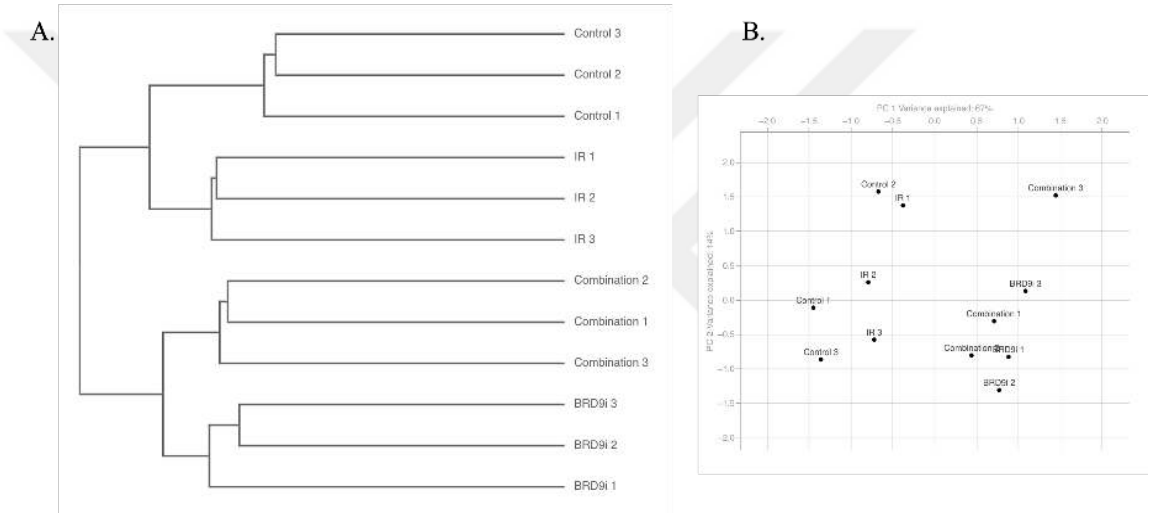

Figure 3.32 Clustering of treated samples of U373 cells in RNA sequencing. A. Hierarchical clustering of RNA sequencing samples. B. Principal component analysis (PCA) plots of RNA sequencing samples

As shown in **Figure 3.32**, samples were evenly clustered and I-BRD9 treated and untreated conditions were differentiated from each other. To investigate the effect of BRD9 inhibition, IR treatment, and their combinatorial effect, pairwise analyses were performed for each condition.

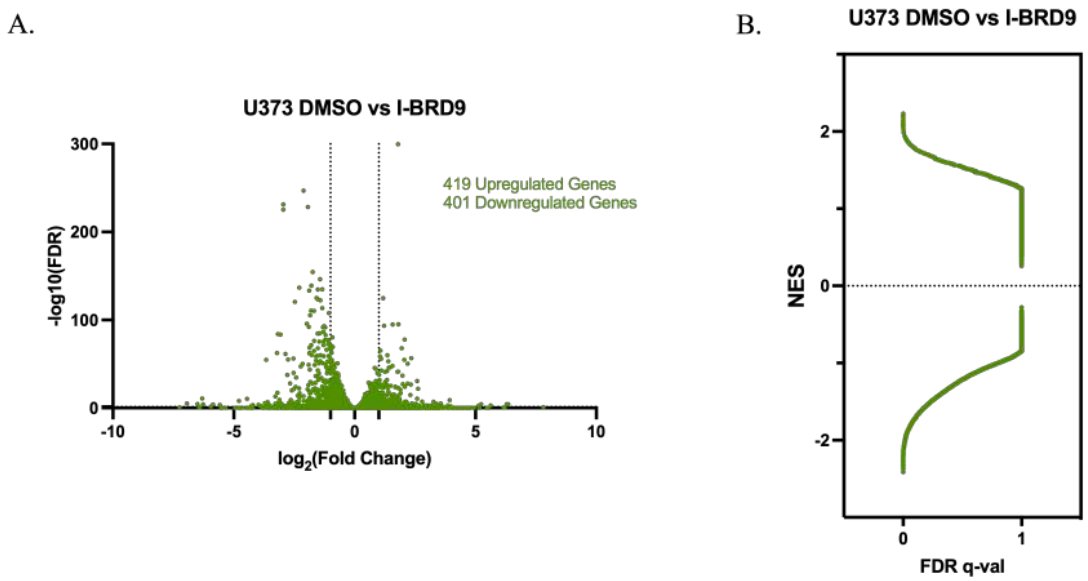

Figure 3.33 Differentially expressed genes upon I-BRD9 treatment. A. Volcano plot representing DEGs upon I-BRD9 treatment in U373 cells. (FDR<0.05, FC>2). B. GSEA analysis for all available gene sets for I-BRD9 treated samples.

For the I-BRD9 treatment itself, over 800 genes were differentially expressed (DEG). 419 genes were upregulated and 401 genes were downregulated, as shown in the volcano plot in **Figure 3.33A.** When Gene Set Enrichment Analysis was performed with all available gene sets as represented in **Figure 3.33B**, there were differentially enriched pathways identified.

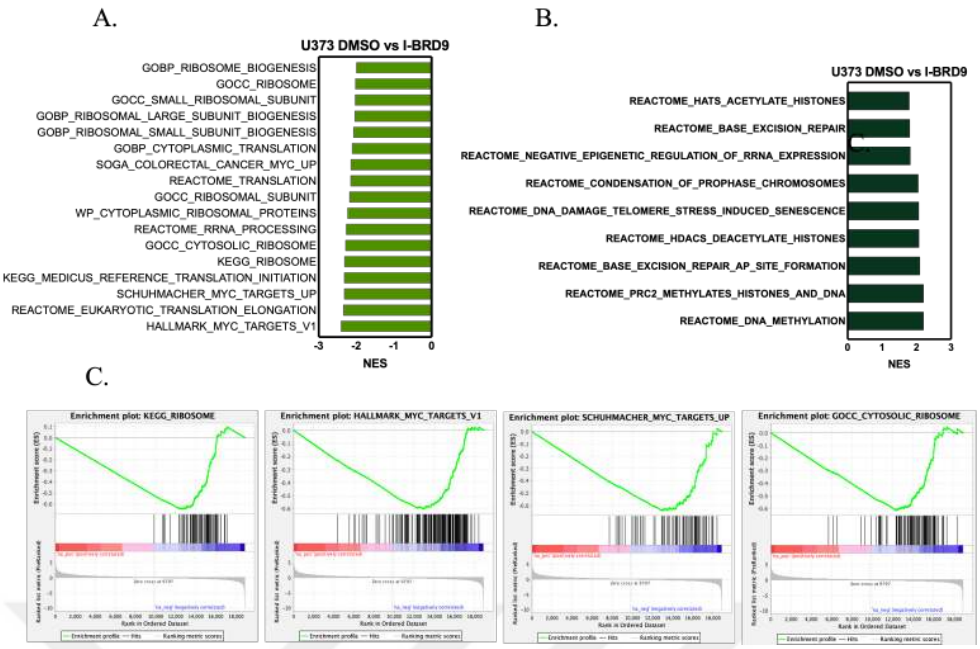

Figure 3.34 Differentially enriched pathways upon I-BRD9 treatment from GSEA. A. Negatively enriched pathways upon I-BRD9 treatment with GSEA ($p<0.05$). B. Positively enriched pathways upon I-BRD9 treatment upon I-BRD9 treatment with GSEA ($p<0.05$). C. NES plots for plots for significantly altered pathways upon I-BRD9 treatment

Pathways related to translation and ribosomal biogenesis such as *Eukaryotic Translation Elongation, Translation Initiation, GOCC_CYTOSOLIC_RIBOSOME,* and *Ribosomal Subunit Biogenesis* were commonly downregulated upon treatment. In addition, *MYC*-related pathways were also significantly downregulated upon I-BRD9 treatment **Figure 3.34A**. On the other hand, pathways related to DNA repair, histone acetylation, histone methylation, DNA methylation, and stress-induced senescence were significantly upregulated (**Figure 3.34B**). The most significantly downregulated pathways were KEGG_RIBOSOME, HALLMARK_MYC_TARGETS_V1, SCHUMACHER_MYC_TARGETS_UP and GOCC_CYTOSOLIC_RIBOSOME. Their NES plots are shown in **Figure 3.34C**.

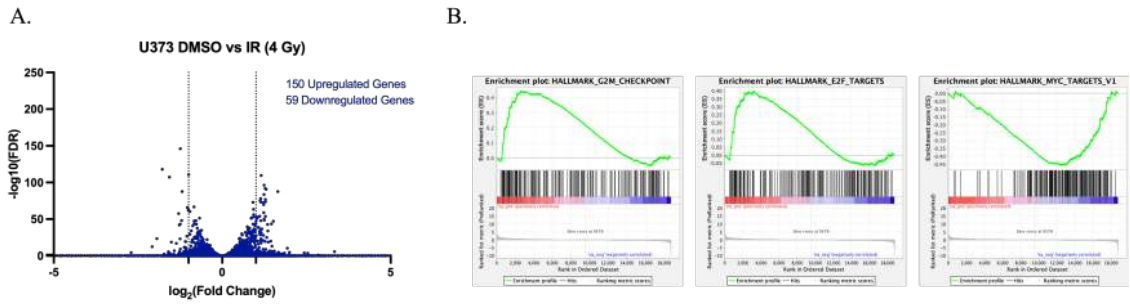

Figure 3.35 Differentially expressed genes upon IR treatment. A. Volcano plot representing DEGs upon IR (4 Gy) treatment (FDR<0.05, FC>2). B. NES plots for G2M Checkpoint, E2F Targets and Myc Targets pathways (p<0.05).

For only IR-treated samples, around 200 genes were differentially expressed. 150 genes were upregulated and 59 genes were downregulated upon IR treatment **(Figure 3.35A).** Since the number of differentially expressed genes was lower than I-BRD9 samples, GSEA analysis resulted in a lower number of significant pathways. Hallmark pathways such as G2/M Checkpoint and E2F targets were upregulated, whereas MYC Targets were downregulated. NES plots are shown in **Figure 3.35C**.

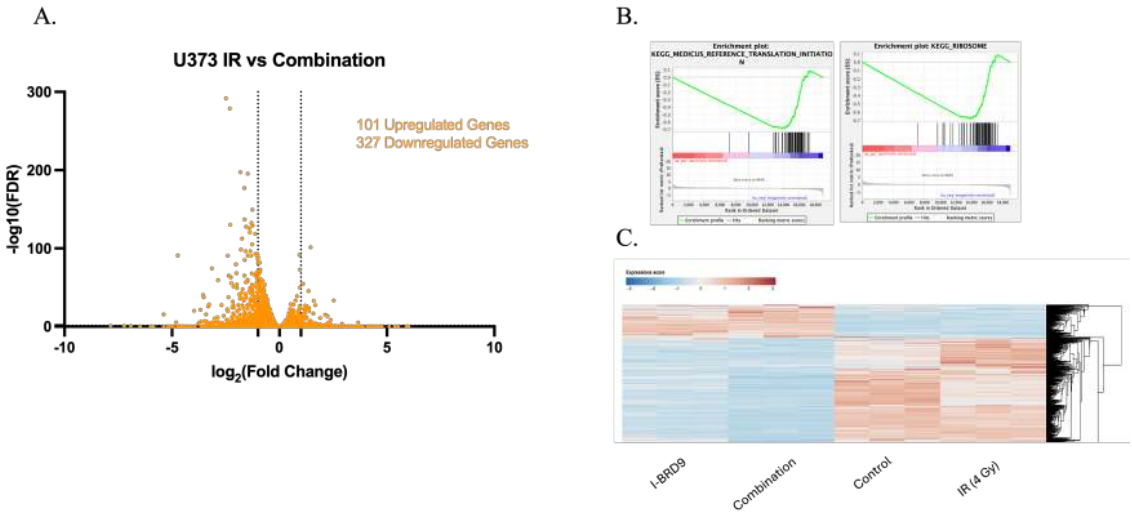

Figure 3.36 Differentially expressed genes among IR treated and Combination treated samples. A. Volcano plot representing DEGs in comparison of IR vs combination treatment (FDR<0.05, FC>2). B. NES plot representing pathways negatively enriched. C. Heatmaps representing DEGs from IR vs Combination treated samples in all conditions.

Furthermore, to observe the distinct effect of I-BRD9 in combination, the analysis was extended to compare IR-treated samples with combination-treated samples. This analysis showed that around 500 genes were differentially expressed, 101 genes were upregulated and 327 genes were downregulated, as shown in a volcano plot in **Figure 3.36A**. GSEA analysis showed in **Figure 3.36B** that pathways related to translation initiation and ribosomal biogenesis were negatively enriched. In addition, the genes that were differentially expressed commonly with I-BRD9 and Combination conditions were inversely differentially expressed in IR-treated and Control conditions.

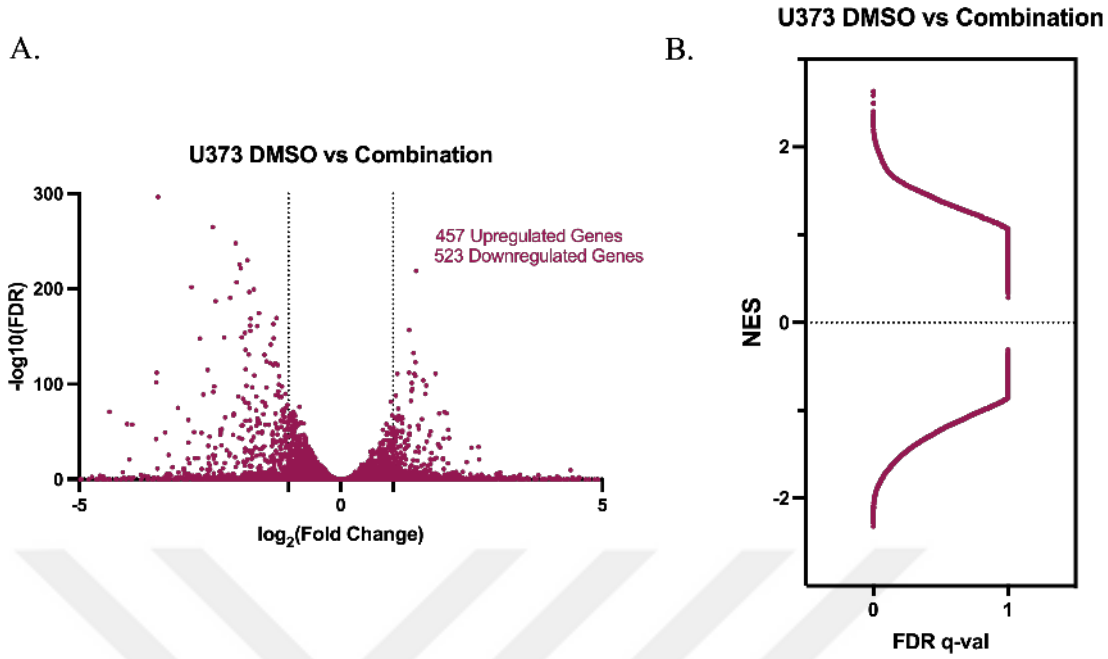

Figure 3.37 Differentially expressed genes upon combination treatment. A. Volcano plot representing DEGs upon combination treatment in U373 cells. (FDR<0.05, FC>2). B. GSEA analysis for all available gene sets for combination treated samples.

The highest number of DEGs came from the analysis of samples treated with the combination of I-BRD9 and 4 Gy. Around 1000 genes were differentially expressed, 457 genes were upregulated and 523 genes were downregulated in combination samples, volcano plot is shown in **Figure 3.37A.** When GSEA was performed with all available gene sets as represented in **Figure 3.37B,** there were commonly differentially enriched pathways identified.

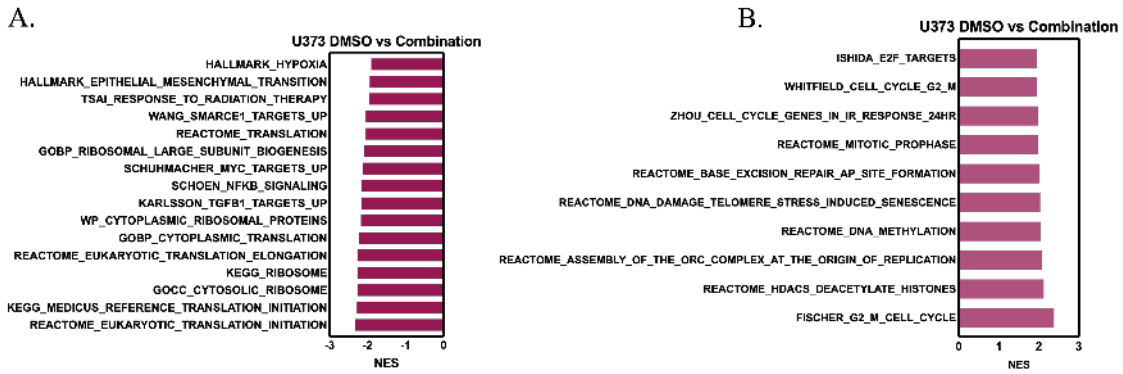

Figure 3.38 Differentially enriched pathways upon combinatorial treatment from GSEA. A. Negatively enriched pathways upon combination treatment with GSEA ($p<0.05$). B. Positively enriched pathways upon combination treatment upon I-BRD9 treatment with GSEA ($p<0.05$).

Similar to I-BRD9 treated samples, pathways related to ribosomal biogenesis, translation initiation, and ribosomal genes were downregulated. In addition to ribosomal pathway downregulation, pathways related to MYC and its targets were downregulated upon combinatorial treatment **(Figure 3.38A)**. As for pathways related to the cell cycle, specifically, the G2/M phase, stress-induced senescence, histone methylation and acetylation, and DNA damage repair were positively enriched upon combinatorial treatment, listed in **Figure 3.38B**. As with the heatmap representation of differentially enriched pathways shown in **Figure 3.39**, the majority of the genes in Hallmark E2F Targets and Hallmark G2/M Checkpoint pathways were upregulated. In addition, the majority of the genes in Hallmark p53 Pathway and MYC Targets were downregulated.

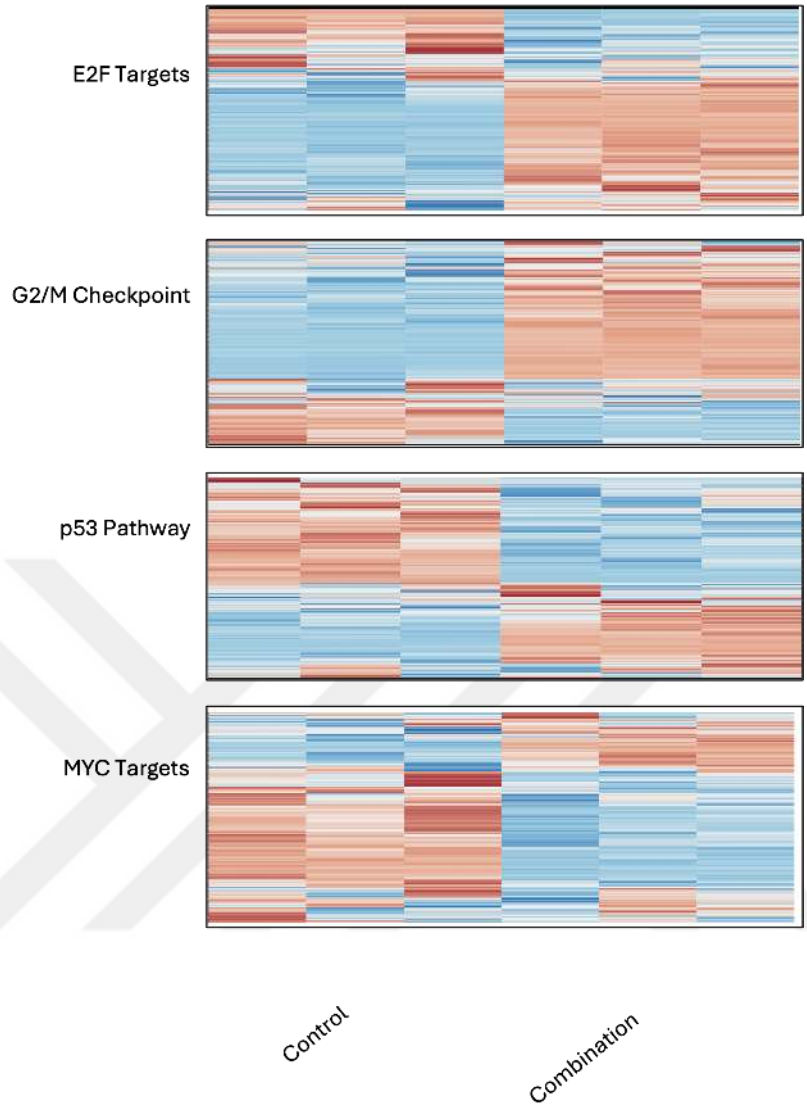

Figure 3.39 Heatmaps representing Hallmark Pathways for control and combination samples

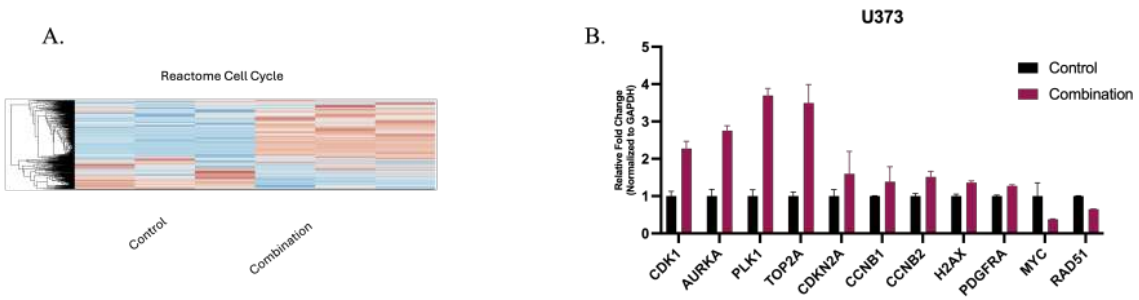

Figure 3.40 Alterations in cell cycle related genes upon combinatorial treatment A. Heatmap representing Reactome Cell Cycle pathways on control and combination treated samples B. Gene expression levels of cell cycle related genes in U373 cells

Cell cycle related genes and pathways, specifically G2/M checkpoint related genes were differentially expressed upon BRD9 inhibition. Again, Reactome cell cycle pathway was highly enriched upon combination treatment, shown as heatmap in **Figure 3.40A.** Indeed, validation of cell cycle related genes with qRT-PCR shows that cell cycle related genes were highly upregulated and *myc* was downregulated in combination treated samples (**Figure 3.40B)**.

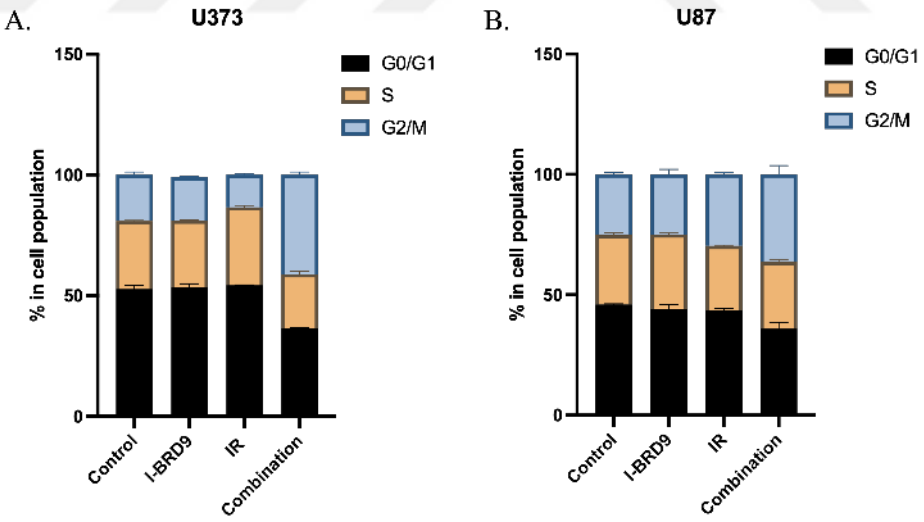

Figure 3.41 Cell cycle analysis of U373 and U87 cells. A. Cell cycle distribution of U373 cells upon I-BRD9 and/or IR treatment. B. Cell cycle distribution of U87 cells upon I-BRD9 and/or IR treatment.

In order to investigate cell cycle alterations observed in transcriptomic level, cell cycle analysis was performed on U373 and U87 cells. After 3 days of I-BRD9 treatment, IR treatment was performed. Cells were collected for cell cycle staining 24 hours after IR treatment. Indeed, single treatment of I-BRD9 and IR did not affect cell cycle distribution in the population both in U373 and U87 cells. Strikingly, combination treatment causes increase in percentage in G2/M phase in U373 cells, shown in **Figure 3.41A.** In U87 cells slight arrest in G2/M phase was observed.

These results suggest that combination treatment causes distinct transcriptional alterations in glioblastoma cells, specifically pathways related with cell cycle regulation.

3.8.2 Transcriptomic analysis of U87 cells upon genetic ablation of BRD9

Transcriptomic analysis was also performed for U87 BRD9 KO cells. As the highest efficiency, BRD9-g3 transduced samples were collected with its NT1 transduced pair. Again, NT1 and BRD9 KO samples were clustered as replicates shown in **Figure 3.42**.

RNA-seq analysis showed that 2422 genes were downregulated, and 135 genes were upregulated upon BRD9 KO **(Figure 3.43A).** GSEA analysis showed that pathways such

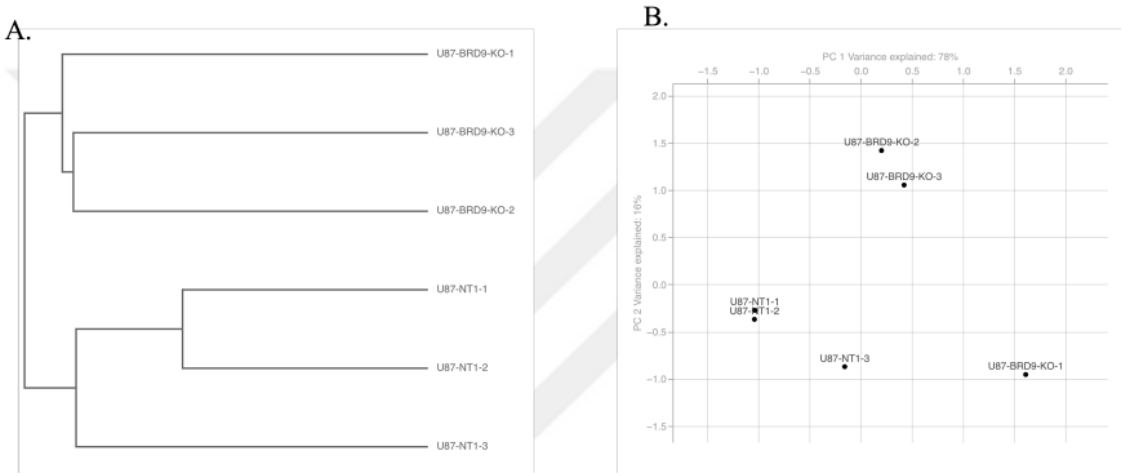

Figure 3.42 Clustering of treated samples of U373 cells in RNA sequencing. A. Hierarchical clustering of RNA sequencing samples. B. Principal component analysis (PCA) plots of U87 NT and BRD9 KO samples.

as Myc targets, E2F Targets, G2/M Checkpoint, and DNA repair were significantly downregulated upon BRD9 loss (**Figure 3.43B, Figure 3.43C**).

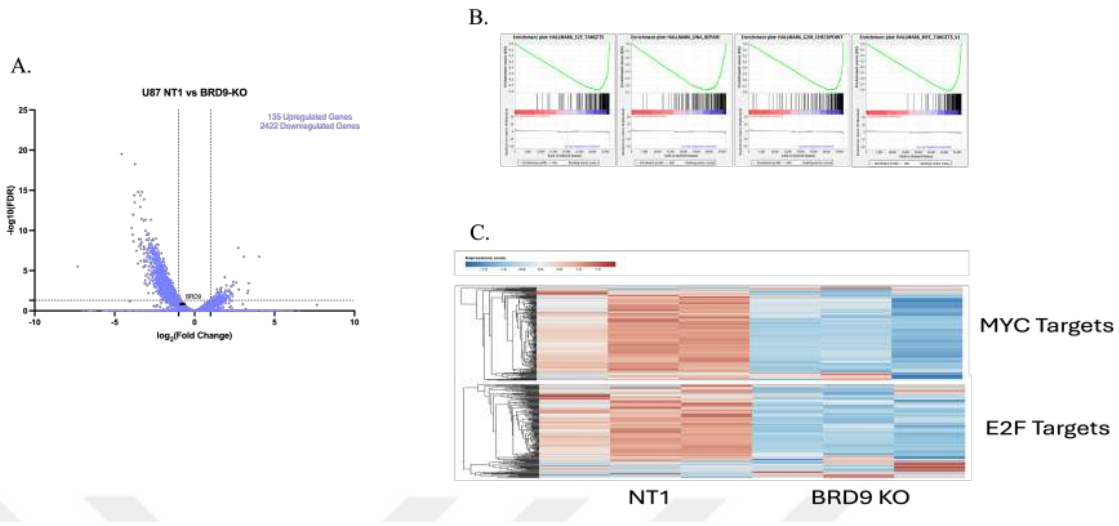

Figure 3.43 Differentially expressed genes upon BRD9 loss on U87 cells. A. Volcano plot showing DEGs upon BRD9 KO (FDR<0.05, FC>2). B. NES plots for negatively enriched pathways upon BRD9 KO C. Heatmaps representing DEGs in MYC Targets and E2F Targets Pathways.

Similar to U373 cells treated with I-BRD9 treatment, BRD9 loss on U87 cells causes significant alterations in cell cycle regulation. When DEGs were analyzed in Reactome and GO Biological Processes, the most enriched pathways were related to cell cycle regulation and cell cycle checkpoints **Figure 3.44**.

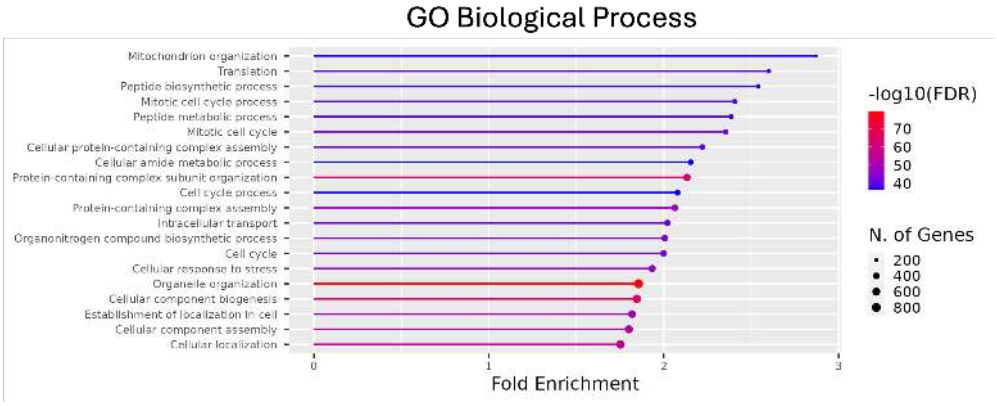

Figure 3.44 Reactome analysis of DEGs upon BRD9 loss in U87 cells

DISCUSSION

Glioblastoma, which is classified as a Grade IV IDH wildtype tumor, is one the most prevalent and aggressive types of brain tumors. The standardized treatment strategy is surgery, followed by chemotherapy and radiotherapy. Since the established "Stupp protocol", which involves concomitant radiotherapy with the golden standard chemotherapeutic agent Temozolomide, there has been no treatment strategy that significantly increases overall survival and progression-free survival of glioblastoma patients (Stupp et al., 2005). There are several reasons affecting therapy response and tumor recurrence in glioblastoma patients, which makes this disease so destructive. Limitations in drug delivery through BBB, tumor heterogeneity, immune evasion, epigenetic factors, hypoxia, and cancer stem cells are some of the factors of therapy resistance in glioblastoma. Although the exact mechanisms are not elucidated yet, current technologies provide a better understanding of therapy response. For instance, intrinsic and adaptive factors that cause intratumoral and intertumoral heterogeneity are one the reasons for therapy resistance, which is currently one of the most studied concepts with the development of single-cell sequencing technologies (Castro et al., 2021; Patel et al., 2014).

Overcoming this recurrence and therapy resistance is only possible if we understand the underlying mechanisms of resistance and develop novel strategies to sensitize these tumors to therapy. In addition to recurrence, another lifetime and life-quality-threatening challenge is the overtreatment of tumor patients. Not only does the therapy develop resistant tumors and fail, but also current treatment options give rise to long-term symptoms. For this reason, it is important to develop novel, tumor-specific treatment strategies to enhance the efficacy of treatments and increase patients' quality of life.

Radiotherapy aims to induce DNA damage in the remaining tumor cells and eradicate them. Regardless of the genetic profiles of their tumors, all patients receive RT. Due to recent technological advancements, improved RT treatments are leading to better palliative care for patients. However, despite the refined RT regimens and TMZ administration, recurrence occurs. Therefore, there is a continuous effort to deliver RT in a more effective way with lower doses, causing less harm to non-malignant tissue.

In this thesis, we performed an epigenetic drug screen in glioblastoma cells to identify epigenetic mechanisms regulating radiotherapy response. With this high-throughput approach, we identified novel radiosensitizers in glioblastoma and ascribed a new role for one epigenetic protein, BRD9, as a regulator of radiotherapy response.

Epigenetic library screen identifies several potential radiosensitizers

Chemical library screens provide large-scale identification of potential drug candidates and target pathways, not only for cancer or other illnesses but also to elucidate different cellular mechanisms. Depending on the library, these screens can be tailored to answer more specific questions (Badr et al., 2011). In this study, our main question was identifying novel epigenetic targets that can be utilized for radiosensitization. Since cancer cells undergo not only genetic but also epigenetic alterations, it is crucial to identify epigenetic vulnerabilities. In the last decade, there have been several epigenetic modifiers identified regarding gliomagenesis and therapy response (Raviraj et al., 2020). Although there is evidence for epigenetic regulation of radiotherapy response in different cancer types, it is not elucidated yet in glioblastoma.

In this thesis, we utilized an epigenetic chemical library consisting of 125 inhibitors targeting over 25 classes of epigenetic modifiers. To remain faithful to the notion of "radiosensitization" and to eliminate the cytotoxicity of inhibitors, we used 1:10 of the working concentration of the chemical library, so that the inhibitor treatment itself could not decrease cell viability. Implementing low-dose screens also carries translational value, which further could be implemented in clinics. Minimizing the harm from radiotherapy by combining low-dose IR and low-dose epigenetic inhibitors potentiates a clinical value.

Primarily, we have performed epigenetic drug screens on U373 cells with replicates. And selected hits taking IR-only control samples as a reference (**Figure 3.2**, **Figure 3.3).** This screen was also conducted on U87 cells as n=1 (**Figure 6.1)**. When we analyze U373 and U87 screens and chemicals that are common between the two screens, Bromodomain and HDAC inhibitors hold the majority as potential radiosensitizers (**Table 7.1)**. Recently, it shown in various cancers that HDAC and Bromodomain family members have a role in tumorigenesis and therapy response (Morel et al., 2020). In addition, with the increasing number of preclinical and clinical trials regarding epi-drugs,

it is reported that Bromodomain and extra-terminal domain inhibitors (BETi) showing alterations in oncogenic transcription and DDR signaling (Morel et al., 2020). Specifically, it is known that HDAC inhibitors have a radiosensitizer effect in glioblastoma (McClure et al., 2018). PRMT family members, which have recently been shown to have a role in DNA damage response and regulation of stemness in glioblastoma are also among the hits from our screen (Jarrold & Davies, 2019; Sachamitr et al., 2021).

BRD9 inhibition primes glioblastoma cells to radiotherapy

For this thesis, BRD9 inhibitors were selected as potential radiosensitizers. Although the exact function of BRD9 is not extensively elucidated yet, its role in cellular reprogramming and cancer cell survival in synovial sarcoma and rhabdomyosarcoma has been studied. A high number of chemical inhibitors and PROTAC-based degraders targeting BRD9 provide useful tools to interrogate and study the function of BRD9 in various contexts. From 3 out of 4 inhibitors targeting BRD9 in our library showed sensitization in combination with IR. While focusing on I-BRD9, which has the highest specificity to BRD9, we also used two different inhibitors, BI-9564 and BI-7273. BI-9564 and BI-7273 show a slight decrease in cell viability in U373 cells (**Figure 3.6**,**Figure 3.7**)**.** While it requires high doses of these inhibitors, BI-9564 could be useful in *in vivo* radiosensitization experiments (Martin et al., 2016). In addition to chemical inhibition, we have also implemented a PROTAC, Von Hippel Lindau (VHL)-based BRD9 targeting degrader VZ185. PROTACs are state-of-the-art chemicals targeting specific proteins and leading to proteasomal degradation. This technology provides a useful tool for eliminating protein itself without disruption of the gene (Zoppi et al., 2019). Although we have observed a slight decrease in colony density (**Figure 3.8)**, it requires further optimizations to observe the maximum effect of this degrader. Another BRD9 degrader, dBRD9 (Remillard et al., 2017), could be utilized to understand the radiosensitization effect of BRD9 degradation. To fully understand the specificity of BRD9 on radiosensitization, investigation other members of SWI/SNF complex and targeting and its role on radiosensitization would be crucial. And to complement the chemical approach understanding role of epigenetic modifiers in radiosensitization, CRISPR/Cas9 based targeting epigenetic modifiers (EPIKOL) could be also implemented to identify additional candidates to combine with I-BRD9 and other BRD9 inhibitors.

In the chemical inhibition of BRD9, we see the radiosensitization effect with only pre-treatment of the cells with the inhibitor. This "priming" could suggest that the cell death was not caused by simultaneous action of inhibitor and IR, but by long-term changes that BRD9 inhibition causes, which makes glioblastoma cells more vulnerable to IR. This vulnerable state could originate from alterations in the transcriptional level, specifically in chromatin conformation. BRD9 inhibition results in disruption in SWI/SNF complex and "acetyl reads" (Wang et al., 2019), therefore required epigenetic modifications could be disrupted or activated. This may cause cells to become more vulnerable to IR, which also alters access of DDR machinery to damaged sequences after IR. Further work is needed to test this model, whereby the activation of DDR signaling components as well as the repairing of the DSBs upon IR treatment will be explored by comprehensive methodologies.

After the establishment of a pre-treatment strategy and working doses of I-BRD9 and IR; we tried this combination in various cell lines to observe the specificity of this radiosensitization effect. In both adherent cell lines and patient-derived primary glioblastoma cells growing in suspension, we observed a cumulative effect on cell viability with increasing doses of I-BRD9 and IR. As a non-malignant cell line, we used I-NHA. Although we did not observe any radiosensitization in I-NHA through BRD9 inhibition, further characterization of this combination treatment would provide a better understanding of the cancer-specific effects of BRD9. We also observed slightly different effects of U87 and U373 cells. This difference might have originated from the genetic background of these cells, where U373 is p53-wt, whereas U87 cells are p53-mutant (Cerrato et al., 2001).

In addition to glioblastoma cells, we tried this combination treatment for prostate adenocarcinoma and breast cancer cells as a proof-of-concept. Since we also observed a radiosensitization effect on these cells, this could hint that radiosensitization caused by BRD9 inhibition may be applicable to several other cancer types besides glioblastoma. In addition, to establish the effect of BRD9 inhibition on malignant cell lines, non-malignant cell lines could be implemented for further studies. To support this notion, this combination treatment can be expanded to several different cancer types and their non-malignant pairs. Since it is shown that BRD9 inhibition causes a decrease in cell survival in hematological malignancies and sarcomas, this low-dose combination treatment could be implemented on these cell lines.

Combination treatment of I-BRD9 and IR causes an increased number of apoptotic cells and a delay in DNA damage repair

Since the cell viability and colony density of glioblastoma cells decreased after combination treatment, we performed Annexin staining to identify the mechanism of cell death. Combination treatment causes a higher number of apoptotic cells in U87 cells than in U373 cells. Since radiotherapy can drive the cells to different cell death mechanisms, such as ferroptosis, pyroptosis, apoptosis, autophagy, or cells undergoing senescence, the governing population of the cells might not be apoptotic after combination treatment (Jiao et al., 2022). Although we showed that combination treatment causes a decrease in cell number and cell viability, the main mechanism of cell death should be elucidated in future studies. Future work will involve using inhibitors of these cell death modalities, such as Caspase Inhibitors like ZVAD-FMK (F Van Noorden, 2001), ferroptosis inhibitors like Ferrostatin (Lei et al., 2021b), and autophagy or pyroptosis inhibitors (Y. Fang et al., 2020), and testing whether these inhibitors could abrogate I-BRD9 mediated radiosensitization.

As the main mechanism of action of radiotherapy is to generate DNA damage, and the most cytotoxicity originates from DNA DSBs, γH2AX analysis is a good indicator to investigate both generated DNA damage and the repair efficiency. In our cell lines, increased DNA damage burden was observed as expected, by increasing H2AX activation after IR treatment which was gradually cleared in control groups. On the other hand, activated H2AX levels were not higher in the combination group as IR-only treated samples, so the clearance of H2AX foci failed. These results were also complemented with immunofluorescence staining with H2AX and 53BP1. A similar pattern was observed with H2AX activation, where foci clearance was impaired compared with the control groups. Again, also 53BP1 foci clearance was slower in combination treatment. On the other hand, I-BRD9 treatment possibly causes increased expression of H2AX and 53BP1, which may lead to cells preferring NHEJ, rather than HR.

All these results suggest that combination treatment causes high damage burden and prior I-BRD9 treatment causes alterations in DNA repair efficiency that radiosensitization effect occurs. Since H2AX activation and 53BP1 accumulation and clearance show only the initiation of DDR, it would be useful to incorporate and analyze

downstream DDR effectors to fully comprehend alterations in DNA repair. In addition to those, comet assay can be utilized in order understand the differences in DNA damage generation.

BRD9 levels affect the radiotherapy response

To complement the chemical approach, genetic ablation of BRD9 was performed to see the effect on radiotherapy response. Although the clinical translation of CRISPR/Cas9 based genetic manipulation is rather more difficult, this approach provides incredible insights on understanding the role and mechanism of gene of interest, and a model for studying the chronic effects of loss-of-function. We showed that BRD9 KO was detrimental to the growth of U87 cells, but not to U373 cells or I-NHAs. While I-NHAs were not radiosensitized by BRD9 KO, U373 cells were markedly more radiosensitive, as BRD9 KO cells exhibited far less growth upon IR, compared to controls. This effect was also observed in our own radiotherapy persistent, IR-surv cells, which serve as a useful source to understand the role of cell signaling pathway alterations in radiotherapy response. This study provided little evidence about role of BRD9 in radiotherapy persistence, where we also showed that BRD9 basal expression levels were changed in IR-surv cells. Further experiments and studies could provide better understanding about role of epigenetic modifiers in radiotherapy resistance.

To model increased expression of BRD9 and test its function in IR response, we employed gain-of-function approach with overexpression vectors. While we successfully generated BRD9-overexpressing cells, the basal response to IR was not markedly altered, prompting further studies. Perhaps the increased BRD9 protein levels may not necessarily affect the radiotherapy response in control cells, therefore these experiments will be conducted in BRD9 KO cells using PAM-mutant versions.

In order to investigate the levels on BRD9 on a translational level, histological staining for glioblastoma patients samples could be performed for I-BRD9. This also could be expanded to primary tumor versus recurrent tumor and BRD9 staining levels.

Cell cycle and ribosome-related pathways are altered upon BRD9 perturbation

Transcriptomic analysis provides useful resources and understanding in complex cellular pathways and alterations in cellular response. RNA-seq we performed with chemicals had 4 conditions: control (DMSO), IR only, I-BRD9 only and combination. We performed pairwise analysis for every comparison possible. But since our ultimate question was to understand to role of BRD9, DMSO vs I-BRD9, DMSO vs Combination and IR-Only vs Combination comparisons provided better understanding on underlying mechanisms. Overall, BRD9 inhibition, itself or in combination causes downregulation of ribosomal pathways, translation and myc related pathways. It is previously shown BRD9 serves as a transcription factor for myc, which regulates its transcription (Bell et al., 2019; Woodley et al., 2021). The association between BRD9 and ribosomal biogenesis is also previously reported (Kurata et al., 2023). Decrease in translation could be reflected as reduction of DNA repair proteins, inhibition of survival pathways and induction of cellular stress, all of which make cells vulnerable to IR. Furthermore, increased expression of proteins related with histone acetylation and histone methylation also could result in decreased transcription, therefore downregulation in translation. These findings will be elaborated with experiments in the future, where we will test the histone levels, as well translation activity, in cells treated with combination.

It is also striking that in comparison of IR vs Combination conditions, the differentially expressed genes in combination treatment is exclusive to I-BRD9 only treatment, also same with control and IR only samples, shown in **Figure 3.36C**. This could suggest that the effect I-BRD9 causes at transcriptional level has a distinct signature, completely different than IR. This shows that this combination treatment does not increase the efficacy of IR in an additive manner, but targets two distinct pathways to cause cell death, in an orthogonal manner.

From RNA-seq analysis, both for chemical aspect and genetic ablation of BRD9, cell cycle dysregulation caught our attention. Even though cancer cells have already disrupted cell cycle regulation, significant upregulation of proteins involves in cell cycle and G2/M phase showed that BRD9 inhibition causes cell cycle aberrations. The underlying reasons could be mitotic catastrophe, loss of cell cycle checkpoint control and increased levels of DNA damage and cellular stress. Since cell cycle is a balanced process to ensure successful division, upregulation of cell cycle activators can disrupt this balance, leading to uncontrolled cell division. In addition, this imbalance often results in

cellular stress and activation of apoptotic pathways to eliminate these cells (Dipaola, 2002). We showed that several genes involved in cell cycle, such as PLK1, CDK1, AURKA, CCNB1 and CCNB2 were upregulated upon combination treatment. Studies show that upregulation and activation of PLK1 and CDK1 are crucial in progression of cells to mitosis (Metselaar et al., 2022; Xu et al., 2021; Z. Zhang et al., 2020). These results could suggest that although we observe cell cycle arrest at G2/M phase, further upregulation of these genes may result in progression to mitosis without proper repair of generated DNA damage. This could cause the cell death we have been observing in combination treatment. In addition, we observe cell death several days later after cell cycle arrest, this findings also support our hypothesis **Figure 4.1**. Further investigation regarding cell cycle and checkpoint regulation could provide better understanding of vulnerability of cells deficient in BRD9.

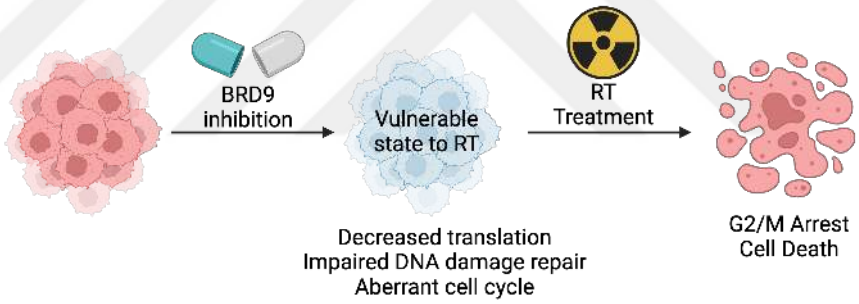

Figure 4.1 Proposed mechanism for radiosensitization through BRD9

FUTURE DIRECTIONS

In this thesis, we identified BRD9 as a novel regulator for IR response in glioblastoma. We showed the radiosensitization effect through different BRD9 inhibitors and different glioblastoma cell lines. BRD9 holds the potential for further investigation of ionizing radiation response and its epigenetic regulation. Since this combination treatment is tested in U87 cells and with *in vivo* compatible BRD9 inhibitor, BI-9564, it would be valuable to test the combination effect in an *in vivo* setup, either with drug treatment or with irradiation of BRD9 KO cells. We already started optimizing in vivo studies, as shown in **Appendix C.**

After showing the effect of combination treatment in the context of DNA damage generation and DNA damage response, it would be extremely valuable to fully understand the effect of BRD9 inhibition on DNA damage response and repair, starting with investigating downstream effectors in DDR and repair pathway of choice.

We showed that genetic ablation of BRD9 KO sensitizes cells to IR, to fully understand the generated phenotype and complement the genetic approach, a competition assay between NT1 and BRD9 KO cells will be useful. In addition, to investigate the rescue effect of BRD9 overexpression on BRD9 KO cells, cloning, and transduction of PAM-resistant overexpression plasmid will propose a broader understanding of the effect of BRD9 levels on therapy response.

We have performed RNA-seq on U373 cells treated with I-BRD9 and IR, and also U87 cells, NT1, and BRD9 KO conditions. Although transcriptomic analysis has provided insights about transcriptomic alterations, to fully understand it we need to expand our RNA-seq experiments to U373 NT1 and BRD9 KO and/or U87 cells treated with I-BRD9 and IR. In addition to RNA-seq, it is important to identify genes that are transcriptionally regulated by BRD9 and their role in therapy response. It would be extremely useful to perform ATAC-seq and ChIP-seq to identify genes regulated by BRD9 which could be the source of radiosensitizing effect.

Lastly, we have shown that I-BRD9 and IR combination treatment causes cell cycle alterations and arrest at the G2/M phase. We will investigate aberrations in the cell cycle and cell cycle checkpoints in a broader concept to fully uncover the mechanism of this treatment strategy.

Appendix A. U373 epigenetic library screen results

Table 6.1 Epigenetic library screen results for U373 cells

	Drug Only			Drug + IR (4 Gy)		
Drug Number	**% Cell viability**	**% SEM**	**Rep #**	**% Cell viability**	**% SEM**	**Rep #**
Control	100	2,87884421	36	66,938061	9,69963926	36
DMSO	101,906233	2,05614315	105	68,5920955	5,06595463	105
25	141,039234	10,5779819	3	88,4982018	12,7485763	3
10	136,542295	6,2187181	3	92,3797913	27,9268449	3
68	130,034265	7,1268583	3	89,4293758	8,99533217	3
19	127,748101	8,67088154	3	100,077768	8,84106354	3
32	127,377261	5,65613731	3	83,4898308	15,1223354	3
60	126,010045	3,41114241	3	83,1923441	5,68949798	3
84	124,958654	5,69875532	3	77,7295928	5,90091505	3
29	123,772783	5,87778244	3	89,3539853	7,16989898	3
85	123,416206	9,3506305	3	73,6320199	13,7196173	3
105	122,389266	9,51330039	3	100,375254	14,2278994	3
18	122,324063	9,54518894	3	90,9921995	9,81511593	3
43	122,23441	3,5956379	3	87,3754954	14,5500504	3
21	122,209959	5,00385294	3	96,4243871	2,240114	3
106	121,839119	1,95507182	3	89,8246663	4,47950801	3
97	121,20747	5,49460376	3	108,541874	6,15097032	3
26	120,738826	3,8613514	3	54,067179	8,64960199	3
113	118,78275	0,87775189	3	101,162779	13,0964088	3
30	118,611593	0,39447591	3	71,6474172	6,5126497	3
79	118,501564	8,35636498	3	76,6354125	17,6197646	3
46	117,285129	6,5124806	3	104,912944	7,2252725	3
33	116,983567	3,41652589	3	88,2190534	7,31573886	3
50	116,726832	3,80184276	3	84,9945834	32,0767563	3
61	116,182798	6,90139751	3	65,0823352	18,5588454	3
70	114,789094	1,44027267	3	86,892589	7,36058387	3
62	114,479381	6,32882388	3	83,8402945	7,6047202	3
128	114,403991	8,50925273	3	39,2621244	4,3145059	3
81	113,906821	4,70125145	3	78,3429043	10,0549257	3
47	112,456065	7,79586412	3	87,6281553	14,0739879	3
90	111,304832	7,9545984	3	109,244839	2,31774624	3

51	111,084774	4,87792352	3	76,9614252	6,64893687	3
108	110,447011	2,48250572	3	92,5142715	8,65556817	3
166	110,381808	6,42058718	3	29,644748	6,0606048	3
117	110,300305	4,31383468	3	27,2291972	7,7420042	3
118	109,742008	4,36026039	3	121,502919	22,6377857	3
49	108,818985	4,72207046	3	40,539687	1,40350739	3
110	108,560212	5,23430506	3	87,4834871	14,5096272	3
109	108,228087	8,73999377	3	66,4658519	15,8938278	3
54	107,873548	4,00063297	3	57,514764	3,36699621	3
6	107,714617	5,43620236	3	91,5749473	6,19550681	3
16	107,372303	5,35149056	3	90,1955058	5,77641061	3
38	107,188921	5,30622319	3	91,0451765	6,69490653	3
77	107,068704	1,28020665	3	88,1783018	8,78178887	3
20	105,850231	7,58664117	3	74,6976741	12,3476733	3
1	105,628135	11,819578	3	70,596026	5,19633723	3
75	105,226732	8,85986754	3	54,4950708	4,24962887	3
66	104,183491	2,66028534	3	98,2745095	10,9597538	3
164	103,735223	1,61982246	3	80,9387809	10,19927	3
80	103,51109	6,42492774	3	77,7204237	10,9664172	3
91	102,907966	4,56205347	3	30,8876716	5,88174857	3
45	101,803598	4,77186464	3	92,9900464	2,97615352	3
107	101,691531	1,73513607	3	48,0828072	2,0720255	3
5	101,550938	3,51029099	3	21,5412933	3,3827504	3
163	100,06758	8,30766419	3	83,2585655	8,94096876	3
63	99,397216	7,14317616	3	41,3221176	3,91338598	3
96	99,3849905	7,3655231	3	44,0728503	13,8036379	3
2	99,3788778	3,53337048	3	137,062897	5,95917786	3
78	98,8837459	10,3442076	3	64,0156622	19,6902565	3
158	98,7309274	16,9244297	3	65,9279308	23,0858931	3
9	97,7345509	4,48365053	3	29,4634034	2,10053062	3
58	97,6326719	4,1987468	3	109,748121	2,0968455	3
99	97,5226426	13,4057477	3	35,7748067	5,2359452	3
123	97,3494483	12,2712149	3	77,4728577	4,1097361	3
37	97,2516445	6,17592429	3	60,9256725	9,80582329	3
122	96,9806464	4,96534438	3	9,97599052	16,7784499	3
132	96,6953852	12,6571603	3	6,95935368	11,3649574	3
121	96,3306584	8,79606922	3	16,6419327	6,723602	3
131	95,7479106	19,051706	3	12,3385643	7,2394483	3
65	95,6358437	6,11328726	3	66,1785531	10,9149481	3

39	95,5747164	8,0171198	3	73,4119613	18,3416807	3
67	95,3791087	8,08813756	3	54,4645071	16,2199657	3
17	94,8309997	0,90812396	3	50,8182581	3,45219881	3
22	94,6353921	0,96023939	3	87,6057419	9,85028241	3
124	94,5212876	13,4146268	3	19,7176594	5,008273	3
127	94,4479347	10,8272604	3	23,6664889	1,9502444	3
15	93,7408946	2,89433035	3	40,7322382	14,734556	3
35	93,4617461	3,86365351	3	43,1834467	1,19622615	3
101	93,0623805	2,98846178	3	80,1991395	10,2155986	3
133	90,7823287	8,14913256	3	38,4307919	5,493595	3
126	90,6132096	5,22083159	3	34,4269477	8,720778	3
83	90,4277899	2,98603057	3	56,4226212	4,26958119	3
165	90,4277899	8,33600075	3	18,1120465	6,80643454	3
100	89,8083656	4,64336076	3	70,455433	13,1291585	3
92	89,4416013	6,0845051	3	101,737376	20,9011547	3
86	89,307121	5,28419979	3	41,8997715	4,6634172	3
4	88,0051075	1,33032108	3	87,3693826	4,53577475	3
55	86,3404049	17,9349382	3	39,0237276	9,0501992	3
3	86,1325717	6,88491771	3	44,7330261	17,305086	3
120	85,9512271	12,858284	3	33,3694438	7,3754788	3
57	84,7307169	11,721777	3	60,714783	6,9671989	3
64	84,6981156	8,13080177	3	21,6666044	9,6992911	3
134	83,8769709	13,3237737	3	62,4049554	7,7343054	3
148	83,4409289	5,54601555	3	24,8788489	7,30232814	3
143	83,1556677	11,5669078	3	53,4131159	21,354486	3
152	82,8398428	6,97956909	3	60,8910336	5,6499409	3
149	82,780753	12,8465167	3	39,2071098	7,0934648	3
154	82,625897	8,02977187	3	26,1105659	8,3319444	3
27	82,5912581	5,9000382	3	101,132215	5,17450914	3
104	81,8781052	3,92916932	3	60,7056139	27,7482223	3
161	81,389086	5,59456275	3	69,6791151	17,5724592	3
150	80,7941128	5,52939378	3	31,9431379	6,85474011	3
125	80,6392567	17,068764	3	1,6718342	1,0614417	3
82	79,4004082	2,83041593	3	43,351547	5,89461717	3
144	78,7748712	8,03965968	3	24,8258718	4,7661924	3
112	78,6954056	9,50057672	3	19,6432877	4,73865294	3
146	78,1635973	12,659539	3	38,8739655	3,3749959	3
167	76,6456004	18,8542114	3	18,3779507	7,7025194	3
88	74,2269932	29,6549452	3	31,5509038	16,0008969	3

129	73,6727715	6,24798669	3	40,3542672	14,1421517	3
116	71,2256382	6,61724229	3	5,51369084	12,8905139	3
151	69,1208183	17,0840916	3	73,2122785	14,6353247	3
153	63,9474033	8,67313904	3	70,2679757	21,1246478	3
135	60,5772463	10,5838693	3	48,5229245	17,0467462	3
28	45,9963256	8,04845401	3	37,0309746	13,3685109	3
114	43,1253757	22,1556218	3	34,5522588	6,6133855	3
53	43,1111126	11,7401983	3	31,0527156	6,04571113	3
162	38,9116607	35,1120194	3	26,9714433	9,98178127	3
69	37,6422485	15,7796363	3	72,9738816	12,6235483	3
24	36,4074752	15,3381924	3	11,0885091	6,6355618	3
76	35,3581216	14,5099237	3	29,363562	3,1447329	3
89	22,03235	5,61592099	3	23,0878163	5,4565808	3
23	18,1222344	12,139462	3	6,89211355	3,4340687	3
159	15,7504916	13,7309004	3	14,342524	2,7427065	3
115	1,36517844	6,30232607	3	0,82827617	1,5838663	3

Appendix B. U87 epigenetic library screen results

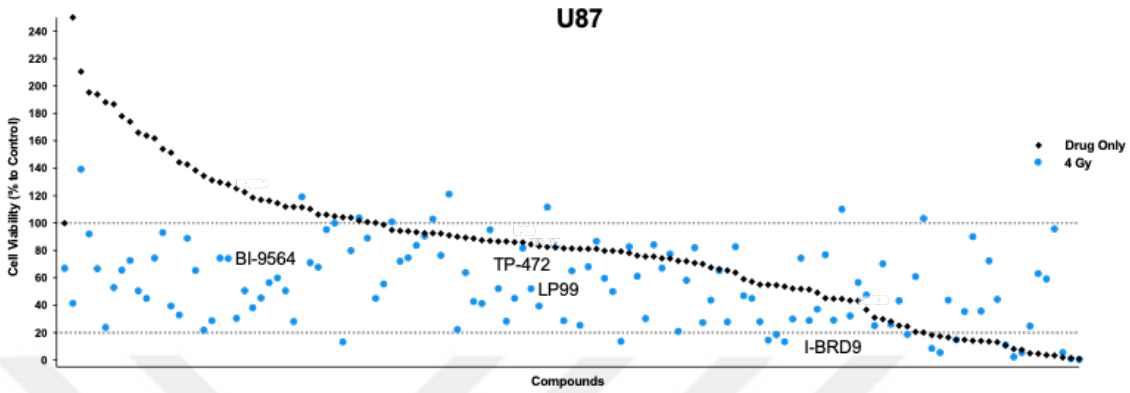

Figure 6.1 Epigenetic library screen for U87 cells. Scatter plot representation of epigenetic drug screen on U87 cells. Colored dots show the changes in cell viability when Taxol given epigenetic chemical is combined with IR.

Epigenetic chemical library is also implemented in U87 cells. The same protocol was used as library treatment and IR treatment and results were analyzed using CTG assay. For the U87 screen, the replicate number was n=1. Library screen results are represented in **Figure 6.1**. When both U373 and U87 screens were analyzed according to "Combination%-Drug Only%", common radiosensitizer candidates are listed in **Table 7.1**. In addition, raw results for the epigenetic screen for U87 cells are listed in **Table 7.2**

Table 7.1 Common chemicals from screens performed onU373 and U87 cells

No	Drug	Class
132	AGK2	HDAC
131	TMP269	HDAC
166	Cyclophosphamide	
5	Bromosporine	Bromodomain
121	TP-064	PRMT
124	A-395N	Methyl Lysine Binder
165	Staurosporine	

49	LLY-507	Histone MethylTransferase
9	SGC-CBP30	Bromodomain
112	NVS-CECR-C	Bromodomain
167	MS-275	
63	UNC1215	Methyl Lysine Binder
154	PFI-5	Histone MethylTransferase
133	GSK6853	Bromodomain
75	GSK484	PAD4
85	KDOAM-25a	KDM
84	Tubastatin A	HDAC
10	I-CBP112	Bromodomain
17	PB1/SMARCA	Bromodomain
60	ML324	Hisyone demethylase
3	PFI-1	Bromodomain
146	TDO20824a	Methyl Lysine Binder
37	UNC0642	Histone MethylTransferase
82	PCI-34051	HDAC
1	JQ1	Bromodomain
78	NI-57	Bromodomain

Table 7.2 Epigenetic library screen results for U87 cells

	Drug Only%	**Drug + IR (4Gy)**
DMSO	100	67
70	250	41,5
60	210,6	139,4
121	195,4	92
77	193,9	66,7
154	188,2	23,9
108	186,8	52,9
110	178	65,7
10	174	72,7
39	166	50,5
97	163,8	45,1
105	161,8	74,4
123	154,1	93,1
146	151,4	39,5
165	144,3	32,9
132	142,7	88,9
133	138,5	65,4
167	134,4	21,9
75	131,3	28,8
124	129,7	74,4
90	128,1	74,2
164	125,3	30,5
92	122,6	50,7
53	118,6	38,2
63	117	45,3
16	116,2	56,5
6	114,5	60
49	111,9	50,7
78	111,8	28,1
152	111,5	119,1
129	110,2	71,2
85	106,2	67,8
54	106,1	95,2
106	104,9	99,9
5	104,3	13,3
128	104	79,9
47	101,7	103,8

38	100,8	89
163	100,2	45,1
50	98,8	55,5
25	94,9	101
51	94,4	72,1
91	94	74,7
21	93,4	83,7
20	92,7	90,6
150	92,6	102,9
55	92,4	76,5
22	91	121,1
45	90	22,3
151	89,3	63,9
84	88,7	42,8
80	87,5	41,4
127	87	95,1
18	86,6	52,2
131	86,6	28,3
166	86	45,1
126	85,9	81,7
79	84,4	52,1
112	83,2	39,5
43	82,6	111,7
46	82,3	82,9
66	81,6	28,7
81	81,4	65,1
37	81,2	25,4
148	81,1	68,2
19	81,1	86,7
130	79,8	59,7
62	79,8	50,1
1	79,3	13,7
120	78,2	82,7
30	76,3	61,2
9	75,6	30,3
96	75,6	84,2
99	74,3	67,2
134	74,1	77,5
4	72,5	21

33	72,1	58,2
158	70,8	82
58	70,1	27,5
32	67,5	43,8
109	66,4	65,3
17	65,4	27,9
67	63,9	82,7
101	59,1	47
104	57,2	45,1
107	55,1	28
3	55	14,6
82	54,7	18,6
57	53,7	13,4
15	52,2	30
122	51,9	74,5
86	51,5	28,9
113	49,2	37,2
161	45,2	76,9
35	44,8	29,1
149	44,6	110,1
125	43,5	32,3
90	43,3	56,7
28	36,7	47,5
117	31,1	25,1
61	29,9	70,3
2	28,1	26,1
88	25,1	43,3
26	24,6	18,7
69	20,5	61
100	20,1	103,4
24	18,3	8,5
23	17,4	5,5
64	16,5	43,8
116	14,9	14,8
118	14,9	35,5
29	14,1	90,1
27	14	35,8
153	13,6	72,5
83	13,1	44,3

76	10,9	11
89	8,1	2,4
114	7,6	5,5
65	4,9	24,8
135	4,6	63,1
144	3,7	59,3
143	3,4	95,8
162	2	5,5
159	1,4	1
115	0,9	0,4

Appendix C. In vivo irradiation optimization and investigation of metabolic analysis upon irradiation

These experiments were performed with approval of Koç University Ethical Committee with approval number 2020.HADYEK.007. In order to investigate effect of ionizing radiation in vivo and optimize the dosage for further experiments, firstly C57BL/6 mice were treated either 1 Gy or 2 Gy daily for two weeks until total exposed dose reach to 10 Gy or 20 Gy. At the end of each week, mice were weighed, and blood samples were collected. 2 day holiday were set between two weeks (**Figure 8.1**).

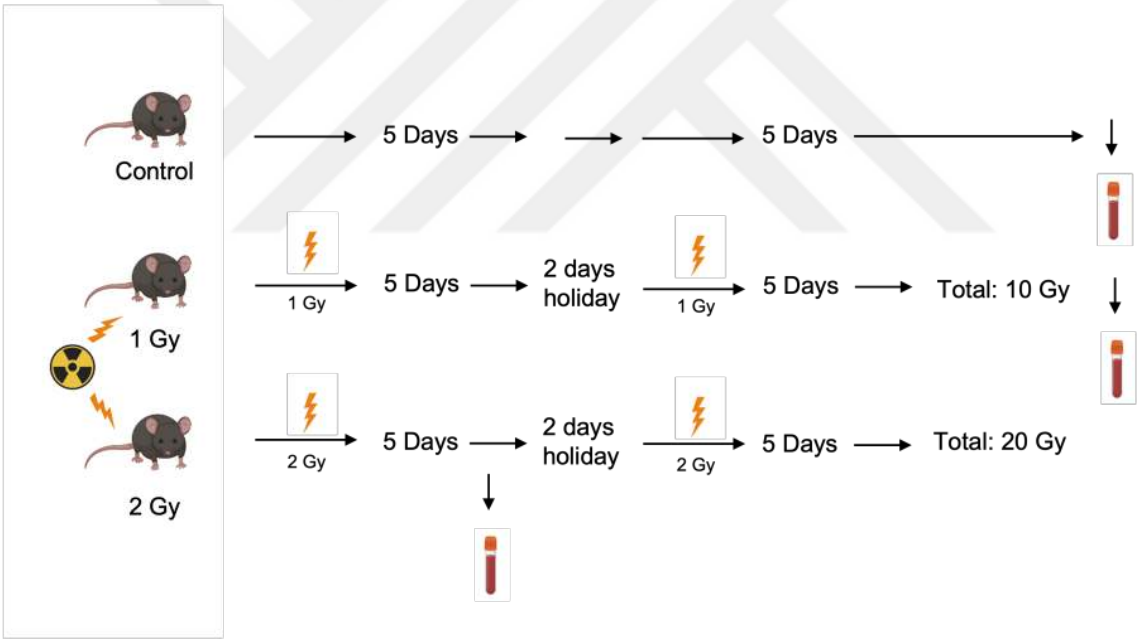

Figure 8.1 Schematic representation of in vivo irradiation optimization studies

Compared to control, irradiated groups were lost around 2 grams at the end of the setup **(Figure 8.2).**

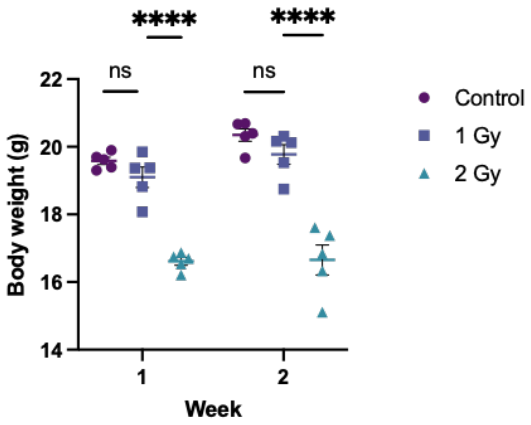

Figure 8.2 Body weight changes upon ionizing radiation treatment

The blood analysis results showed that white blood cell levels, hemoglobin levels and red blood cell levels were decreased upon ionizing radiation. At week 3 HGB and RBC levels were significantly decreased at 10 Gy IR received mice. **(Figure 8.3).**

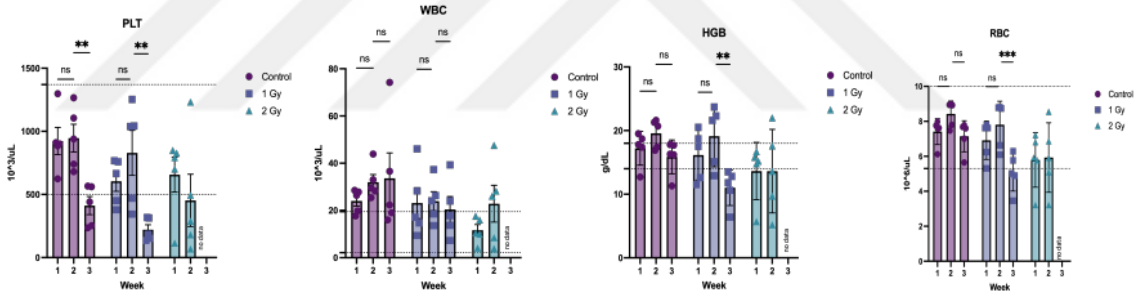

Figure 8.3 Platelet (PLT), White Blood Cell (WBC), Hemoglobin (HGB) and Red Blood Cell levels upon 2-week exposure to ionizing radiation.

After the irradiation experiment, 20 Gy IR received mice were dead, the blood samples were not collected. At week 4, 10 Gy IR received mice were transferred to metabolic cage in order to investigate the fundamental metabolic alterations upon ionizing radiation. Oxygen consumption, carbon dioxide production levels, feeding and water intake habits were analyzed for 5 days.

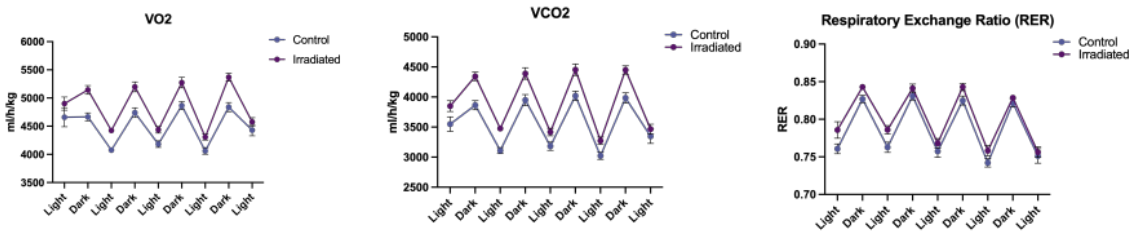

Figure 8.4 Respiratory alterations upon IR exposure

It is shown that irradiated mice have higher oxygen consumption and carbon dioxide production rate compared to control groups. Respiratory exchange ratio (RER) also showed that irradiated mice have higher respiration rate **Figure 8.4**. As DNA repair and genomic maintenance requires high energy, these results may suggest that irradiated mice have higher energy consumption when compared with non- irradiated mice. We observed that food intake is also altered, irradiated mice have higher food intake. Any significant change in water intake between control and irradiated groups did not observed **Figure 8.5**.

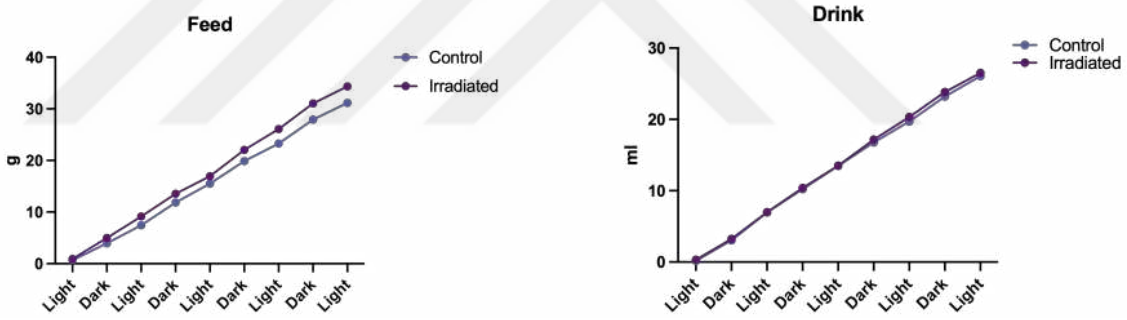

Figure 8.5 Cumulative Feed and water intake amounts of control and irradiated mice

BIBLIOGRAPHY

An, Z., Aksoy, O., Zheng, T., Fan, Q. W., & Weiss, W. A. (2018). Epidermal growth factor receptor and EGFRvIII in glioblastoma: Signaling pathways and targeted therapies. In *Oncogene* (Vol. 37, Issue 12, pp. 1561–1575). Nature Publishing Group. https://doi.org/10.1038/s41388-017-0045-7

Andreoli, A., Bertorelle, R., Leonardi, M., Blatt, V., Ermani, M., Bartolini, S., Franceschi, E., Pession, A., Tallini, G., Tosoni, A., Calbucci, F., Spagnolli, F., Brandes, A. A., & Frezza, G. (2008). MGMT Promoter Methylation Status Can Predict the Incidence and Outcome of Pseudoprogression After Concomitant Radiochemotherapy in Newly Diagnosed Glioblastoma Patients . *Journal of Clinical Oncology*, *26*(13), 2192–2197. https://doi.org/10.1200/jco.2007.14.8163

Annovazzi, L., Mellai, M., & Schiffer, D. (2017). Chemotherapeutic drugs: DNA damage and repair in glioblastoma. *Cancers*, *9*(6), 1–17. https://doi.org/10.3390/cancers9060057

Aparicio, T., Baer, R., & Gautier, J. (2014). DNA double-strand break repair pathway choice and cancer. *DNA Repair*, *19*, 169–175. https://doi.org/10.1016/j.dnarep.2014.03.014

Auffinger, B., Spencer, D., Pytel, P., Ahmed, A. U., & Lesniak, M. S. (2015). The role of glioma stem cells in chemotherapy resistance and glioblastoma multiforme recurrence. *Expert Review of Neurotherapeutics*, *15*(7), 741–752. https://doi.org/10.1586/14737175.2015.1051968

Awasthi, P., Foiani, M., & Kumar, A. (2016). ATM and ATR signaling at a glance. *Journal of Cell Science*, *129*(6), 1285–1285. https://doi.org/10.1242/jcs.188631

Badr, C. E., Wurdinger, T., & Tannous, B. A. (2011). Functional drug screening assay reveals potential glioma therapeutics. *Assay and Drug Development Technologies*, *9*(3), 281–289. https://doi.org/10.1089/adt.2010.0324

Bakir, B., Chiarella, A. M., Pitarresi, J. R., & Rustgi, A. K. (2020). EMT, MET, Plasticity, and Tumor Metastasis. *Trends in Cell Biology*, *30*(10), 764–776. https://doi.org/10.1016/j.tcb.2020.07.003

Balentova, S., & Adamkov, M. (2015). Molecular, cellular and functional effects of radiation-induced brain injury: A review. *International Journal of Molecular Sciences*, *16*(11), 27796–27815. https://doi.org/10.3390/ijms161126068

Bannister, A. J., & Kouzarides, T. (2011). Regulation of chromatin by histone modifications. In *Cell Research* (Vol. 21, Issue 3, pp. 381–395). https://doi.org/10.1038/cr.2011.22

Barnaba, N., & LaRocque, J. R. (2021). Targeting cell cycle regulation via the G2-M checkpoint for synthetic lethality in melanoma. *Cell Cycle*, *20*(11), 1041–1051. https://doi.org/10.1080/15384101.2021.1922806

Baskar, R., Dai, J., Wenlong, N., Yeo, R., & Yeoh, K. W. (2014a). Biological response of cancer cells to radiation treatment. In *Frontiers in Molecular Biosciences* (Vol. 1, Issue NOV). Frontiers Media S.A. https://doi.org/10.3389/fmolb.2014.00024

Baskar, R., Dai, J., Wenlong, N., Yeo, R., & Yeoh, K.-W. (2014b). Biological response of cancer cells to radiation treatment. *Frontiers in Molecular Biosciences*, *1*(November), 1–9. https://doi.org/10.3389/fmolb.2014.00024

Baskar, R., Lee, K. A., Yeo, R., & Yeoh, K. (2012). Cancer and Radiation Therapy: Current Advances and Future Directions. *International Journal of Medical Sciences*, *9*(3), 193–199. https://doi.org/10.7150/ijms.3635

Begg, K., & Tavassoli, M. (2020). Inside the hypoxic tumour: reprogramming of the DDR and radioresistance. In *Cell Death Discovery* (Vol. 6, Issue 1). Springer Nature. https://doi.org/10.1038/s41420-020-00311-0

Békés, M., Langley, D. R., & Crews, C. M. (2022). PROTAC targeted protein degraders: the past is prologue. In *Nature Reviews Drug Discovery* (Vol. 21, Issue 3, pp. 181–200). Nature Research. https://doi.org/10.1038/s41573-021-00371-6

Bell, C. M., Raffeiner, P., Hart, J. R., & Vogt, P. K. (2019). PIK3CA cooperates with KRAS to promote MYC activity and tumorigenesis via the bromodomain protein BRD9. *Cancers*, *11*(11). https://doi.org/10.3390/cancers11111634

Bouleftour, W., Rowinski, E., Louati, S., Sotton, S., Wozny, A.-S., Moreno-Acosta, P., Mery, B., Rodriguez-Lafrasse, C., & Magne, N. (2021). A Review of the Role of Hypoxia in Radioresistance in Cancer Therapy. *Medical Science Monitor*, *27*, 1–7. https://doi.org/10.12659/MSM.934116

Boustani, J., Grapin, M., Laurent, P. A., Apetoh, L., & Mirjolet, C. (2019). The 6th R of radiobiology: Reactivation of anti-tumor immune response. *Cancers*, *11*(6), 1–16. https://doi.org/10.3390/cancers11060860

Brandes, A. A., Tosoni, A., Franceschi, E., Reni, M., Gatta, G., & Vecht, C. (2008). Glioblastoma in adults. *Critical Reviews in Oncology/Hematology*, *67*(2), 139–152. https://doi.org/10.1016/j.critrevonc.2008.02.005

Brem, S., & Abdullah, K. G. (2017). Glioblastoma. In S. De Vleeschouwer (Ed.), *Glioblastoma*. Codon Publications. https://doi.org/10.15586/codon.glioblastoma.2017

Brien, G. L., Remillard, D., Shi, J., Hemming, M. L., Chabon, J., Wynne, K., Dillon, E. T., Cagney, G., Van Mierlo, G., Baltissen, M. P., Vermeulen, M., Qi, J., Fröhling, S., Gray, N. S., Bradner, J. E., Vakoc, C. R., & Armstrong, S. A. (2018). Targeted degradation of BRD9 reverses oncogenic gene expression in synovial sarcoma. *ELife*, *7*. https://doi.org/10.7554/eLife.41305

Burgess, R. C., & Misteli, T. (2015). Not All DDRs Are Created Equal: Non-Canonical DNA Damage Responses. *Cell*, *162*(5), 944–947. https://doi.org/10.1016/j.cell.2015.08.006

Canela, A., Maman, Y., Jung, S., Wong, N., Callen, E., Day, A., Kieffer-Kwon, K. R., Pekowska, A., Zhang, H., Rao, S. S. P., Huang, S. C., Mckinnon, P. J., Aplan, P. D., Pommier, Y., Aiden, E. L., Casellas, R., & Nussenzweig, A. (2017). Genome Organization Drives Chromosome Fragility. *Cell*, *170*(3), 507-521.e18. https://doi.org/10.1016/j.cell.2017.06.034

Castro, L. N. G., Tirosh, I., & Suvà, M. L. (2021). Decoding cancer biology one cell at a time. *Cancer Discovery*, *11*(4), 960–970. https://doi.org/10.1158/2159-8290.CD-20-1376

Cerrato, J. A., Yung, W. K. A., & Liu, T.-J. (2001). Introduction of mutant p53 into a wild-type p53-expressing glioma cell line confers sensitivity to Ad-p53-induced apoptosis 1. In *Neuro-Oncology* (Vol. 3).

Chaddad, A., Kucharczyk, M. J., Daniel, P., Sabri, S., Jean-Claude, B. J., Niazi, T., & Abdulkarim, B. (2019). Radiomics in glioblastoma: Current status and challenges facing clinical implementation. *Frontiers in Oncology*, *9*(MAY), 1–9. https://doi.org/10.3389/fonc.2019.00374

Chapman, C. H., Hara, J. H., Molinaro, A. M., Clarke, J. L., Oberheim Bush, N. A., Taylor, J. W., Butowski, N. A., Chang, S. M., Fogh, S. E., Sneed, P. K., Nakamura, J. L., Raleigh, D. R., & Braunstein, S. E. (2019). Reirradiation of recurrent high-grade glioma and development of prognostic scores for progression

and survival. *Neuro-Oncology Practice*, *6*(5), 364–374. https://doi.org/10.1093/nop/npz017

Chen, H. H. W., & Kuo, M. T. (2017). Improving radiotherapy in cancer treatment: Promises and challenges. *Oncotarget*, *8*(37), 62742–62758. https://doi.org/10.18632/oncotarget.18409

Chen, J. (2016). The cell-cycle arrest and apoptotic functions of p53 in tumor initiation and progression. *Cold Spring Harbor Perspectives in Medicine*, *6*(3). https://doi.org/10.1101/cshperspect.a026104

Cheng, B., Pan, W., Xing, Y., Xiao, Y., Chen, J., & Xu, Z. (2022). Recent advances in DDR (DNA damage response) inhibitors for cancer therapy. In *European Journal of Medicinal Chemistry* (Vol. 230). Elsevier Masson s.r.l. https://doi.org/10.1016/j.ejmech.2022.114109

Christmann, M., & Kaina, B. (2017). Epigenetic regulation of DNA repair genes and implications for tumor therapy. *Mutation Research - Reviews in Mutation Research*, *October*, 1–15. https://doi.org/10.1016/j.mrrev.2017.10.001

Clark, P. G. K., Vieira, L. C. C., Tallant, C., Fedorov, O., Singleton, D. C., Rogers, C. M., Monteiro, O. P., Bennett, J. M., Baronio, R., Müller, S., Daniels, D. L., Méndez, J., Knapp, S., Brennan, P. E., & Dixon, D. J. (2015). LP99: Discovery and Synthesis of the First Selective BRD7/9 Bromodomain Inhibitor. *Angewandte Chemie*, *127*(21), 6315–6319. https://doi.org/10.1002/ange.201501394

Cochran, A. G., Conery, A. R., & Sims, R. J. (2019). Bromodomains: a new target class for drug development. *Nature Reviews Drug Discovery*, *18*(8), 609–628. https://doi.org/10.1038/s41573-019-0030-7

Crusio, W. E., Dong, H., & Radeke, H. H. (2021). Histone Mutations and Cancer. In D. Fang & J. Han (Eds.), *Advances in Experimental Medicine and Biology* (Vol. 1283). Springer Singapore. https://doi.org/10.1007/978-981-15-8104-5

Davis, M. E. (2016). Glioblastoma: Overview of Disease and Treatment. *Clinical Journal of Oncology Nursing*, *20*(5), S2–S8. https://doi.org/10.1188/16.CJON.S1.2-8

Del Gaudio, N., Di Costanzo, A., Liu, N. Q., Conte, L., Migliaccio, A., Vermeulen, M., Martens, J. H. A., Stunnenberg, H. G., Nebbioso, A., & Altucci, L. (2019). BRD9 binds cell type-specific chromatin regions regulating leukemic cell survival via

STAT5 inhibition. *Cell Death and Disease*, *10*(5). https://doi.org/10.1038/s41419-019-1570-9

Desouky, O., Ding, N., & Zhou, G. (2015). Targeted and non-targeted effects of ionizing radiation. *Journal of Radiation Research and Applied Sciences*, *8*(2), 247–254. https://doi.org/10.1016/j.jrras.2015.03.003

Dewhirst, M. W., Cao, Y., & Moeller, B. (2008). Cycling hypoxia and free radicals regulate angiogenesis and radiotherapy response. *Nature Reviews Cancer*, *8*(6), 425–437. https://doi.org/10.1038/nrc2397

Di Nunno, V., Aprile, M., Gatto, L., Tosoni, A., Ranieri, L., Bartolini, S., & Franceschi, E. (2023). Tumor Microenvironment in Gliomas: A Treatment Hurdle or an Opportunity to Grab? In *Cancers* (Vol. 15, Issue 4). MDPI. https://doi.org/10.3390/cancers15041042

Dillon, M. T., Good, J. S., & Harrington, K. J. (2014). Selective Targeting of the G2/M Cell Cycle Checkpoint to Improve the Therapeutic Index of Radiotherapy. *Clinical Oncology*, *26*(5), 257–265. https://doi.org/10.1016/j.clon.2014.01.009

Dipaola, R. S. (2002). To Arrest or Not To G 2-M Cell-Cycle Arrest Commentary re: A. K. Tyagi et al., Silibinin Strongly Synergizes Human Prostate Carcinoma DU145 Cells to Doxorubicin-induced Growth Inhibition, G 2-M Arrest. In *Clin. Cancer Res* (Vol. 8). http://aacrjournals.org/clincancerres/article-pdf/8/11/3311/2082085/df1102003311.pdf

Du, J., Liu, Y., Wu, X., Sun, J., Shi, J., Zhang, H., Zheng, A., Zhou, M., & Jiang, X. (2023). BRD9-mediated chromatin remodeling suppresses osteoclastogenesis through negative feedback mechanism. *Nature Communications*, *14*(1). https://doi.org/10.1038/s41467-023-37116-5

Erasimus, H., Gobin, M., Niclou, S., & Van Dyck, E. (2016). DNA repair mechanisms and their clinical impact in glioblastoma. *Mutation Research - Reviews in Mutation Research*, *769*, 19–35. https://doi.org/10.1016/j.mrrev.2016.05.005

Etcheverry, A., Aubry, M., de Tayrac, M., Vauleon, E., Boniface, R., Guenot, F., Saikali, S., Hamlat, A., Riffaud, L., Menei, P., Quillien, V., & Mosser, J. (2010). DNA methylation in glioblastoma: Impact on gene expression and clinical outcome. *BMC Genomics*, *11*(1). https://doi.org/10.1186/1471-2164-11-701

F Van Noorden, C. J. (2001). The history of Z-VAD-FMK, a tool for understand-ing the significance of caspase inhibition*. In *acta histochem* (Vol. 103). Urban & Fischer Verlag. http://www.urbanfischer.de/journals/actahist

Fang, Y., Tian, S., Pan, Y., Li, W., Wang, Q., Tang, Y., Yu, T., Wu, X., Shi, Y., Ma, P., & Shu, Y. (2020). Pyroptosis: A new frontier in cancer. In *Biomedicine and Pharmacotherapy* (Vol. 121). Elsevier Masson SAS. https://doi.org/10.1016/j.biopha.2019.109595

Feinberg, A. P., Koldobskiy, M. A., & Göndör, A. (2016). Epigenetic modulators, modifiers and mediators in cancer aetiology and progression. *Nature Reviews Genetics*, *17*(5), 284–299. https://doi.org/10.1038/nrg.2016.13

Friedman, H. S., Kerby, T., & Calvert, H. (2000). Temozolomide and treatment of malignant glioma. *Clinical Cancer Research*, *6*(7), 2585–2597.

Gatchalian, J., Malik, S., Ho, J., Lee, D. S., Kelso, T. W. R., Shokhirev, M. N., Dixon, J. R., & Hargreaves, D. C. (2018). A non-canonical BRD9-containing BAF chromatin remodeling complex regulates naive pluripotency in mouse embryonic stem cells. *Nature Communications*, *9*(1). https://doi.org/10.1038/s41467-018-07528-9

Gérard, M., Corroyer-Dulmont, A., Lesueur, P., Collet, S., Chérel, M., Bourgeois, M., Stefan, D., Limkin, E. J., Perrio, C., Guillamo, J.-S., Dubray, B., Bernaudin, M., Thariat, J., & Valable, S. (2019). Hypoxia Imaging and Adaptive Radiotherapy: A State-of-the-Art Approach in the Management of Glioma. *Frontiers in Medicine*, *6*(June). https://doi.org/10.3389/fmed.2019.00117

Goldstein, M., & Kastan, M. B. (2015). The DNA Damage Response: Implications for Tumor Responses to Radiation and Chemotherapy. *Annual Review of Medicine*, *66*(1), 129–143. https://doi.org/10.1146/annurev-med-081313-121208

Goodarzi, A. A., & Jeggo, P. A. (2013). The Repair and Signaling Responses to DNA Double-Strand Breaks. In *Advances in Genetics* (1st ed., Vol. 82). Elsevier Inc. https://doi.org/10.1016/B978-0-12-407676-1.00001-9

Grabowski, M. M., Recinos, P. F., Nowacki, A. S., Schroeder, J. L., Angelov, L., Barnett, G. H., & Vogelbaum, M. A. (2014). Residual tumor volume versus extent of resection: Predictors of survival after surgery for glioblastoma. *Journal of Neurosurgery*, *121*(5), 1115–1123. https://doi.org/10.3171/2014.7.JNS132449

Gusyatiner, O., & Hegi, M. E. (2018). Glioma epigenetics: From subclassification to novel treatment options. *Seminars in Cancer Biology*, *51*(November), 50–58. https://doi.org/10.1016/j.semcancer.2017.11.010

Hakem, R. (2008). DNA-damage repair; the good, the bad, and the ugly. *EMBO Journal*, *27*(4), 589–605. https://doi.org/10.1038/emboj.2008.15

Han, X., Xue, X., Zhou, H., & Zhang, G. (2017). A molecular view of the radioresistance of gliomas. *Oncotarget*, *8*(59), 100931–100941. https://doi.org/10.18632/oncotarget.21753

Hauge, S., Eek Mariampillai, A., Rødland, G. E., Bay, L. T. E., Landsverk, H. B., & Syljuåsen, R. G. (2023). Expanding roles of cell cycle checkpoint inhibitors in radiation oncology. In *International Journal of Radiation Biology* (Vol. 99, Issue 6, pp. 941–950). Taylor and Francis Ltd. https://doi.org/10.1080/09553002.2021.1913529

Hegi, M. E., Diserens, A.-C., Gorlia, T., Hamou, M.-F., de Tribolet, N., Weller, M., Kros, J. M., Hainfellner, J. A., Mason, W., Mariani, L., Bromberg, J. E. C., Hau, P., Mirimanoff, R. O., Cairncross, J. G., Janzer, R. C., & Stupp, R. (2005). MGMT Gene Silencing and Benefit from Temozolomide in Glioblastoma. *New England Journal of Medicine*, *352*(10), 997–1003. https://doi.org/10.1056/nejmoa043331

Hein, A. L., Ouellette, M. M., & Yan, Y. (2014). Radiation-induced signaling pathways that promote cancer cell survival (Review). *International Journal of Oncology*, *45*(5), 1813–1819. https://doi.org/10.3892/ijo.2014.2614

Hipólito, A., Xavier, R., Brito, C., Tomás, A., Lemos, I., Cabaço, L. C., Silva, F., Oliva, A., Barral, D. C., Vicente, J. B., Gonçalves, L. G., Pojo, M., & Serpa, J. (2024). BRD9 status is a major contributor for cysteine metabolic remodeling through MST and EAAT3 modulation in malignant melanoma. *Biochimica et Biophysica Acta - Molecular Basis of Disease*, *1870*(2). https://doi.org/10.1016/j.bbadis.2023.166983

Hodges, C., Kirkland, J. G., & Crabtree, G. R. (2016). The many roles of BAF (mSWI/SNF) and PBAF complexes in cancer. *Cold Spring Harbor Perspectives in Medicine*, *6*(8). https://doi.org/10.1101/cshperspect.a026930

Hohmann, A. F., Martin, L. J., Minder, J. L., Roe, J. S., Shi, J., Steurer, S., Bader, G., McConnell, D., Pearson, M., Gerstberger, T., Gottschamel, T., Thompson, D., Suzuki, Y., Koegl, M., & Vakoc, C. R. (2016). Sensitivity and engineered

resistance of myeloid leukemia cells to BRD9 inhibition. *Nature Chemical Biology*, *12*(9), 672–679. https://doi.org/10.1038/nchembio.2115

Hohmann, A. F., & Vakoc, C. R. (2014). A rationale to target the SWI/SNF complex for cancer therapy. *Trends in Genetics*, *30*(8), 356–363. https://doi.org/10.1016/j.tig.2014.05.001

Horsman, M. R., Mortensen, L. S., Petersen, J. B., Busk, M., & Overgaard, J. (2012). Imaging hypoxia to improve radiotherapy outcome. *Nature Reviews Clinical Oncology*, *9*(12), 674–687. https://doi.org/10.1038/nrclinonc.2012.171

Huang, B., Li, X., Li, Y., Zhang, J., Zong, Z., & Zhang, H. (2021). Current Immunotherapies for Glioblastoma Multiforme. In *Frontiers in Immunology* (Vol. 11). Frontiers Media S.A. https://doi.org/10.3389/fimmu.2020.603911

Inbar-Feigenberg, M., Choufani, S., Butcher, D. T., Roifman, M., & Weksberg, R. (2013). Basic concepts of epigenetics. *Fertility and Sterility*, *99*(3), 607–615. https://doi.org/10.1016/j.fertnstert.2013.01.117

Inoue, D., Chew, G. L., Liu, B., Michel, B. C., Pangallo, J., D'Avino, A. R., Hitchman, T., North, K., Lee, S. C. W., Bitner, L., Block, A., Moore, A. R., Yoshimi, A., Escobar-Hoyos, L., Cho, H., Penson, A., Lu, S. X., Taylor, J., Chen, Y., … Bradley, R. K. (2019). Spliceosomal disruption of the non-canonical BAF complex in cancer. *Nature*, *574*(7778), 432–436. https://doi.org/10.1038/s41586-019-1646-9

Jamasbi, E., Hamelian, M., Hossain, M. A., & Varmira, K. (2022a). The cell cycle, cancer development and therapy. In *Molecular Biology Reports* (Vol. 49, Issue 11, pp. 10875–10883). Springer Science and Business Media B.V. https://doi.org/10.1007/s11033-022-07788-1

Jamasbi, E., Hamelian, M., Hossain, M. A., & Varmira, K. (2022b). The cell cycle, cancer development and therapy. In *Molecular Biology Reports* (Vol. 49, Issue 11, pp. 10875–10883). Springer Science and Business Media B.V. https://doi.org/10.1007/s11033-022-07788-1

Jarrold, J., & Davies, C. C. (2019). PRMTs and Arginine Methylation: Cancer's Best-Kept Secret? *Trends in Molecular Medicine*, *xx*(xx), 1–16. https://doi.org/10.1016/j.molmed.2019.05.007

Jeggo, P. A., Pearl, L. H., & Carr, A. M. (2016). DNA repair, genome stability and cancer: A historical perspective. *Nature Reviews Cancer*, *16*(1), 35–42. https://doi.org/10.1038/nrc.2015.4

Jiao, Y., Cao, F., & Liu, H. (2022). Radiation-induced Cell Death and Its Mechanisms. In *Health Physics* (Vol. 123, Issue 5, pp. 376–386). Lippincott Williams and Wilkins. https://doi.org/10.1097/HP.0000000000001601

Jones, P. A., Issa, J. P. J., & Baylin, S. (2016). Targeting the cancer epigenome for therapy. *Nature Reviews Genetics*, *17*(10), 630–641. https://doi.org/10.1038/nrg.2016.93

Kadoch, C., Hargreaves, D. C., Hodges, C., Elias, L., Ho, L., Ranish, J., & Crabtree, G. R. (2013). Proteomic and bioinformatic analysis of mammalian SWI/SNF complexes identifies extensive roles in human malignancy. *Nature Genetics*, *45*(6), 592–601. https://doi.org/10.1038/ng.2628

Karakaidos, P., Karagiannis, D., & Rampias, T. (2020). Resolving DNA damage: Epigenetic regulation of DNA repair. *Molecules*, *25*(11), 1–28. https://doi.org/10.3390/molecules25112496

Karim, R. M., & Schönbrunn, E. (2016). An Advanced Tool to Interrogate BRD9. *Journal of Medicinal Chemistry*, *59*(10), 4459–4461. https://doi.org/10.1021/acs.jmedchem.6b00550

Karschnia, P., Young, J. S., Dono, A., Häni, L., Sciortino, T., Bruno, F., Juenger, S. T., Teske, N., Morshed, R. A., Haddad, A. F., Zhang, Y., Stoecklein, S., Weller, M., Vogelbaum, M. A., Beck, J., Tandon, N., Hervey-Jumper, S., Molinaro, A. M., Rudà, R., … Tonn, J. C. (2023). Prognostic validation of a new classification system for extent of resection in glioblastoma: A report of the RANO resect group. *Neuro-Oncology*, *25*(5), 940–954. https://doi.org/10.1093/neuonc/noac193

Katagi, H., Louis, N., Unruh, D., Sasaki, T., He, X., Zhang, A., Ma, Q., Piunti, A., Shimazu, Y., Lamano, J. B., Carcaboso, A. M., Tian, X., Seluanov, A., Gorbunova, V., Laurie, K. L., Kondo, A., Wadhwani, N. R., Lulla, R., Goldman, S., … Hashizume, R. (2019). Radiosensitization by histone H3 demethylase inhibition in diffuse intrinsic pontine glioma. *Clinical Cancer Research*, *25*(18), 5572–5583. https://doi.org/10.1158/1078-0432.CCR-18-3890

Kaya, V. O., & Adebali, O. (2024). UV-induced reorganization of 3D genome mediates DNA damage response. *Biorxiv*. https://doi.org/https://doi.org/10.1101/2024.05.27.595922

Kayabolen, A., Sahin, G. N., Seker-Polat, F., Cingoz, A., Isik, B., Acar, S., Wakimoto, H., Cahill, D. P., Solaroglu, I., Cribbs, A., Oppermann, U., & Bagci-Onder, T. (2020). Combined inhibition of KDM6A/B and HDACs exacerbates integrated stress response and mediates therapeutic effects in IDH1-mutant glioma. *BioRxiv*, 1–34. https://doi.org/10.1101/2020.11.26.400234

Kayabolen, A., Yilmaz, E., & Bagci-Onder, T. (2021). IDH mutations in glioma: Double-edged sword in clinical applications? *Biomedicines*, *9*(7). https://doi.org/10.3390/biomedicines9070799

Kim, J. G., Bae, J. H., Kim, J. A., Heo, K., Yang, K., & Yi, J. M. (2014). Combination effect of epigenetic regulation and ionizing radiation in colorectal cancer cells. *PLoS ONE*, *9*(8), 1–10. https://doi.org/10.1371/journal.pone.0105405

Kim, W., Lee, S., Seo, D., Kim, D., Kim, K., Kim, E., Kang, J., Seong, K. M., Youn, H., & Youn, B. (2019). Cellular stress responses in radiotherapy. In *Cells* (Vol. 8, Issue 9). MDPI. https://doi.org/10.3390/cells8091105

Kinner, A., Wu, W., Staudt, C., & Iliakis, G. (2008). Gamma-H2AX in recognition and signaling of DNA double-strand breaks in the context of chromatin. *Nucleic Acids Research*, *36*(17), 5678–5694. https://doi.org/10.1093/nar/gkn550

Kohsaka, S., & Tanak, S. (2013). Chemotherapeutic Agent for Glioma. In *Clinical Management and Evolving Novel Therapeutic Strategies for Patients with Brain Tumors*. InTech. https://doi.org/10.5772/54353

Kouzarides, T. (2007a). Chromatin Modifications and Their Function. *Cell*, *128*(4), 693–705. https://doi.org/10.1016/j.cell.2007.02.005

Kouzarides, T. (2007b). Chromatin Modifications and Their Function. In *Cell* (Vol. 128, Issue 4, pp. 693–705). https://doi.org/10.1016/j.cell.2007.02.005

Krämer, K. F., Moreno, N., Frühwald, M. C., & Kerl, K. (2017). BRD9 inhibition, alone or in combination with cytostatic compounds as a therapeutic approach in rhabdoid tumors. *International Journal of Molecular Sciences*, *18*(7), 1–12. https://doi.org/10.3390/ijms18071537

Kurata, K., Samur, M. K., Liow, P., Wen, K., Yamamoto, L., Liu, J., Morelli, E., Gulla, A., Tai, Y. T., Qi, J., Hideshima, T., & Anderson, K. C. (2023). BRD9

Degradation Disrupts Ribosome Biogenesis in Multiple Myeloma. *Clinical Cancer Research*, *29*(9), 1807–1821. https://doi.org/10.1158/1078-0432.CCR-22-3668

Kurt, I. C., Sur, I., Kaya, E., Cingoz, A., Kazancioglu, S., Kahya, Z., Toparlak, O. D., Senbabaoglu, F., Kaya, Z., Ozyerli, E., Karahüseyinoglu, S., Lack, N. A., Gümüs, Z. H., Onder, T. T., & Bagci-Onder, T. (2017). KDM2B, an H3K36-specific demethylase, regulates apoptotic response of GBM cells to TRAIL. *Cell Death & Disease*, *8*(6), e2897. https://doi.org/10.1038/cddis.2017.288

Labun, K., Montague, T. G., Krause, M., Torres Cleuren, Y. N., Tjeldnes, H., & Valen, E. (2019). CHOPCHOP v3: Expanding the CRISPR web toolbox beyond genome editing. *Nucleic Acids Research*, *47*(W1), W171–W174. https://doi.org/10.1093/nar/gkz365

Lei, G., Mao, C., Yan, Y., Zhuang, L., & Gan, B. (2021a). Ferroptosis, radiotherapy, and combination therapeutic strategies. In *Protein and Cell* (Vol. 12, Issue 11, pp. 836–857). Higher Education Press Limited Company. https://doi.org/10.1007/s13238-021-00841-y

Lei, G., Mao, C., Yan, Y., Zhuang, L., & Gan, B. (2021b). Ferroptosis, radiotherapy, and combination therapeutic strategies. In *Protein and Cell* (Vol. 12, Issue 11, pp. 836–857). Higher Education Press Limited Company. https://doi.org/10.1007/s13238-021-00841-y

Li, X., Zhao, L., Li, W., Gao, P., & Zhang, N. (2024). HER2-targeting CAR-T cells show highly efficient anti-tumor activity against glioblastoma both in vitro and in vivo. *Genes and Immunity*. https://doi.org/10.1038/s41435-024-00275-6

Lin, Y. J., Mashouf, L. A., & Lim, M. (2022). CAR T Cell Therapy in Primary Brain Tumors: Current Investigations and the Future. In *Frontiers in Immunology* (Vol. 13). Frontiers Media S.A. https://doi.org/10.3389/fimmu.2022.817296

Ling, R., Wang, J., Fang, Y., Yu, Y., Su, Y., Sun, W., Li, X., & Tang, X. (2023). HDAC-an important target for improving tumor radiotherapy resistance. In *Frontiers in Oncology* (Vol. 13). Frontiers Media SA. https://doi.org/10.3389/fonc.2023.1193637

Liu, B., Bhatt, D., Oltvai, Z. N., Greenberger, J. S., & Bahar, I. (2014). Significance of p53 dynamics in regulating apoptosis in response to ionizing radiation, and polypharmacological strategies. *Scientific Reports*, *4*. https://doi.org/10.1038/srep06245

Liu, R., Bian, Y., Liu, L., Liu, L., Liu, X., & Ma, S. (2022). Molecular pathways associated with oxidative stress and their potential applications in radiotherapy (Review). In *International Journal of Molecular Medicine* (Vol. 49, Issue 5). Spandidos Publications. https://doi.org/10.3892/IJMM.2022.5121

Lomax, M. E., Folkes, L. K., & O'Neill, P. (2013). Biological consequences of radiation-induced DNA damage: Relevance to radiotherapy. *Clinical Oncology*, *25*(10), 578–585. https://doi.org/10.1016/j.clon.2013.06.007

Lord, C. J., & Ashworth, A. (2012). The DNA damage response and cancer therapy. *Nature*, *481*(7381), 287–294. https://doi.org/10.1038/nature10760

Louis, D. N., Perry, A., Wesseling, P., Brat, D. J., Cree, I. A., Figarella-Branger, D., Hawkins, C., Ng, H. K., Pfister, S. M., Reifenberger, G., Soffietti, R., Von Deimling, A., & Ellison, D. W. (2021). The 2021 WHO classification of tumors of the central nervous system: A summary. *Neuro-Oncology*, *23*(8), 1231–1251. https://doi.org/10.1093/neuonc/noab106

Lu, C., & Shervington, A. (2008). Chemoresistance in gliomas. *Molecular and Cellular Biochemistry*, *312*(1–2), 71–80. https://doi.org/10.1007/s11010-008-9722-8

Mallick, S., Rath, G. K., & Benson, R. (2020). Practical Radiation Oncology. In S. Mallick, G. K. Rath, & R. Benson (Eds.), *Practical Radiation Oncology* (Vol. 4, Issue 4). Springer Singapore. https://doi.org/10.1007/978-981-15-0073-2

Mann, J., Ramakrishna, R., Magge, R., & Wernicke, A. G. (2018). Advances in radiotherapy for glioblastoma. *Frontiers in Neurology*, *8*(JAN), 1–11. https://doi.org/10.3389/fneur.2017.00748

Marcu, L. G., Toma Dasu, I., & Dasu, A. (2015). The Six Rs of Head and Neck Cancer Radiotherapy. In *Contemporary Issues in Head and Neck Cancer Management: Vol. i* (Issue tourism, p. 13). InTech. https://doi.org/10.5772/60015

Marín, A., Martín, M., Liñán, O., Alvarenga, F., López, M., Fernández, L., Büchser, D., & Cerezo, L. (2015). Bystander effects and radiotherapy. *Reports of Practical Oncology and Radiotherapy*, *20*(1), 12–21. https://doi.org/10.1016/j.rpor.2014.08.004

Martin, L. J., Koegl, M., Bader, G., Cockcroft, X. L., Fedorov, O., Fiegen, D., Gerstberger, T., Hofmann, M. H., Hohmann, A. F., Kessler, D., Knapp, S., Knesl, P., Kornigg, S., Müller, S., Nar, H., Rogers, C., Rumpel, K., Schaaf, O., Steurer, S., … McConnell, D. (2016). Structure-Based Design of an in Vivo Active

Selective BRD9 Inhibitor. *Journal of Medicinal Chemistry*, *59*(10), 4462–4475. https://doi.org/10.1021/acs.jmedchem.5b01865

Matsui, J. K., Perlow, H. K., Facer, B. D., McCalla, A., Marrazzo, L., Detti, B., Scorsetti, M., Clerici, E., Scoccianti, S., Navarria, P., Trifiletti, D. M., Gondi, V., Bovi, J., Huang, J., Brown, P. D., & Palmer, J. D. (2022). Radiotherapy for elderly patients with glioblastoma: an assessment of hypofractionation and modern treatment techniques. In *Chinese Clinical Oncology* (Vol. 11, Issue 5). AME Publishing Company. https://doi.org/10.21037/cco-22-76

McClure, J. J., Li, X., & Chou, C. J. (2018). Advances and Challenges of HDAC Inhibitors in Cancer Therapeutics. In *Advances in Cancer Research* (1st ed., Vol. 138). Elsevier Inc. https://doi.org/10.1016/bs.acr.2018.02.006

McFaline-Figueroa, J. L., Braun, C. J., Stanciu, M., Nagel, Z. D., Mazzucato, P., Sangaraju, D., Cerniauskas, E., Barford, K., Vargas, A., Chen, Y., Tretyakova, N., Lees, J. A., Hemann, M. T., White, F. M., & Samson, L. D. (2015). Minor changes in expression of the mismatch repair protein MSH2 exert a major impact on glioblastoma response to temozolomide. *Cancer Research*, *75*(15), 3127–3138. https://doi.org/10.1158/0008-5472.CAN-14-3616

Merrifield, M., & Kovalchuk, O. (2013). Epigenetics in radiation biology: A new research frontier. *Frontiers in Genetics*, *4*(APR), 1–16. https://doi.org/10.3389/fgene.2013.00040

Metselaar, D. S., du Chatinier, A., Meel, M. H., ter Huizen, G., Waranecki, P., Goulding, J. R., Bugiani, M., Koster, J., Kaspers, G. J. L., & Hulleman, E. (2022). AURKA and PLK1 inhibition selectively and synergistically block cell cycle progression in diffuse midline glioma. *IScience*, *25*(6). https://doi.org/10.1016/j.isci.2022.104398

Michelhaugh, S. K., Kiousis, S., Michelhaugh, S. A., Klinger, N. V., & Mittal, S. (2018). *Abstract 4398: In vitro Tumor Treating Fields (TTFields) alter proliferation and morphology of patient-derived high-grade meningioma cell lines*. *September 2021*, 4398–4398. https://doi.org/10.1158/1538-7445.am2018-4398

Millán-Zambrano, G., Burton, A., Bannister, A. J., & Schneider, R. (2022). Histone post-translational modifications — cause and consequence of genome function. In *Nature Reviews Genetics* (Vol. 23, Issue 9, pp. 563–580). Nature Research. https://doi.org/10.1038/s41576-022-00468-7

Moeller, B. J., Richardson, R. A., & Dewhirst, M. W. (2007). Hypoxia and radiotherapy: Opportunities for improved outcomes in cancer treatment. *Cancer and Metastasis Reviews*, *26*(2), 241–248. https://doi.org/10.1007/s10555-007-9056-0

Montoya, M., Gallus, M., Phyu, S., Haegelin, J., de Groot, J., & Okada, H. (2024). A Roadmap of CAR-T-Cell Therapy in Glioblastoma: Challenges and Future Perspectives. In *Cells* (Vol. 13, Issue 9). Multidisciplinary Digital Publishing Institute (MDPI). https://doi.org/10.3390/cells13090726

Morel, D., Jeffery, D., Aspeslagh, S., Almouzni, G., & Postel-Vinay, S. (2020). Combining epigenetic drugs with other therapies for solid tumours — past lessons and future promise. In *Nature Reviews Clinical Oncology* (Vol. 17, Issue 2, pp. 91–107). Nature Research. https://doi.org/10.1038/s41571-019-0267-4

Nakada, M., Furuta, T., Hayashi, Y., Minamoto, T., & Hamada, J. (2012). The strategy for enhancing temozolomide against malignant glioma. *Frontiers in Oncology*, *2*(August), 1–5. https://doi.org/10.3389/fonc.2012.00098

Nguyen, H. S., Shabani, S., Awad, A. J., Kaushal, M., & Doan, N. (2018). Molecular markers of therapy-resistant glioblastoma and potential strategy to combat resistance. *International Journal of Molecular Sciences*, *19*(6). https://doi.org/10.3390/ijms19061765

Nicholson, T. B., Veland, N., & Chen, T. (2015). Writers, Readers, and Erasers of Epigenetic Marks. In *Epigenetic Cancer Therapy* (pp. 31–66). Elsevier Inc. https://doi.org/10.1016/B978-0-12-800206-3.00003-3

Nickoloff, J. A., Jones, D., Lee, S.-H., Williamson, E. A., & Hromas, R. (2017). Drugging the Cancers Addicted to DNA Repair. *JNCI: Journal of the National Cancer Institute*, *109*(11), 1–13. https://doi.org/10.1093/jnci/djx059

O'Connor, M. J. (2015). Targeting the DNA Damage Response in Cancer. *Molecular Cell*, *60*(4), 547–560. https://doi.org/10.1016/j.molcel.2015.10.040

Ornelas, A. S., Porter, A. B., Sharma, A., Knox, M. G., Marks, L. A., Wingerchuk, D. M., & O'Carroll, C. B. (2019). What is the role of tumor-Treating fields in newly diagnosed glioblastoma? *Neurologist*, *24*(2), 71–73. https://doi.org/10.1097/NRL.0000000000000222

Pajonk, F., Vlashi, E., & McBride, W. H. (2010). Radiation Resistance of Cancer Stem Cells: The 4 R's of Radiobiology Revisited. *STEM CELLS*, *28*(4), 639–648. https://doi.org/10.1002/stem.318

Patel, A. P., Tirosh, I., Trombetta, J. J., Shalek, A. K., Gillespie, S. M., Wakimoto, H., Cahill, D. P., Nahed, B. V., Curry, W. T., Martuza, R. L., Louis, D. N., Rozenblatt-Rosen, O., Suvà, M. L., Regev, A., & Bernstein, B. E. (2014). Single-cell RNA-seq highlights intratumoral heterogeneity in primary glioblastoma. *Science*, *344*(6190), 1396–1401. https://doi.org/10.1126/science.1254257

Peng, Q., Weng, K., Li, S., Xu, R., Wang, Y., & Wu, Y. (2021). A Perspective of Epigenetic Regulation in Radiotherapy. *Frontiers in Cell and Developmental Biology*, *9*(February), 1–15. https://doi.org/10.3389/fcell.2021.624312

Perazzoli, G., Prados, J., Ortiz, R., Caba, O., Cabeza, L., Berdasco, M., Gónzalez, B., & Melguizo, C. (2015). Temozolomide resistance in glioblastoma cell lines: Implication of MGMT, MMR, P-glycoprotein and CD133 expression. *PLoS ONE*, *10*(10), 1–23. https://doi.org/10.1371/journal.pone.0140131

Pilié, P. G., Tang, C., Mills, G. B., & Yap, T. A. (2019). State-of-the-art strategies for targeting the DNA damage response in cancer. *Nature Reviews Clinical Oncology*, *16*(2), 81–104. https://doi.org/10.1038/s41571-018-0114-z

Pinarbasi-Degirmenci, N., Sur-Erdem, I., Akcay, V., Bolukbasi, Y., Selek, U., Solaroglu, I., & Bagci-Onder, T. (2022). Chronically Radiation-Exposed Survivor Glioblastoma Cells Display Poor Response to Chk1 Inhibition under Hypoxia. *International Journal of Molecular Sciences*, *23*(13). https://doi.org/10.3390/ijms23137051

Rakotomalala, A., Escande, A., Furlan, A., Meignan, S., & Lartigau, E. (2021). Hypoxia in Solid Tumors: How Low Oxygenation Impacts the "Six Rs" of Radiotherapy. *Frontiers in Endocrinology*, *12*(September), 1–17. https://doi.org/10.3389/fendo.2021.742215

Ramaiah, M. J., Tangutur, A. D., & Manyam, R. R. (2021). Epigenetic modulation and understanding of HDAC inhibitors in cancer therapy. In *Life Sciences* (Vol. 277). Elsevier Inc. https://doi.org/10.1016/j.lfs.2021.119504

Ramirez, Y. P., Weatherbee, J. L., Wheelhouse, R. T., & Ross, A. H. (2013). Glioblastoma multiforme therapy and mechanisms of resistance. *Pharmaceuticals*, *6*(12), 1475–1506. https://doi.org/10.3390/ph6121475

Raviraj, R., Nagaraja, S. G. S., Selvakumar, I., Mohan, S., & Nagarajan, D. (2020). The epigenetics of brain tumors and its modulation during radiation: A review. In *Life Sciences* (Vol. 256). Elsevier Inc. https://doi.org/10.1016/j.lfs.2020.117974

Reisz, J. A., Bansal, N., Qian, J., Zhao, W., & Furdui, C. M. (2014). Effects of Ionizing Radiation on Biological Molecules—Mechanisms of Damage and Emerging Methods of Detection. *Antioxidants & Redox Signaling*, *21*(2), 260–292. https://doi.org/10.1089/ars.2013.5489

Remillard, D., Buckley, D. L., Paulk, J., Brien, G. L., Sonnett, M., Seo, H.-S., Dastjerdi, S., Wühr, M., Dhe-Paganon, S., Armstrong, S. A., & Bradner, J. E. (2017). Degradation of the BAF Complex Factor BRD9 by Heterobifunctional Ligands. *Angewandte Chemie International Edition*, *56*(21), 5738–5743. https://doi.org/10.1002/anie.201611281

Sachamitr, P., Ho, J. C., Ciamponi, F. E., Ba-Alawi, W., Coutinho, F. J., Guilhamon, P., Kushida, M. M., Cavalli, F. M. G., Lee, L., Rastegar, N., Vu, V., Sánchez-Osuna, M., Coulombe-Huntington, J., Kanshin, E., Whetstone, H., Durand, M., Thibault, P., Hart, K., Mangos, M., … Dirks, P. B. (2021). PRMT5 inhibition disrupts splicing and stemness in glioblastoma. *Nature Communications*, *12*(1), 1–17. https://doi.org/10.1038/s41467-021-21204-5

Sak, A., Kübler, D., Bannik, K., Groneberg, M., Strunz, S., Kriehuber, R., & Stuschke, M. (2017). Epigenetic silencing and activation of transcription: influence on the radiation sensitivity of glioma cell lines. *International Journal of Radiation Biology*, *93*(5), 494–506. https://doi.org/10.1080/09553002.2017.1270472

Sanders, J. T., Freeman, T. F., Xu, Y., Golloshi, R., Stallard, M. A., Hill, A. M., San Martin, R., Balajee, A. S., & McCord, R. P. (2020). Radiation-induced DNA damage and repair effects on 3D genome organization. *Nature Communications*, *11*(1). https://doi.org/10.1038/s41467-020-20047-w

Sansom, C. (2009). Temozolomide – birth of a blockbuster. *Chemistry World*, *6*(July), 48–51.

Saraç, H., Morova, T., Pires, E., McCullagh, J., Kaplan, A., Cingöz, A., Bagci-Onder, T., Önder, T., Kawamura, A., & Lack, N. A. (2020). Systematic characterization of chromatin modifying enzymes identifies KDM3B as a critical regulator in castration resistant prostate cancer. *Oncogene*, *39*(10), 2187–2201. https://doi.org/10.1038/s41388-019-1116-8

Seker-polat, F., Degirmenci, N. P., Solaroglu, I., & Bagci-onder, T. (2022). *Tumor Cell Infiltration into the Brain in Glioblastoma : From*.

Sevinç, K., Sevinç, G. G., Cavga, A. D., Philpott, M., Kelekçi, S., Can, H., Cribbs, A. P., Yıldız, A. B., Yılmaz, A., Ayar, E. S., Arabacı, D. H., Dunford, J. E., Ata, D., Sigua, L. H., Qi, J., Oppermann, U., & Onder, T. T. (2022). BRD9-containing non-canonical BAF complex maintains somatic cell transcriptome and acts as a barrier to human reprogramming. *Stem Cell Reports*, *17*(12), 2629–2642. https://doi.org/10.1016/j.stemcr.2022.10.005

Shaltiel, I. A., Krenning, L., Bruinsma, W., & Medema, R. H. (2015). The same, only different - DNA damage checkpoints and their reversal throughout the cell cycle. *Journal of Cell Science*, *128*(4), 607–620. https://doi.org/10.1242/jcs.163766

Shen, W., Hu, J. A., & Zheng, J. S. (2014). Mechanism of temozolomide-induced antitumour effects on glioma cells. *Journal of International Medical Research*, *42*(1), 164–172. https://doi.org/10.1177/0300060513501753

Smits, K. M., Melotte, V., Niessen, H. E. C., Dubois, L., Oberije, C., Troost, E. G. C., Starmans, M. H. W., Boutros, P. C., Vooijs, M., Van Engeland, M., & Lambin, P. (2014). Epigenetics in radiotherapy: Where are we heading? *Radiotherapy and Oncology*, *111*(2), 168–177. https://doi.org/10.1016/j.radonc.2014.05.001

Squatrito, M., Brennan, C. W., Helmy, K., Huse, J. T., Petrini, J. H., & Holland, E. C. (2010). Loss of ATM/Chk2/p53 Pathway Components Accelerates Tumor Development and Contributes to Radiation Resistance in Gliomas. *Cancer Cell*, *18*(6), 619–629. https://doi.org/10.1016/j.ccr.2010.10.034

Stepanenko, A. A., & Chekhonin, V. P. (2019). On the Critical Issues in Temozolomide Research in Glioblastoma: Clinically Relevant Concentrations and MGMT-independent Resistance. *Biomedicines*, *7*(4), 92. https://doi.org/10.3390/biomedicines7040092

Stupp, R., Hegi, M. E., Mason, W. P., van den Bent, M. J., Taphoorn, M. J., Janzer, R. C., Ludwin, S. K., Allgeier, A., Fisher, B., Belanger, K., Hau, P., Brandes, A. A., Gijtenbeek, J., Marosi, C., Vecht, C. J., Mokhtari, K., Wesseling, P., Villa, S., Eisenhauer, E., … Mirimanoff, R. O. (2009). Effects of radiotherapy with concomitant and adjuvant temozolomide versus radiotherapy alone on survival in glioblastoma in a randomised phase III study: 5-year analysis of the EORTC-NCIC

trial. *The Lancet Oncology*, *10*(5), 459–466. https://doi.org/10.1016/S1470-2045(09)70025-7

Stupp, R., Mason, W. P., van den Bent, M. J., Weller, M., Fisher, B., Taphoorn, M. J. B., Belanger, K., Brandes, A. A., Marosi, C., Bogdahn, U., Curschmann, J., Janzer, R. C., Ludwin, S. K., Gorlia, T., Allgeier, A., Lacombe, D., Cairncross, J. G., Eisenhauer, E., Mirimanoff, R. O., … National Cancer Institute of Canada Clinical Trials Group. (2005). Radiotherapy plus concomitant and adjuvant temozolomide for glioblastoma. *The New England Journal of Medicine*, *352*(10), 987–996. https://doi.org/10.1056/NEJMoa043330

Stupp, R., Taillibert, S., Kanner, A., Read, W., Steinberg, D. M., Lhermitte, B., Toms, S., Idbaih, A., Ahluwalia, M. S., Fink, K., Di Meco, F., Lieberman, F., Zhu, J. J., Stragliotto, G., Tran, D. D., Brem, S., Hottinger, A. F., Kirson, E. D., Lavy-Shahaf, G., … Ram, Z. (2017). Effect of tumor-treating fields plus maintenance temozolomide vs maintenance temozolomide alone on survival in patients with glioblastoma a randomized clinical trial. *JAMA - Journal of the American Medical Association*, *318*(23), 2306–2316. https://doi.org/10.1001/jama.2017.18718

Tesileanu, C. M. S., Dirven, L., Wijnenga, M. M. J., Koekkoek, J. A. F., Vincent, A. J. P. E., Dubbink, H. J., Atmodimedjo, P. N., Kros, J. M., Van Duinen, S. G., Smits, M., Taphoorn, M. J. B., French, P. J., & Van Den Bent, M. J. (2020). Survival of diffuse astrocytic glioma, IDH1/2 wildtype, with molecular features of glioblastoma, WHO grade IV: A confirmation of the cIMPACT-NOW criteria. *Neuro-Oncology*, *22*(4), 515–523. https://doi.org/10.1093/neuonc/noz200

Theodoulou, N. H., Bamborough, P., Bannister, A. J., Becher, I., Bit, R. A., Che, K. H., Chung, C. W., Dittmann, A., Drewes, G., Drewry, D. H., Gordon, L., Grandi, P., Leveridge, M., Lindon, M., Michon, A. M., Molnar, J., Robson, S. C., Tomkinson, N. C. O., Kouzarides, T., … Humphreys, P. G. (2016). Discovery of I-BRD9, a Selective Cell Active Chemical Probe for Bromodomain Containing Protein 9 Inhibition. *Journal of Medicinal Chemistry*, *59*(4), 1425–1439. https://doi.org/10.1021/acs.jmedchem.5b00256

Tomar, M. S., Kumar, A., Srivastava, C., & Shrivastava, A. (2021). Elucidating the mechanisms of Temozolomide resistance in gliomas and the strategies to overcome the resistance. In *Biochimica et Biophysica Acta - Reviews on Cancer* (Vol. 1876, Issue 2). Elsevier B.V. https://doi.org/10.1016/j.bbcan.2021.188616

Tong, S., Wang, Y., Wu, J., Long, J., Zhong, P., & Wang, B. (2021). Comprehensive pharmacogenomics characterization of temozolomide response in gliomas. In *European Journal of Pharmacology* (Vol. 912). Elsevier B.V. https://doi.org/10.1016/j.ejphar.2021.174580

Torgovnick, A., & Schumacher, B. (2015). DNA repair mechanisms in cancer development and therapy. *Frontiers in Genetics*, *6*(APR), 1–15. https://doi.org/10.3389/fgene.2015.00157

Uddin, M. S., Mamun, A. Al, Alghamdi, B. S., Tewari, D., Jeandet, P., Sarwar, M. S., & Ashraf, G. M. (2022). Epigenetics of glioblastoma multiforme: From molecular mechanisms to therapeutic approaches. In *Seminars in Cancer Biology* (Vol. 83, pp. 100–120). Academic Press. https://doi.org/10.1016/j.semcancer.2020.12.015

Virga, J., Szivos, L., Hortobágyi, T., Chalsaraei, M. K., Zahuczky, G., Steiner, L., Tóth, J., Reményi-Puskár, J., Bognár, L., & Klekner, A. (2019). Extracellular matrix differences in glioblastoma patients with different prognoses. *Oncology Letters*, *17*(1), 797–806. https://doi.org/10.3892/ol.2018.9649

Vlatkovic, T., Veldwijk, M. R., Giordano, F. A., & Herskind, C. (2022). Targeting Cell Cycle Checkpoint Kinases to Overcome Intrinsic Radioresistance in Brain Tumor Cells. *Cancers*, *14*(3), 1–18. https://doi.org/10.3390/cancers14030701

Wakimoto, H., Tanaka, S., Curry, W. T., Loebel, F., Zhao, D., Tateishi, K., Chen, J., Klofas, L. K., Lelic, N., Kim, J. C., Dias-Santagata, D., Ellisen, L. W., Borger, D. R., Fendt, S. M., Vander Heiden, M. G., Batchelor, T. T., John Iafrate, A., Cahill, D. P., & Chi, A. S. (2014). Targetable signaling pathway mutations are associated with malignant phenotype in IDH-mutant gliomas. *Clinical Cancer Research*, *20*(11), 2898–2909. https://doi.org/10.1158/1078-0432.CCR-13-3052

Wallace, S. S. (2014). Base excision repair: A critical player in many games. *DNA Repair*, *19*(1), 14–26. https://doi.org/10.1016/j.dnarep.2014.03.030

Wang, X., Wang, S., Troisi, E. C., Howard, T. P., Haswell, J. R., Wolf, B. K., Hawk, W. H., Ramos, P., Oberlick, E. M., Tzvetkov, E. P., Vazquez, F., Hahn, W. C., Park, P. J., & Roberts, C. W. M. (2019). BRD9 defines a SWI/SNF sub-complex and constitutes a specific vulnerability in malignant rhabdoid tumors. *Nature Communications*, *10*(1). https://doi.org/10.1038/s41467-019-09891-7

Weisberg, E., Chowdhury, B., Meng, C., Case, A. E., Ni, W., Garg, S., Sattler, M., Azab, A. K., Sun, J., Muz, B., Sanchez, D., Toure, A., Stone, R. M., Galinsky, I.,

Winer, E., Gleim, S., Gkountela, S., Kedves, A., Harrington, E., … Griffin, J. D. (2022). BRD9 degraders as chemosensitizers in acute leukemia and multiple myeloma. *Blood Cancer Journal*, *12*(7). https://doi.org/10.1038/s41408-022-00704-7

Wickström, M., Dyberg, C., Milosevic, J., Einvik, C., Calero, R., Sveinbjörnsson, B., Sandén, E., Darabi, A., Siesjö, P., Kool, M., Kogner, P., Baryawno, N., & Johnsen, J. I. (2015). Wnt/β-catenin pathway regulates MGMT gene expression in cancer and inhibition of Wnt signalling prevents chemoresistance. *Nature Communications*, *6*. https://doi.org/10.1038/ncomms9904

Wirsching, H. G., Galanis, E., & Weller, M. (2016). Glioblastoma. *Handbook of Clinical Neurology*, *134*, 381–397. https://doi.org/10.1016/B978-0-12-802997-8.00023-2

Woodley, C. M., Romer, A. S., Wang, J., Guarnaccia, A. D., Elion, D. L., Maxwell, J. N., Guerrazzi, K., McCann, T. S., Popay, T. M., Matlock, B. K., Flaherty, D. K., Lorey, S. L., Liu, Q., Tansey, W. P., & Weissmiller, A. M. (2021). Multiple interactions of the oncoprotein transcription factor MYC with the SWI/SNF chromatin remodeler. *Oncogene*, *40*(20), 3593–3609. https://doi.org/10.1038/s41388-021-01804-7

Wu, Y., Song, Y., Wang, R., & Wang, T. (2023). Molecular mechanisms of tumor resistance to radiotherapy. In *Molecular Cancer* (Vol. 22, Issue 1). BioMed Central Ltd. https://doi.org/10.1186/s12943-023-01801-2

Xu, G., Yan, X., Hu, Z., Zheng, L., Ding, K., Zhang, Y., Qing, Y., Liu, T., Cheng, L., & Shi, Z. (2021). Glucocappasalin Induces G2/M-Phase Arrest, Apoptosis, and Autophagy Pathways by Targeting CDK1 and PLK1 in Cervical Carcinoma Cells. *Frontiers in Pharmacology*, *12*. https://doi.org/10.3389/fphar.2021.671138

Yard, B. D., Adams, D. J., Chie, E. K., Tamayo, P., Battaglia, J. S., Gopal, P., Rogacki, K., Pearson, B. E., Phillips, J., Raymond, D. P., Pennell, N. A., Almeida, F., Cheah, J. H., Clemons, P. A., Shamji, A., Peacock, C. D., Schreiber, S. L., Hammerman, P. S., & Abazeed, M. E. (2016). A genetic basis for the variation in the vulnerability of cancer to DNA damage. *Nature Communications*, *7*. https://doi.org/10.1038/ncomms11428

Yi, G. Z., Huang, G., Guo, M., Zhang, X., Wang, H., Deng, S., Li, Y., Xiang, W., Chen, Z., Pan, J., Li, Z., Yu, L., Lei, B., Liu, Y., & Qi, S. (2019). Acquired temozolomide

resistance in MGMT-deficient glioblastoma cells is associated with regulation of DNA repair by DHC2. *Brain : A Journal of Neurology*, *142*(8), 2352–2366. https://doi.org/10.1093/brain/awz202

Yoshimoto, K., Mizoguchi, M., Hata, N., Murata, H., Hatae, R., Amano, T., Nakamizo, A., & Sasaki, T. (2012). Complex DNA repair pathways as possible therapeutic targets to overcome temozolomide resistance in glioblastoma. *Frontiers in Oncology*, *2*(December), 1–8. https://doi.org/10.3389/fonc.2012.00186

Yun, M., Wu, J., Workman, J. L., & Li, B. (2011). Readers of histone modifications. *Cell Research*, *21*(4), 564–578. https://doi.org/10.1038/cr.2011.42

Zhang, J., F.G. Stevens, M., & D. Bradshaw, T. (2011). Temozolomide: Mechanisms of Action, Repair and Resistance. *Current Molecular Pharmacology*, *5*(1), 102–114. https://doi.org/10.2174/1874467211205010102

Zhang, Z., Zou, Z., Dai, H., Ye, R., Di, X., Li, R., Ha, Y., Sun, Y., & Gan, S. (2020). Key genes involved in cell cycle arrest and DNA damage repair identified in anaplastic thyroid carcinoma using integrated bioinformatics analysis. *Translational Cancer Research*, *9*(7), 4188–4203. https://doi.org/10.21037/tcr-19-2829

Zheng, Y., Li, H., Bo, X., & Chen, H. (2023). Ionizing radiation damage and repair from 3D-genomic perspective. *Trends in Genetics*, *39*, 1–4. https://doi.org/10.1016/j.tig

Zhou, Q., Huang, J., Zhang, C., Zhao, F., Kim, W., Tu, X., Zhang, Y., Nowsheen, S., Zhu, Q., Deng, M., Chen, Y., Qin, B., Luo, K., Liu, B., Lou, Z., Mutter, R. W., & Yuan, J. (2020). The bromodomain containing protein BRD-9 orchestrates RAD51–RAD54 complex formation and regulates homologous recombination-mediated repair. *Nature Communications*, *11*(1). https://doi.org/10.1038/s41467-020-16443-x

Zhu, N., Chen, S., Jin, Y., Wang, M., Fang, L., Xue, L., Hua, D., Zhang, Z., Jia, M., Hao, M., & Zhang, C. (2024). Enhancing Glioblastoma Immunotherapy with Integrated Chimeric Antigen Receptor T Cells through the Re-Education of Tumor-Associated Microglia and Macrophages. *ACS Nano*, *18*(17), 11165–11182. https://doi.org/10.1021/acsnano.4c00050

Zhu, X., Liao, Y., & Tang, L. (2020). Targeting brd9 for cancer treatment: A new strategy. *OncoTargets and Therapy*, *13*, 13191–13200. https://doi.org/10.2147/OTT.S286867

Zoppi, V., Hughes, S. J., Maniaci, C., Testa, A., Gmaschitz, T., Wieshofer, C., Koegl, M., Riching, K. M., Daniels, D. L., Spallarossa, A., & Ciulli, A. (2019). Iterative Design and Optimization of Initially Inactive Proteolysis Targeting Chimeras (PROTACs) Identify VZ185 as a Potent, Fast, and Selective von Hippel-Lindau (VHL) Based Dual Degrader Probe of BRD9 and BRD7. *Journal of Medicinal Chemistry*, *62*(2), 699–726. https://doi.org/10.1021/acs.jmedchem.8b01413